TECHNICAL MEMORANDUM

X-800

AN INVESTIGATION OF THE SUBSONIC, TRANSONIC, AND SUPERSONIC

AERODYNAMIC CHARACTERISTICS OF A PROPOSED ARROW-WING

TRANSPORT AIRPLANE CONFIGURATION

By Richard T. Whitcomb, James C. Patterson, Jr.,
and Thomas C. Kelly

Langley Research Center
Langley Station, Hampton, Va.

NATIONAL AERONAUTICS AND SPACE ADMINISTRATION

WASHINGTON   January 1963

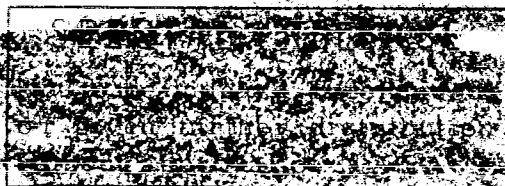NATIONAL AERONAUTICS AND SPACE ADMINISTRATION

TECHNICAL MEMORANDUM X-800

AN INVESTIGATION OF THE SUBSONIC, TRANSONIC, AND SUPERSONIC

AERODYNAMIC CHARACTERISTICS OF A PROPOSED ARROW-WING

TRANSPORT AIRPLANE CONFIGURATION*

By Richard T. Whitcomb, James C. Patterson, Jr.,
and Thomas C. Kelly

ABSTRACT

The principal feature of the configuration investigated is the integration of the engine nacelles into the rearward part of the wing. Wind-tunnel measurements of the aerodynamic forces and moments and sonic-boom intensity have been made at Mach numbers from 0.5 to 3.5. Various means for improving the off-design characteristics have been investigated at Mach numbers from 0.5 to 2.0.

---

*Title, Unclassified.

NATIONAL AERONAUTICS AND SPACE ADMINISTRATION

TECHNICAL MEMORANDUM X-800

AN INVESTIGATION OF THE SUBSONIC, TRANSONIC, AND SUPERSONIC

AERODYNAMIC CHARACTERISTICS OF A PROPOSED ARROW-WING

TRANSPORT AIRPLANE CONFIGURATION*

By Richard T. Whitcomb, James C. Patterson, Jr.,
and Thomas C. Kelly

SUMMARY

The results of a wind-tunnel investigation of the aerodynamic characteristics at high subsonic, transonic, and supersonic flight conditions are presented for a proposed improved arrow-wing transport airplane configuration designed for a maximum cruise Mach number of 3.2. The principal feature of the combination is the integration of the engine nacelles into the rearward part of the wing. Estimates based on the experimental results presented suggest that an airplane based on the proposed combination would achieve relatively high supersonic lift-drag ratios, acceptable lift-drag ratios at subsonic and transonic speeds with trailing-edge flaps deflected a small amount, and a sonic-boom level at the ground of about 1.5 pounds per square foot for reasonable operating altitudes.

INTRODUCTION

It is generally agreed that the attainment of a competitive, long-range supersonic commercial aircraft will require, among other factors, the achievement of supersonic lift-drag ratios substantially higher than those obtained with a simple delta-wing configuration similar to present long-range supersonic cruise military airplanes. Further, to provide acceptable sonic-boom levels at the ground with a reasonable climb-acceleration flight path for such an airplane, sonic-boom pressure signatures substantially lower than those for the delta-wing configuration (ref. 1) will be required. One approach for accomplishing these objectives, a special treatment of a highly swept arrow wing, is proposed in reference 2.

Although the supersonic characteristics for the representative transport configuration based on the proposed approach of reference 2 appeared quite promising, exploratory investigations of this airplane indicated unacceptable low lift-drag ratios at high subsonic and transonic speeds. Therefore, a number of means for improving the off-design characteristics of this configuration have

---

*Title, Unclassified.

been investigated. Also, to provide a basis for the evaluation of the overall feasibility of an airplane based on the proposed approach, the aerodynamic characteristics of the representative configuration for the range of probable operating speeds and attitudes have been obtained. Further, a limited study has been made of the effects of changes in certain key design parameters, such as fuselage size and wing sweep. Finally, experimental measurements have been made to evaluate the probable sonic-boom level for the proposed combination. Selected results from these investigations and analyses are presented herein for the Mach number range from 0.50 to 3.50. Results obtained for the proposed configuration at landing and take-off speeds (Mach number of 0.20) may be found in reference 3.

SYMBOLS

A aspect ratio

b wing span

C_D drag coefficient, $\dfrac{\text{Drag}}{qS}$

ΔC_D incremental drag coefficient

$C_{D,b}$ nacelle base drag coefficient, $\dfrac{\text{Nacelle base drag}}{qS}$

$C_{D,i}$ internal duct drag coefficient, $\dfrac{\text{Internal duct drag}}{qS}$

C_L lift coefficient, $\dfrac{\text{Lift}}{qS}$

ΔC_L incremental lift coefficient

C_m pitching-moment coefficient, $\dfrac{\text{Pitching moment}}{qS\bar{c}}$

ΔC_m incremental pitching-moment coefficient

$\bar{c}$ mean geometric chord

d diameter

i incidence of wing section, deg

L characteristic length of sonic-boom model (1 inch was used for present investigation)

M free-stream Mach number

m/c	ratio of maximum deviation of section mean chord line from a straight line from leading to trailing edge to chord
p	free-stream static pressure
p_t	free-stream total pressure
Δp	incremental pressure above or below ambient due to flow field of sonic-boom model
Δp_{max}	maximum value of Δp at bow shock
$\left(\dfrac{\Delta p}{p}\right)_{max}$	maximum pressure ratio at bow shock
q	free-stream dynamic pressure
R	Reynolds number
S	wing area
t/c	thickness ratio of wing section
V	total volume of airplane
W	weight of airplane
X,Y	Cartesian coordinates of sonic-boom field, point X measured in free-stream direction
ΔX	distance from point on sonic-boom pressure signature to point of zero incremental pressure
x,y	Cartesian coordinates of airfoil sections, x measured in chordwise direction
α	angle of attack of reference line, top of rear fuselage, deg
β	angle of sideslip of fuselage reference line, deg
Λ	sweepback angle of wing leading edge, deg
δ_a	aileron deflection angle, positive when trailing edge down, deg
δ_e	elevator deflection angle, positive when trailing edge down, deg
δ_f	flap deflection, positive when trailing edge down, deg
δ_r	rudder deflection angle, positive when trailing edge right, deg

L/D lift-drag ratio

$\dfrac{\partial C_L}{\partial \alpha}$ lift-curve slope, per deg

$\dfrac{\partial C_m}{\partial C_L}$ static-longitudinal-stability parameter

C_{l_β} change in rolling-moment coefficient due to sideslip, per deg

C_{n_β} change in yawing-moment coefficient due to sideslip, per deg

C_{Y_β} change in side-force coefficient due to sideslip, per deg

$C_{l_{\delta_a}}$ change in rolling-moment coefficient due to aileron deflection, per deg

$C_{n_{\delta_a}}$ change in yawing-moment coefficient due to aileron deflection, per deg

$C_{Y_{\delta_a}}$ change in side-force coefficient due to aileron deflection, per deg

$C_{m_{\delta_e}}$ change in pitching moment due to elevator deflection, per deg

$C_{l_{\delta_r}}$ change in rolling-moment coefficient due to rudder deflection, per deg

$C_{n_{\delta_r}}$ change in yawing-moment coefficient due to rudder deflection, per deg

$C_{Y_{\delta_r}}$ change in side-force coefficient due to rudder deflection, per deg

$\dfrac{\Delta C_D}{\Delta \beta}$ incremental change in drag coefficient due to sideslip, per deg

$\dfrac{\Delta C_L}{\Delta \beta}$ incremental change in lift coefficient due to sideslip, per deg

$\dfrac{\Delta C_m}{\Delta \beta}$ incremental change in pitching-moment coefficient due to sideslip, per deg

$\dfrac{\Delta C_D}{\Delta \delta_a}$ incremental change in drag coefficient due to aileron deflection, per deg

$\dfrac{\Delta C_L}{\Delta \delta_a}$ incremental change in lift coefficient due to aileron deflection, per deg

$\dfrac{\Delta C_m}{\Delta \delta_a}$ incremental change in pitching-moment coefficient due to aileron deflection, per deg

$\dfrac{\Delta C_D}{\Delta \delta_r}$ incremental change in drag coefficient due to rudder deflection, per deg

$\dfrac{\Delta C_L}{\Delta \delta_r}$ incremental change in lift coefficient due to rudder deflection, per deg

$\dfrac{\Delta C_m}{\Delta \delta_r}$ incremental change in pitching-moment coefficient due to rudder deflection, per deg

Subscripts:

max   maximum

min   minimum

APPARATUS AND METHODS

Experimental Models

The general configuration of the present investigation is similar to that described in reference 2 except for the addition of vertical and horizontal tails. It incorporates a highly swept arrow wing having a low ratio of root chord to length, camber and twist, nacelles (4) integrated into the rearward portion of the wings, and fuselage camber. (See fig. 1.) This configuration is the fourth in a series of supersonic transport combinations being investigated by the National Aeronautics and Space Administration and is generally referred to as SCAT 4.

Basic configuration.- Most of the supersonic tests of this investigation were made for the model described in figures 1(a) and 1(b) and table I, which will be referred to herein as the "basic configuration." The volume factor $\dfrac{V^{2/3}}{S}$ for an airplane based on this model would be about 0.18. In arriving at this factor, the volume of the stream tubes on the engine air ducts was subtracted from the total volume and the rearward end of the fuselage was closed to simulate a proposed airplane configuration. (See fig. 2.)

Leading-edge droop.- During the development of the proposed configuration, leading-edge droop was incorporated in the outboard sections of the basic wing to improve the subsonic characteristics. The effect of this droop, which varied from 0 at the wing-fuselage juncture to a maximum of 0.07 inch at the tip, on the outboard wing section shapes is shown in figures 1(b) and 1(e). The

experimental configurations with and without this droop are identified in the figures presenting results.

Nacelle and fuselage camber deletion.- Experiments were made to determine the separate effects of deleting the nacelles and fuselage camber at supersonic speeds and the combined effects of these changes at subsonic and transonic Mach numbers for the combination with leading-edge droop.

Modifications of fuselage size and shape and dihedral.- Limited experiments were made late in the investigation of the combined effects of a 25-percent reduction in fuselage frontal area, a 4° reduction in dihedral, and a forward movement of the discontinuity of the fuselage contours near the leading edge of the wing-fuselage juncture. (See fig. 1(c).) The supersonic phase of these tests was made for a configuration with the nacelles removed; the transonic part was made with the nacelles and fuselage camber eliminated. The volume factor for a complete airplane configuration with the reduced fuselage would be about 0.16. Photographs of an airplane based on the configuration with the modified fuselage and dihedral are shown in figure 1(d).

Fuselage afterbody closure.- The effect of changing the fuselage afterbody shape from that of the test model with the reduced fuselage size (fig. 1(c)) to one simulating an airplane configuration was evaluated by using the models of figure 3. The wings and forebody of the models of figure 3(a) are similar to those of figure 1 except for removal of the outer portions of the wing panels. At Mach numbers of 3.0 or greater this modification should have only a slight effect on the fuselage afterbody drag since most of the disturbances from these outboard elements pass behind the fuselage for such conditions. Solid bodies simulating the area developments of the forward parts of the inner nacelles with the inlet stream tube removed have been added to the wing.

Two closed afterbody configurations were investigated. One consisted of a simple closure of the test configuration in a generally upward direction. This configuration will be referred to as the "basic closure." (See fig. 3(a).) For the second, the aft portion of the fuselage was lowered 0.015 inch while the trailing edge of the wing near the fuselage was raised 0.015 inch. These changes have been confined within a Mach cone which is aft of the components of this model differing from the complete configuration. Thus, aerodynamic increments obtained should be applicable to the complete configuration. This combination will be referred to as the "closure with raised wing trailing edge."

The two afterbodies of figure 3(b) for the fuselage alone are similar to those of figure 1 except for the removal of a small portion of the extreme rearward part of the closed afterbody configuration.

Flaps and controls.- The effects of partial deflections of the main trailing-edge landing flap and the associated ramp (ref. 3) were investigated in conjunction with downward deflections of the ailerons. (See fig. 1(a).)

Investigations were also made with deflections of the rudder, ailerons, and elevator shown in figure 1(a).

Sonic-boom configuration.- A 1/40-scale model of the basic model configuration (fig. 4) was investigated to determine the far-field pressure intensity. This model is an exact scale model of the basic configuration with the exception that the volume of the engine nacelles has been evenly distributed along the rearward region of the wing rather than at four isolated positions along the span.

Facilities and Techniques

Wind tunnels.- Four variable-density wind-tunnel facilities were utilized for the present investigation. Subsonic and transonic results (Mach numbers 0.50 to 1.30) were obtained in the Langley 8-foot transonic pressure tunnel which is capable of continuous operation through the speed range noted without the usual effects of blockage. Aerodynamic characteristics at a Mach number of 2.01 and measurements of the sonic-boom intensities at Mach numbers of 1.40 and 2.01 were obtained in the Langley 4- by 4-foot supersonic pressure tunnel. High supersonic results (Mach numbers 2.3 to 3.5) were obtained in the high-speed leg of the Langley Unitary Plan wind tunnel. Investigations of afterbody closure for the fuselage alone were made in the 2-foot hypersonic facility at the Langley Research Center.

Afterbody closure investigation.- The truncated wing-fuselage combinations were supported on a centrally located internal strain-gage balance which was attached to a strut passing through the left wing panel and extending well beyond the wing tip as shown in figure 3(a). The strut was connected to the angle-of-attack mechanism through a large diameter sting. The model was oriented with the wing span essentially vertical. For the open afterbody configuration, the aerodynamic effects of the sting holding the complete test model were simulated by an independently mounted dummy sting. The fuselage-alone models of figure 3(b) were supported by a 0.5-inch-diameter sting with a constant area extending 4 base diameters behind the ends of the models.

Sonic boom.- The sonic-boom models were sting mounted on a support system which provided for remotely controlled adjustments of the longitudinal position of the model. (See ref. 4.)

Test Conditions

Range for force tests.- Tests were conducted over a Mach number range from 0.50 to 3.50 at Reynolds numbers indicated in figure 5. Most of the experiments were conducted at tunnel static pressures which are designated "basic" in figure 5. In order to determine the effects of a variation in Reynolds number, limited investigations were conducted at tunnel static pressures indicated as "increased" in figure 5. The angle-of-attack range varied generally from -2° to 6° at Mach numbers from 0.50 to 1.30; and from -2° to 6° at Mach numbers from 2.01 to 3.50. Investigations were made at sideslip angles of -2° for Mach numbers from 0.50 to 1.2 and $\pm 1^\circ$ for Mach numbers from 2.3 to 3.5. Investigations were made for the flap and aileron deflected downward 4° with the ramp at 2° (fig. 1(a)) at Mach numbers to 2.0. Corresponding deflections of 7° and 3° were tested at Mach numbers to 1.2. Elevator deflections of -5° and -7° were

investigated at Mach numbers from 0.50 to 1.2 and -2.25° to -1.75° at Mach numbers of 2.3 to 3.5. Rudder deflections of -5° and -7° at Mach numbers from 0.50 to 1.2, and -5° at Mach numbers of 2.3 to 3.5 were also investigated. Results were obtained with the left aileron down 7°, the right up 7° for the configuration incorporating 7° of flap deflection at Mach numbers from 0.5 to 1.2. In addition to the various control deflections investigated, data were obtained with the complete tail assembly removed.

The afterbody closure investigation utilizing the truncated wing-fuselage combination was conducted at Mach numbers of 2.96, 3.20, and 3.50 for angles of attack from about 0° to 3° and through a sideslip-angle range from -2° to 2°. Tests of the fuselage alone (with and without afterbody closure) were conducted at Mach numbers from 3.0 to 3.5 and at angles of attack from 0° to 4°.

Transition strips.- All experiments were conducted with boundary-layer transition fixed. The transition strips, composed of carborundum grains set in a plastic adhesive, were 0.010 inch wide and were located with the forward edges 3/16 inch aft of the wing and tail leading edges, 1/8 inch aft of the inlet lip, and 3 inches aft of the fuselage nose. The strip on the fuselage nose was composed of No. 60 carborundum grains for all Mach numbers. The other strips were composed of No. 120 carborundum grains for the tests at Mach numbers from 0.50 to 3.50. In an attempt to assure a turbulent boundary layer most of the studies were made with a relatively high grain density, approximately 100 grains per frontal inch. Fluorescent-oil flow investigations, which are described later, indicated that the transition strips used produced flow patterns typical of those generally observed with the presence of turbulent boundary-layer flow over a model. In addition, tests conducted at two Reynolds numbers indicated a change in drag with Reynolds number close to that predicted using turbulent skin-friction theory. In order to determine the effect of a decrease in transition-strip grain density, one experiment was conducted at a Mach number of 2.01 with approximately 20 grains per frontal inch.

Recent unpublished experiments through a wider range of Reynolds numbers than for the present investigation for a supersonic transport configuration with transition strips similar to those on the present model have indicated that the boundary layer was not fully turbulent at supersonic Mach numbers for Reynolds numbers of the order of the present tests, even though oil-flow surveys indicated completely turbulent flow. Such a condition may have existed on the present model at low angles of attack. It is probable, however, that the boundary layer would become completely turbulent as angle of attack is increased to values close to those for the full-scale maximum lift-drag condition.

Sonic boom.- Studies with the sonic-boom model were made at Mach numbers of 1.40 and 2.01 at Reynolds numbers per foot of 3.0×10^6 and 2.5×10^6, respectively. Model angles of attack were adjusted to obtain lift coefficients of 0, 0.15, and 0.3 at a Mach number of 1.4 and lift coefficients of 0, 0.1, and 0.2 at $M = 2.01$.

Forces.- Measurements of all forces and moments were obtained from an internally mounted, sting-supported, six-component electrical strain-gage balance.

The static pressure at the base of the fuselage and in the balance chamber was measured simultaneously by a single pressure transducer. The measurements were used to adjust the force and moment results to the condition of stream static pressure at the base of the fuselage. Similar corrections were made for the static pressures measured at the bases of the nacelles and the base of the open afterbody of the afterbody closure investigations.

The measured angle of attack has been corrected for tunnel flow angularity and tunnel sting and balance deflection and is estimated to be accurate within ±0.10°.

Internal duct drag.- Previous investigations have indicated that accurate determination of internal duct drag, particularly at the higher supersonic Mach numbers, is quite difficult. (See ref. 5.) In order to insure adequate measurements for the present investigation, several precautions (based on exploratory tests) have been taken. The internal ducting, shown in figure 6, was designed to provide relatively low Mach numbers in the flow ahead of the exit and sonic flow at the exit. In addition, the ducting cross section was reduced just behind the inlet in order to provide reduced mass-flow ratios at subsonic speeds, more closely simulating conditions which would be experienced in actual flight. (See fig. 7.) Each inlet had a capture area of about 0.63 square inch, a minimum area of roughly 0.41 square inch, a maximum area ahead of the exit of 1.23 square inches, and an exit nozzle area of 0.61 square inch. The design of the exit nozzle shape was such as to provide a smooth acceleration of the duct air flow to a Mach number of 1.0 (at stream Mach numbers greater than 1.0). In order to provide sufficient length for this air-flow acceleration, the nacelles were extended beyond the wing trailing edge by an amount somewhat greater than that proposed for an actual airplane. (See fig. 1(a).)

Exploratory tests indicated irregular variations of the static and total pressures across each duct exit at supersonic stream Mach numbers. In an attempt to reduce these variations as well as any stream cross flows or fluctuations which might be present, divider plates were installed which extended into the exit nozzles approximately 1.2 inches and which separated each exit into four segments having equal areas. (See fig. 6.) Subsequent static-pressure measurements, both in the stream and at the wall, indicated that there was essentially no variation in static pressure within each segment; therefore, only the static-pressure orifices in each segment wall were used for the rest of the investigations.

Measurements of total pressures in each duct exit showed that, for two segments, total pressures were fairly constant within the segment whereas for the other two segments variations in total pressure occurred. The available number of total-pressure tubes for each exit were then arranged so there were six total-pressure measurements made in the segments having noticeable total-pressure variations and three in those having a fairly constant total pressure across the segment. Actual tube locations were selected to provide measurements at the

center-of-equal-area portions and also to provide a good indication of the total-pressure variation near the duct outer surface.

Mass-flow ratios and internal drag coefficients have been calculated by using standard procedures. (See ref. 6, for example.) Internal drag coefficients, presented in figure 7, represent a summation of individual point drag values which were obtained for each of the total-pressure tubes. The model drag results have been adjusted for both the internal duct drag and also the skin-friction drag associated with the model nacelle extension which was noted earlier.

The total-pressure measurements on which the internal drag adjustments are based include the energy loss of the wing boundary layer ingested into the inlets. This effect, of course, leads to an erroneously high internal drag correction. It is impossible to calculate the magnitude of this error exactly. However, estimates indicate that it should probably be less than 0.0001 in drag coefficient. The basic results presented include no adjustment for such an error.

Oil flow surveys.- Studies of the flow about several of the configurations investigated were made through the use of the fluorescent-oil film method. As reported in reference 7, the method consists simply of putting a thin film of lubricating oil on the model and observing the model in the dark with use of ultraviolet light. The shearing action of the air passing over the model produced clearly defined patterns of the boundary-layer flow over the surfaces coated with the oil.

Schlieren.- Schlieren photographs at supersonic speeds were taken with the use of a single pass system. (See ref. 8.)

Sonic boom.- Measurements of the pressure signatures of the sonic-boom model were made by means of static-pressure probes located at distances of 12.5, 25, and 50 inches from the model, measured perpendicular to the free-stream direction, as described in reference 4. The repeatability of the data is estimated to be ±0.0003 for $\Delta p/p$ and ±0.03 for $\Delta X/L$. The bow-shock pressure-rise data obtained by the probe located 50 inches from the model (far-field conditions) were adjusted for vibration of the model during the investigation in the manner discussed in reference 4. This adjustment increased the peak pressure by 30 percent. The peak pressures also have been adjusted for the buildup of the laminar boundary layer on the small sonic-boom model. The stream displacement by the boundary layer at $M = 2.0$ is equivalent to an increase of the frontal area of the model of approximately 28 percent. The correction to account for this displacement amounted to a 12-percent decrease in the peak-pressure or sonic-boom level at $C_L = 0$ with lesser correction at other test conditions. Also, the effect of reducing the relative size of the fuselage from that of the boom test model to that of the configuration of figure 1(d) has been estimated on the basis of linear theory.

Results of this investigation are presented in standard coefficient form with the longitudinal and lateral results referred to the stability- and body-axis systems, respectively. Force-test coefficients including those for the afterbody closure investigation are based on wing areas and the mean aerodynamic chord listed in table I. The moment reference center was selected to give static stability at low subsonic speeds and is located at model station 27.87 inches (61 percent of the body length). The results of this investigation are included in the following table:

Flaps.- At subsonic and transonic speeds the drag-due-to-lift factors for the basic configuration without flap deflection (fig. 8(b)) are substantially greater than that predicted by theory. Oil flow surveys indicate that this adverse difference results from boundary-layer separation on the upper surface of the wing. The flap and aileron deflections investigated result in significant improvement of these factors at lift coefficients near those for maximum full-scale lift-drag ratios (fig. 29). Deflections of 7° are most effective at Mach numbers from 0.50 to 0.90; 4° is more satisfactory at M = 0.97 to 1.3. (See fig. 8(b).) (The measured drag-coefficient values at M = 0.97 are lower for the 7° than for the 4° deflection; however, because of the lesser negative shift in the pitching moment associated with the 4° deflection, the maximum trimmed lift-drag ratios at this condition are obtained with the 4° deflection.) These favorable effects of flap deflections result primarily from the fact that they allow a substantial reduction of the wing angle of attack required to obtain a given lift coefficient (about 2° for 7° flap deflection of a Mach number of 0.90) with an associated decrease of the boundary-layer separation on the upper surface. Flow surveys indicate very little separation on the flap even at the critical transonic speeds (fig. 16). However, exploratory experiments indicated substantial separation in the region of the flaps without the ramp of the main flap.

Leading-edge droop.- Drooping the wing leading edge results in a small improvement in the drag at lift coefficients for full-scale maximum lift-drag ratios through the subsonic speed range with little or no effect at the higher Mach numbers. (See figs. 9(b) and 18(b).) With the flaps deflected and leading-edge droop the drag-due-to-lift values at subsonic Mach numbers for lift coefficients near those for maximum full-scale lift-drag ratios (fig. 29) are approximately 1.10 times the theoretical values for these speeds. This difference is of the order of that for a similar swept-wing configuration designed for subsonic speeds (ref. 9). This relatively close approach of the actual factor to the theory results primarily from the near elimination of separation on the wing (fig. 16).

Nacelles and fuselage camber.- At subsonic and transonic speeds, the deletion of the nacelles and fuselage camber from the configuration without flap deflection (fig. 11(b)) provides a significant reduction in drag at angles of attack corresponding to those for maximum lift-drag ratios, approximately 2°, with the flaps deflected. (See figs. 8(b) and 29.) At Mach numbers of 0.90 and 1.2, this reduction in drag coefficient is approximately 0.0020. This decrement is substantially greater than the computed skin-friction drag coefficients of the nacelles of about 0.0009 for these same Mach numbers. The additional difference probably results from inlet spillage associated with the relatively low inlet mass-flow ratios for these conditions (fig. 7) and the effect of fuselage camber. Inlet spillage is probably the larger factor.

At all supersonic test Mach numbers, removal of the engine nacelles from the basic configuration having leading-edge droop (fig. 20(b)) results in a noticeable increase in the drag coefficients at lift coefficients near those for the full-scale maximum lift-drag ratios (see fig. 29) even though the configuration wetted area is significantly reduced by this change.

Deletion of the fuselage camber (from the basic configuration with leading-edge droop and nacelles removed) is seen to have only small effects at supersonic speeds on drag at lift coefficients near those for the maximum lift-drag ratio. (See fig. 20(b).)

Fuselage size and dihedral, combined.- Results showing the combined effects of reductions in fuselage size and dihedral and a forward shift in the longitudinal position of the fuselage corner near the wing-leading-edge—fuselage juncture for the configuration with no flap deflection and with nacelles and body camber removed are given in figures 12(b) and 21(b). At angles of attack (approximately 2°) near those for maximum lift-drag ratios (for the combination with flaps deflected) the total decrements associated with these changes are about 0.0010 at a Mach number of 0.90, and 0.0020 at $M = 1.03$. (See fig. 12(b).) The subsonic difference is approximately 50 percent greater than that estimated for the changes in skin friction and induced drag. The additional change might have resulted from a favorable effect of the more forward location of the fuselage corner. The greater effects of these changes at transonic speeds are approximately equal to the change in wave drag estimated for the differences in the area developments (fig. 2).

The changes noted result in reductions in the drag coefficients at lift coefficients near those for the maximum full-scale lift-drag ratios (fig. 29) at all supersonic Mach numbers (fig. 21(b)). At a Mach number of 3.2 this reduction is approximately 0.0006. Estimates have indicated that of this total reduction, the variation in fuselage size contributes approximately 0.0003; the reduction in wing dihedral, 0.0002; and the forward movement of the fuselage corner, the rest. This latter effect results from a significant reduction of the local slopes of the supersonic-area developments for the combination at longitudinal stations near the leading edge of the wing-fuselage juncture. It might be expected that the decrements due to the variations investigated for the nacelle-on configuration would be approximately similar to these measured values since there would probably be no significant mutual interferences between the effects of nacelles and the influences of the changes investigated.

Afterbody closure.- Because of a considerable question as to the drag increment due to closing the fuselage afterbody from the configuration required for the model tests to one corresponding to a possible airplane configuration, a significant effort was made to evaluate this effect experimentally at supersonic speeds. Results obtained for opened and closed afterbodies of the reduced fuselage in the presence of a simulated wing, but with no tail surfaces (fig. 3(a)) are given in figure 22 for Mach numbers from 2.96 to 3.50. Both the basic closure and that with the wing trailing edge raised result in a drag-coefficient increase of about 0.00015 for angles of attack near those for the full-scale $(L/D)_{max}$, about 2°, at a Mach number of 3.2. For the basic closure the lift coefficient is reduced by about 0.001. With the wing trailing edge raised no change in lift was measured. Application of these increments to the results for the complete configuration indicates that the drag coefficient for a given lift coefficient near that for maximum lift-drag ratio is increased by 0.00025 for the basic closure and 0.00015 for the configuration with the raised trailing edge. The improvement for this latter configuration results primarily from a reduced interference of the flow fields of the wing and fuselage afterbody.

13

An indication of the magnitudes of the aerodynamic interferences between the fields of the wing and fuselage on the wave drag may be obtained by comparing the drag decrements just noted with those obtained from an investigation of the open and closed afterbodies alone. A drag-coefficient decrement of 0.0005 was measured for the closure of the body alone at conditions close to those for which the decrements noted previously for the simulated wing afterbody configurations were obtained. This favorable effect of afterbody closure for the fuselage alone results from the fact that the decrease of skin-friction drag associated with the reduction of wetted area is greater than the relatively small increase of wave drag for the high-fineness-ratio afterbody.

Mach number.- The variations with Mach number of the minimum drag coefficient for the most nearly symmetrical configuration, that is, the basic configuration without leading-edge droop or flap deflection, is shown in figure 29. At supersonic Mach numbers the minimum drag decreases with increase in Mach number approximately as predicted on the basis of turbulent skin-friction theory (ref. 10) and linear-wave theory to a Mach number of approximately 3.2. At a Mach number of 3.5 the minimum drag increases abruptly above the trend defined by the lower Mach number data. As suggested in reference 2, this increase in drag is probably due to the convergence of positive disturbances along the leading edge of the wing.

The variation with Mach number of the drag-due-to-lift factor is also presented in figure 29. These factors were obtained by subtracting the minimum drag coefficients previously described from the drag coefficients for the basic configuration with leading-edge droop and optimum flap deflections at lift coefficients near those that would probably be required to obtain maximum full-scale lift-drag ratios. At supersonic Mach numbers from 2.6 to 3.5, the drag-due-to-lift increase is approximately as predicted by linear theory. At a Mach number of 2.3 the drag due to lift is significantly higher than the trend defined by the data obtained at the higher Mach numbers. This increase in drag can be attributed to separation of the flow on the upper surface of the wing at this off-design condition.

Lift-drag ratios.- Because of the question related to the condition of the boundary layer for the present investigation, which was noted earlier, no attempt is made herein to predict full-scale maximum lift-drag ratios for the proposed configuration. However, estimates (not presented) based on these experimental results suggest that an airplane typified by the proposed combination would achieve relatively high lift-drag ratios at supersonic Mach numbers to 3.20 and satisfactory lift-drag ratios at subsonic and transonic speeds.

Inlet Simulation

Examination of the oil flow and schlieren photographs (figs. 26 and 27) indicates that, in contrast to the condition which existed at transonic speeds and which was noted previously, the inlets are operating properly in the supersonic range and the local entering flow is reasonably alined with the inlet.

14

It may be noted in figure 7 that the mass-flow ratios near the design Mach number (3.2) are noticeably greater than 1.0. This effect is associated with the deceleration of the flow over the wing lower surface just ahead of the inlet, and should allow the use of an inlet somewhat smaller than that which would be required if the inlet was located in the free stream.

No boundary-layer diverter was included in the model inlet system, although a diverter might possibly be required for a proposed full-scale vehicle. It is felt, however, that the drag increment associated with such a diverter would be slight since the distance from the wing leading edge to the inlet is relatively short and the height of the required diverter, therefore, would be small.

Stability and Control

Trimming moments.- For the selected center-of-gravity location the complete configuration with leading-edge droop, 7° of flap deflection, and the basic 0° elevator deflection is trimmed at lift coefficients slightly below those for full-scale maximum lift-drag ratios (fig. 29) at Mach numbers to 0.90 (fig. 9(c)). At transonic Mach numbers the configuration with 4° flap deflection trims at lift coefficients well below those for maximum lift-drag ratio.

Results for the basic configuration with leading-edge droop show that at supersonic speeds, for the selected center-of-gravity location, trim occurs at lift coefficients close to those for the full-scale maximum lift-drag ratios. Examination of the results presented in figure 21(c) indicates that variations in fuselage size and wing dihedral have only slight effects on trim. On the other hand, fuselage camber (fig. 20(c)) and afterbody closure (fig. 22) result in a fairly constant positive shift in pitching moment (and, therefore, increases in lift coefficients for trim) throughout the supersonic Mach number range.

Longitudinal stability.- The flap deflections required to obtain improved $(L/D)_{max}$ for the various subsonic and transonic conditions also significantly increase the lift coefficients for pitch-up (fig. 8(c)). The wing leading-edge droop further increases the lift coefficient for pitch-up in the subsonic speed range with essentially no effect at transonic Mach numbers (fig. 9(c)). With the flap deflection and wing leading-edge droop, the lift coefficient for pitch-up is delayed to coefficients well beyond those required for full-scale maximum lift-drag ratios.

The pitch-up for the configuration with the nacelles and fuselage camber deleted is much more severe than for the complete configuration (fig. 11(c)). This difference results from a favorable effect of the nacelles on the boundary-layer separation similar to that described in reference 11.

At the lift coefficients for maximum lift-drag ratios, the longitudinal stability parameter $\partial C_m / \partial C_L$ is about -0.08 at $M = 0.90$, and -0.14 at $M = 1.2$ (fig. 28). The effect of the tail on the subsonic and transonic longitudinal stability is shown in figure 13(c).

Examination of the supersonic pitching-moment results for the basic configuration (fig. 10(c)) indicates that the variations with lift coefficient are reasonably linear over the probable flight lift-coefficient range. At the lift coefficients for maximum full-scale lift-drag ratio, the longitudinal stability parameter varies from -0.19 at a Mach number of 2.60 to -0.11 at a Mach number of 3.50 (fig. 28). The effect of the horizontal tail on the supersonic longitudinal stability is shown in figure 23(c).

Removal of the nacelles from the basic configuration with a drooped leading edge results in substantial adverse effects on stability (fig. 20(c)). These changes are associated with the increase in upper-surface separation which was noted in the discussion of the transonic characteristics.

Lateral stability.- The limited results in sideslip of figure 14(d) indicate an increase in the positive directional and lateral stability of the configuration with an increase in angle of attack throughout the subsonic and transonic speed ranges. The directional stability parameter for the configuration with empennage on at an angle of attack of 1.5° ranges from 0.0015 at a Mach number of 0.50 to 0.0023 at a Mach number of 1.20. Values of positive effective dihedral at these Mach numbers and $\alpha = 1.5°$ are -0.0031 and -0.0033, respectively.

Lateral stability derivatives for the basic, drooped-leading-edge configuration at Mach numbers near 3.0 and angles of attack near those for maximum lift-drag ratios are given in figure 24 and are seen to be -0.0015, 0.0019, and -0.0071 for C_{l_β}, C_{n_β}, and C_{Y_β}, respectively, for the configuration with empennage on.

Controls.- The results presented in figures 13 and 15(d) indicate that the elevator, rudder, and aileron deflections investigated provide values of $C_{m_{\delta_e}}$, $C_{n_{\delta_r}}$, and $C_{l_{\delta_a}}$ of -0.0026, -0.0011, and -0.0002, respectively, at a Mach number of 0.90 and an angle of attack of 1.5°. The marked change in pitching moment associated with the aileron deflection results from varying the deflection of the right aileron only.

Effectiveness parameters for the horizontal (elevator) and vertical (rudder) tail controls at Mach numbers near 3.0 have values of -0.0006, -0.0004 per degree for $C_{m_{\delta_e}}$ and $C_{n_{\delta_r}}$, respectively. (See figs. 23 and 25.)

Sonic Boom

The bow-shock overpressure (sonic-boom level), as obtained by adjusting tunnel data (fig. 30) for the airplane configuration with the reduced fuselage size (fig. 31), has been extrapolated, on the basis of reference 4, to meet flight conditions for Mach numbers of 1.40 and 2.01 and for a wing loading W/S of 65 lb/sq ft, as shown in figure 32. In the extrapolation of the data, complete reflection of the bow shock at the ground was assumed and, as suggested by reference 4, the reference pressure was chosen simply as the measured atmospheric

pressure at midaltitude. An analysis of the data of figure 32 indicates that a maximum overpressure of 1.5 lb/sq ft would be produced on the ground by the configuration in straight and level flight at 58,000 feet for a Mach number of 2.01 and at 48,000 feet for a Mach number of 1.40. The corresponding lift coefficients for these conditions are $C_L = 0.145$ and $C_L = 0.175$, respectively.

CONCLUDING REMARKS

The experimental results presented herein indicate that the proposed arrow-wing transport airplane configuration has satisfactory high subsonic, transonic, and off-design supersonic aerodynamic characteristics, as well as relatively high lift-drag ratios at the cruise speeds near a Mach number of 3.2 and low sonic-boom pressures.

Langley Research Center,
     National Aeronautics and Space Administration,
          Langley Station, Hampton, Va., January 9, 1963.

REFERENCES

1. Patton, R. J.: Supersonic Transport Design Characteristics and the Sonic Boom. Paper No. 62-23, Inst. Aerospace Sci., Jan. 1962.

2. Whitcomb, Richard T.: An Approach to Obtaining Increased Supersonic Lift-Drag Ratios and Reduced Sonic Boom. NASA TM X-799, 1963.

3. Whitcomb, Richard T., and Loving, Donald L.: An Investigation of the Landing and Take-Off Characteristics of a Proposed Arrow-Wing Transport Airplane Configuration. NASA TM X-801, 1963.

4. Carlson, Harry W.: Wind-Tunnel Measurements of the Sonic-Boom Characteristics of a Supersonic Bomber Model and a Correlation With Flight-Test Ground Measurements. NASA TM X-700, 1962.

5. Carraway, Ausley B., Morris, Owen G., and Carmel, Melvin M.: Aerodynamic Characteristics at Mach Numbers From 0.20 to 4.63 of a Canard-Type Supersonic Commerical Air Transport Configuration. NASA TM X-628, 1962.

6. Pendley, Robert E., Milillo, Joseph R., and Fleming, Frank F.: An Investigation of Three NACA 1-Series Nose Inlets at Subsonic and Transonic Speeds. NACA RM L52J23, 1953.

7. Loving, Donald L., and Katzoff, S.: The Fluorescent-Oil Film Method and Other Techniques for Boundary-Layer Flow Visualization. NASA MEMO 3-17-59L, 1959.

8. Anon.: Manual for Users of the Unitary Plan Wind Tunnel Facilities of the National Advisory Committee for Aeronautics. NACA 1956.

9. Loving, Donald L.: A Wind-Tunnel Investigation of a Transonic-Transport Configuration Utilizing Drag-Reducing Devices at Mach Numbers From 0.20 to 1.03. NASA TN D-636, 1961.

10. Sommer, Simon C., and Short, Barbara J.: Free-Flight Measurements of Turbulent-Boundary-Layer Skin Friction in the Presence of Severe Aerodynamic Heating at Mach Numbers From 2.8 to 7.0. NACA TN 3391, 1955.

11. Whitcomb, Richard T.: Special Bodies Added on a Wing To Reduce Shock-Induced Boundary-Layer Separation at High Subsonic Speeds. NACA TN 4293, 1958.

TABLE I.- DESCRIPTION OF CONFIGURATIONS

(a) Dimensions

	Basic	Small fuselage, reduced dihedral
Wing:		
Sweep, Λ, deg	74.5	74.3
Aspect ratio, A	1.72	1.75
Taper ratio	0.15	0.15
Root chord/Length	0.53	0.53
Area, sq ft	1.43	1.45
Mean aerodynamic chord, ft	1.08	1.08
Span	1.57	1.59
Airfoil section	Modified circular arc	Modified circular arc
t/c (mean)	0.05	0.05
Twist (overall), deg:		
Drooped leading edge	2.8	2.8
Undrooped leading edge	1.9	1.9
Incidence (mean)(leading edge drooped), deg	1.5	1.5
Dihedral (mean), deg	19	15
Horizontal tail (fuselage afterbody closed):		
Sweep, Λ, deg	68	68
Aspect ratio, A	1.72	1.72
Taper ratio	0.25	0.25
Exposed area/Area wing	0.086	0.086
Airfoil	Circular arc	Circular arc
t/c	0.02	0.02
Incidence, deg	1.0	1.0
Dihedral, deg	22	22
Elevator/Stabilizer area (exposed)	0.34	
Vertical tail:		
Sweep, Λ, deg	75	75
Aspect ratio, A	0.48	0.48
Taper ratio	0.20	0.20
Area/Wing area	0.085	0.084
Airfoil section	Circular arc	Circular arc
Rudder/Tail area	0.25	
Fuselage:		
Frontal area/Wing area	0.023	0.016
Fineness ratio	19	22
Airplane:		
$V^{2/3}/S$	0.178	0.162
Total wetted area/Wing area	3.4	3.3

TABLE I.- DESCRIPTION OF CONFIGURATIONS - Continued

(b) Fuselage coordinates

Distance from nose, in.	Fuselage coordinates, in., for -					
	Basic test configuration			Reduced fuselage configuration		
	Side view		Plan view referenced to center line	Side view		Plan view referenced to center line
	Upper surface	Lower surface		Upper surface	Lower surface	
0.25	0	-0.06	0.02	0.20	0.16	0.02
11	.88	-1.12	.99	1.00	-.82	.93
11.50	.92	-1.17	1.03	1.03	-.87	.97
12	.96	-1.21	1.08	1.04	-.92	1.01
12.50	.98	-1.27	1.12	1.03	-.97	1.05
13	.99	-1.32	1.16	1.00	-1.01	1.09
13.50	.98	-1.37	1.19	.95	-1.05	1.11
14	.95	-1.43	1.22	.90	-1.10	1.12
15	.87	-1.52	1.24	.82	-1.19	1.125
16	.78	-1.63	1.25	.74	-1.28	1.125
17	.69	-1.73	1.25	.65	-1.36	1.125
18	.61	-1.81	1.25	.57	-1.44	1.125
19	.53	-1.88	1.25	.50	-1.51	1.125
20	.47	-1.94	1.25	.45	-1.56	1.125
21	.42	-1.99	1.25	.39	-1.62	1.125
22	.38	-2.05	1.25	.35	-1.66	1.125
23	.34	-2.11	1.25	.32	-1.70	1.125
24	.31	-2.15	1.25	.30	-1.72	1.125
25	.29	-2.19	1.25	.28	-1.73	1.125
26	.28	-2.20	1.25	.28	-1.73	1.125
27	.27	-2.21	1.25	.28	-1.73	1.125
28	.26	-2.22	1.25	.27	-1.72	1.125
29	.26	-2.22	1.24	.27	-1.70	1.125
30	.25	-2.21	1.23	.27	-1.68	1.12
31	.25	-2.18	1.22	.28	-1.65	1.10
32	.25	-2.14	1.21	.29	-1.62	1.08
33	.25	-2.10	1.19	.30	-1.59	1.06
34	.25	-2.07	1.16	.31	-1.56	1.05
35	.25	-2.02	1.13	.33	-1.52	1.03
45.75	.25	-1.45	.85	.50	-1.20	.85

TABLE I.- DESCRIPTION OF CONFIGURATIONS - Continued

(b) Fuselage coordinates - Concluded

Distance from nose, in.	Fuselage coordinates, in., for -				
	Side view				Plan view referenced to center line
	Closed afterbody		Closed afterbody with fuselage lowered		
	Upper surface	Lower surface	Upper surface	Lower surface	
0.25	0.20	0.16	0.20	0.16	0.02
11	1.00	-.82	1.00	-.82	.93
11.50	1.03	-.87	1.03	-.87	.97
12	1.04	-.92	1.04	-.92	1.01
12.50	1.03	-.97	1.03	-.97	1.05
13	1.00	-1.01	1.00	-1.01	1.09
13.50	.95	-1.05	.95	-1.05	1.11
14	.90	-1.10	.90	-1.10	1.12
15	.82	-1.19	.82	-1.19	1.125
16	.74	-1.28	.74	-1.28	1.125
17	.65	-1.36	.65	-1.36	1.125
18	.57	-1.44	.57	-1.44	1.125
19	.50	-1.51	.50	-1.51	1.125
20	.45	-1.56	.43	-1.56	1.125
21	.39	-1.62	.37	-1.62	1.125
22	.35	-1.66	.33	-1.66	1.125
23	.32	-1.70	.28	-1.71	1.125
24	.30	-1.72	.24	-1.73	1.125
25	.28	-1.73	.22	-1.76	1.125
26	.28	-1.73	.21	-1.78	1.125
27	.28	-1.73	.20	-1.79	1.125
28	.27	-1.72	.19	-1.80	1.11
29	.27	-1.70	.18	-1.80	1.09
30	.27	-1.68	.17	-1.77	1.07
31	.27	-1.64	.16	-1.73	1.03
32	.27	-1.58	.15	-1.68	.98
33	.26	-1.51	.13	-1.61	.93
34	.26	-1.43	.12	-1.53	.87
35	.25	-1.33	.11	-1.44	.81
47.12	.25	.01	.11	-.12	.11
47.25	.13	.13	0	0	0

TABLE I.- DESCRIPTION OF CONFIGURATIONS - Continued

(c) Airfoil coordinates

Distance from leading edge, in.	Airfoil coordinates, in., for -	
	Drooped leading edge	
	Upper surface	Lower surface
Span station = 1.80 in.		
0	0	0
.2	.075	-.065
.5	.110	-.105
1.0	.130	-.165
2.0	.160	-.270
3.0	.165	-.380
4.0	.165	-.485
5.0	.155	-.580
6.0	.130	-.665
7.0	.095	-.750
8.0	.060	-.815
9.0	-.005	-.860
10.0	-.075	-.895
11.0	-.155	-.895
12.0	-.245	-.895
13.0	-.325	-.880
14.0	-.410	-.845
15.0	-.495	-.815
16.0	-.595	-.740
16.70	-.670	-.670
Span station = 3.04 in.		
0	0	0
.2	.075	-.065
.5	.105	-.100
1.0	.140	-.160
2.0	.170	-.265
3.0	.185	-.370
4.0	.185	-.460
5.0	.160	-.535
6.0	.135	-.605
7.0	.080	-.640
8.0	.025	-.660
9.0	-.065	-.660
10.0	-.165	-.640
11.0	-.290	-.615
12.0	-.420	-.570
12.65	-.510	-.510

TABLE I.- DESCRIPTION OF CONFIGURATIONS - Continued

(c) Airfoil coordinates - Continued

Distance from leading edge, in.	Airfoil coordinates, in., for -			
	Drooped leading edge		Undrooped leading edge	
	Upper surface	Lower surface	Upper surface	Lower surface
Span station = 4.23 in.				
0	0	0		
.2	.085	-.070		
.5	.120	-.115		
1.0	.155	-.980		
2.0	.200	-.975		
3.0	.225	-.950		
4.0	.240	-.945		
5.0	.255	-.955		
6.0	.270	-.960		
7.0	.290	-.980		
8.0	.305	-.995		
9.0	.320	-1.000		
10.0	.335	-1.010		
10.81	.340	1.040		
Span station = 5.42 in.				
0	0	0	0.042	0.042
.2	.060	-.070	.115	-.010
.5	.090	-.095	.150	-.050
1.0	.120	-.140	.185	-.090
2.0	.160	-.205	.220	-.170
3.0	.175	-.260	.220	-.240
4.0	.180	-.295	.195	-.285
5.0	.150	-.305	.150	-.305
6.0	.085	-.300	.085	-.300
7.0	.010	-.275	.010	-.275
8.0	-.070	-.230	-.070	-.230
9.0	-.145	-.170	-.145	-.170
9.025	-.150	-.150	-.150	-.150

TABLE I.- DESCRIPTION OF CONFIGURATIONS - Concluded

(c) Airfoil coordinates - Concluded

Distance from leading edge, in.	Airfoil coordinates, in., for -			
	Drooped leading edge		Undrooped leading edge	
	Upper surface	Lower surface	Upper surface	Lower surface
Span station = 6.60 in.				
0	0	0	0.052	0.052
.2	.095	-.055	.135	-.015
.5	.135	-.085	.170	-.045
1.0	.180	-.740	.210	-.740
2.0	.240	-.880	.260	-.860
3.0	.295	-.850	.310	-.850
4.0	.340	-.830	.355	-.830
5.0	.390	-.820	.405	-.820
6.0	.450	-.810	.450	-.810
7.0	.495	-.800	.495	-.800
7.45	.520	-.800	.520	-.800
Span station = 7.80 in.				
0	0	0	0.061	0.061
.2	.055	-.055	.105	-.005
.5	.095	-.075	.135	-.045
1.0	.135	-.085	.160	-.075
2.0	.190	-.095	.190	-.095
3.0	.190	-.090	.190	-.090
4.0	.160	-.060	.160	-.060
5.0	.100	-.020	.100	-.020
5.9	.030	.030	.030	.030
Span station = 8.98 in.				
0	0	0	0.070	0.070
.2	.075	-.045	.125	.000
.5	.115	-.060	.140	-.005
1.0	.155	-.050	.160	-.030
2.0	.160	-.025	.160	-.025
3.0	.125	.000	.125	.000
4.0	.075	.020	.075	.020
4.42	.050	.050	.050	.050
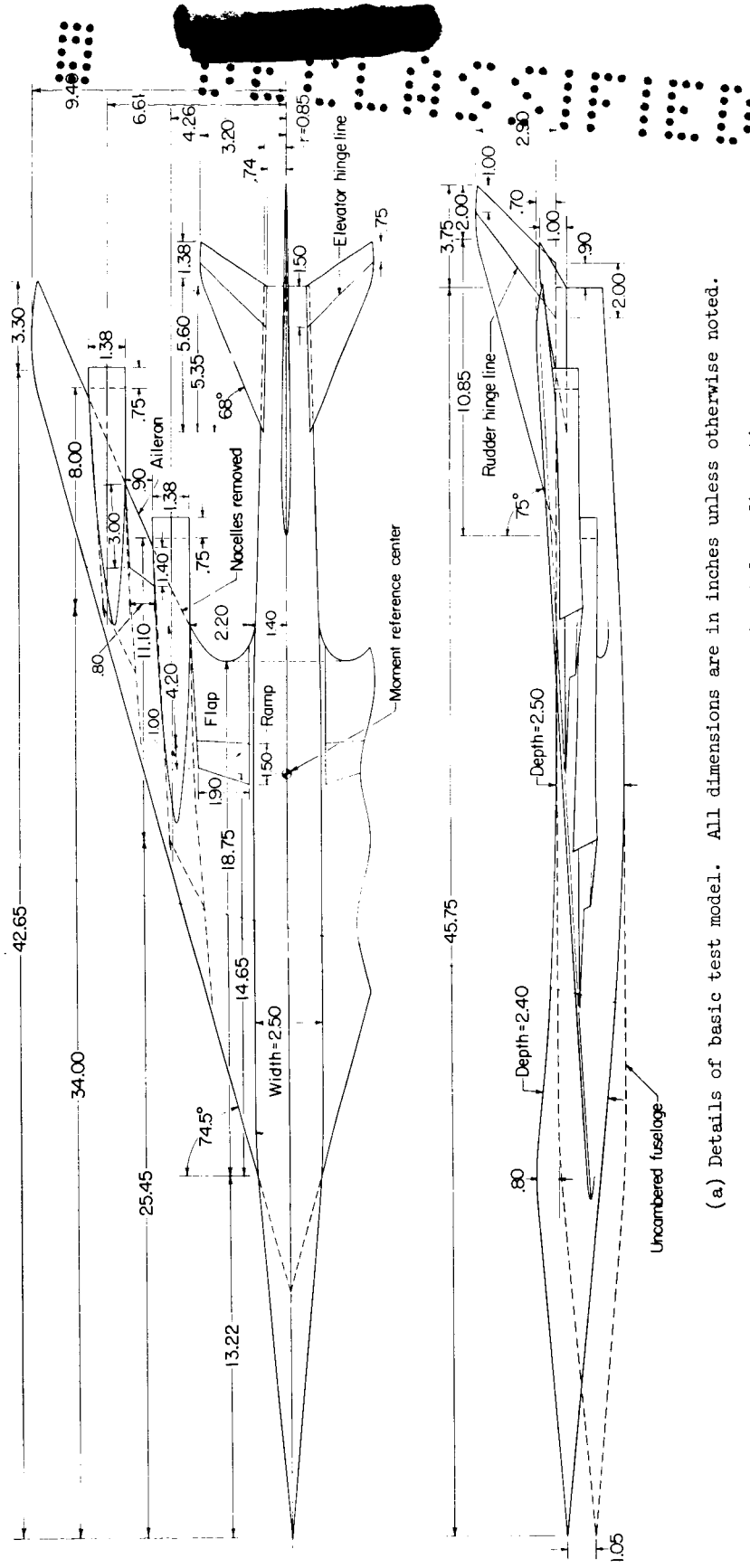
(a) Details of basic test model. All dimensions are in inches unless otherwise noted.

Figure 1.- Description of high-speed experimental configurations.
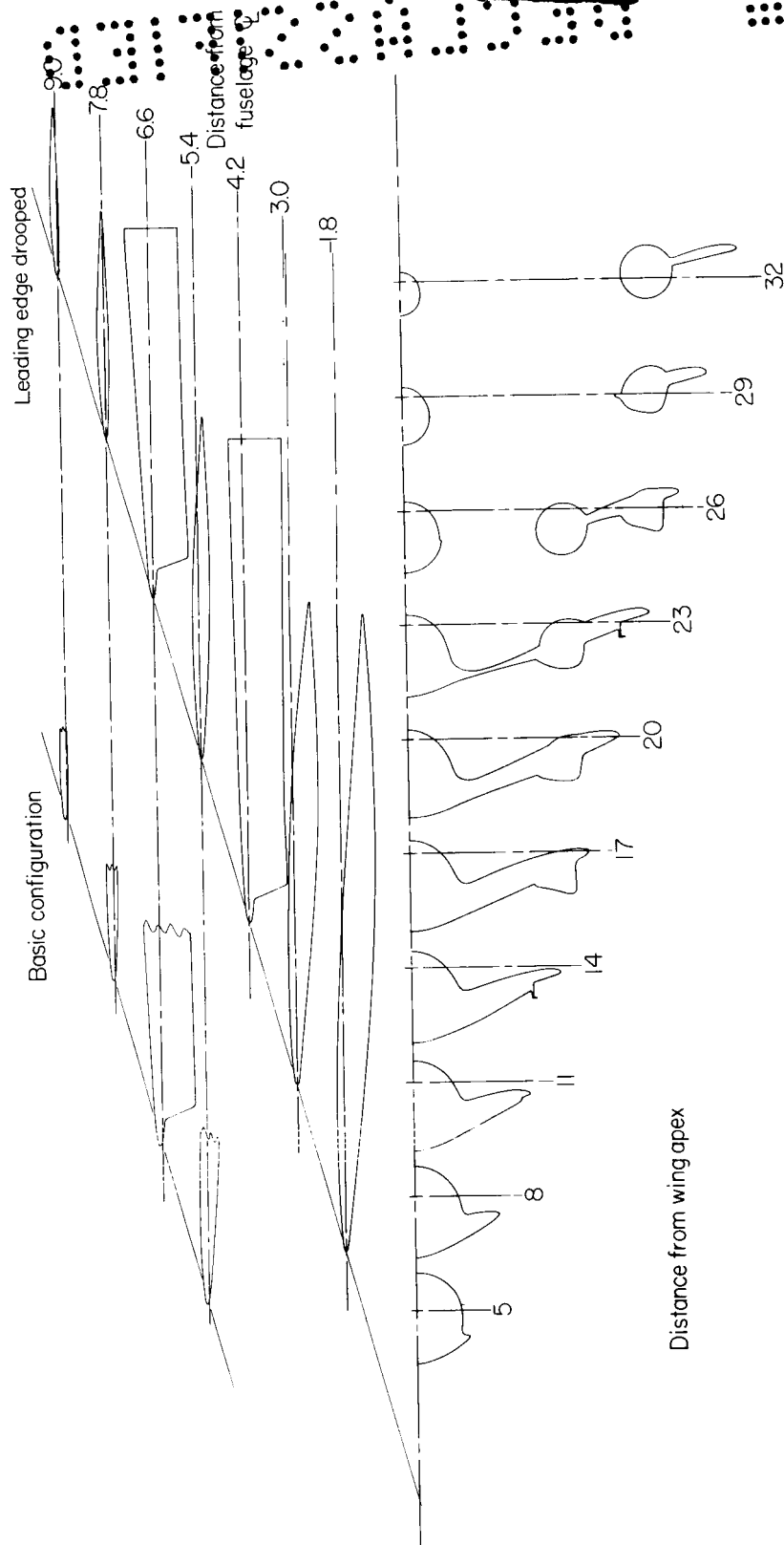
(b) Sections of basic airplane.

Figure 1.- Continued.

9.55

r=0.85

74.3°

13.17

19.13

14.70

Width=2.25

Moment reference center

45.75

Depth=2.00

Depth=2.00
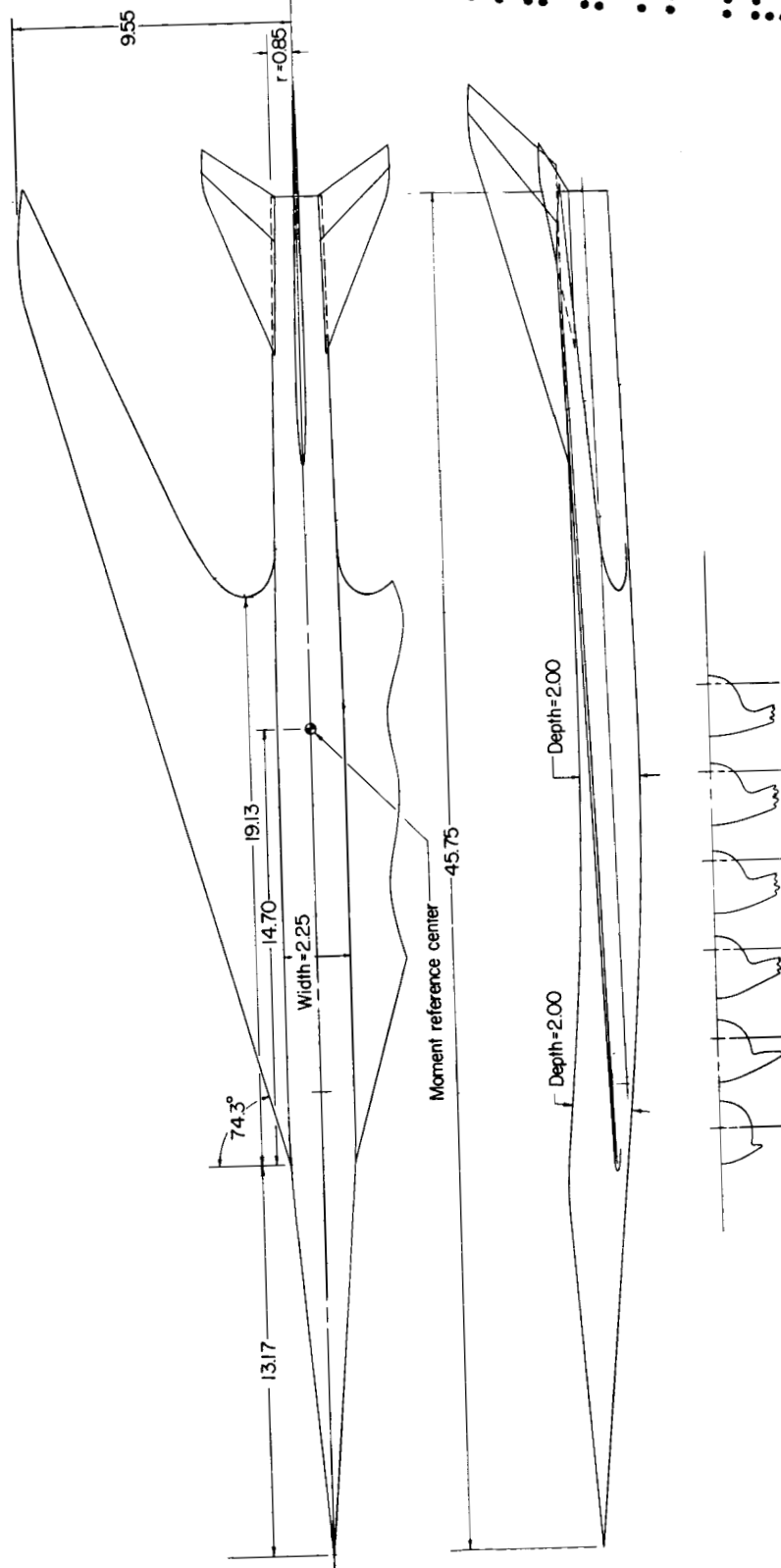
(c) Model with reduced fuselage size, decreased dihedral, and forward movement of fuselage corner. All dimensions are in inches unless otherwise noted.

Figure 1.- Continued.

27
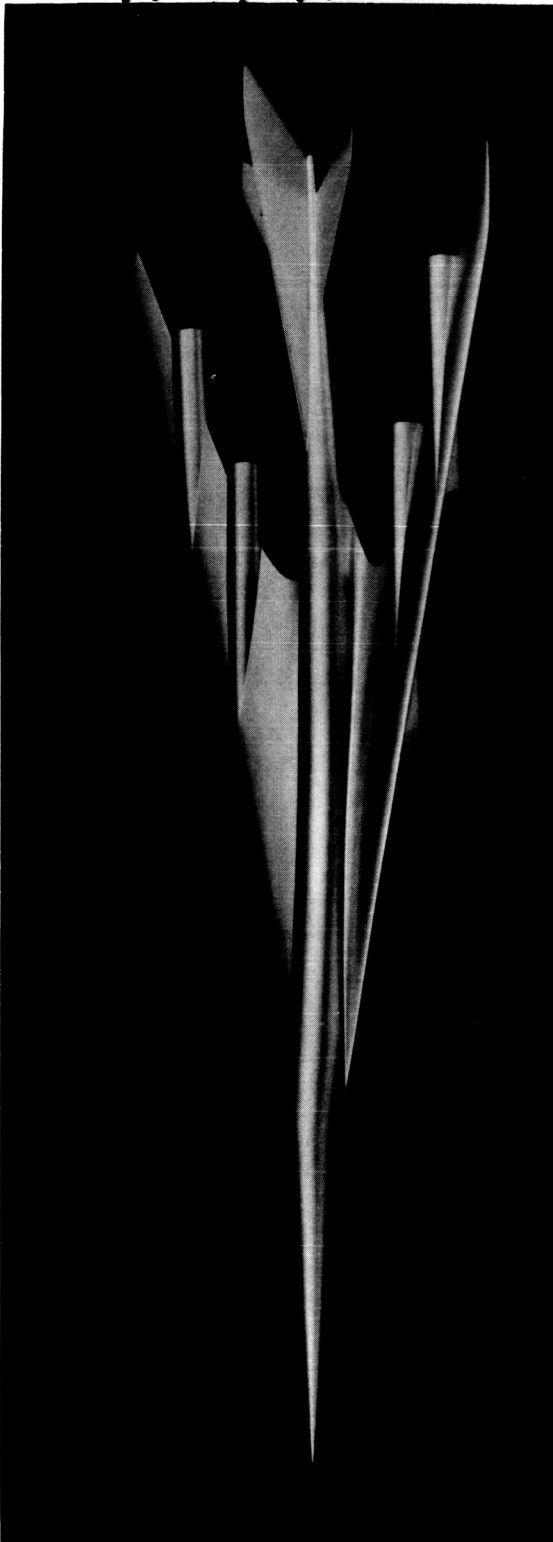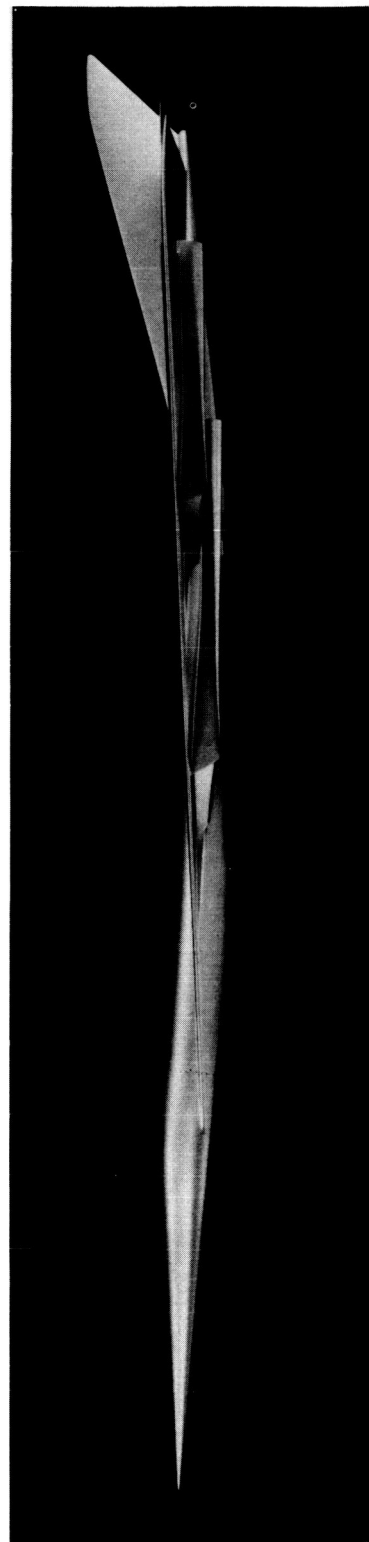
L-62-6137

L-62-6136

(d) Proposed airplane configuration with modified fuselage and dihedral.

Figure 1.- Continued.

——— Outboard L.E. undrooped
— — — Outboard L.E. drooped
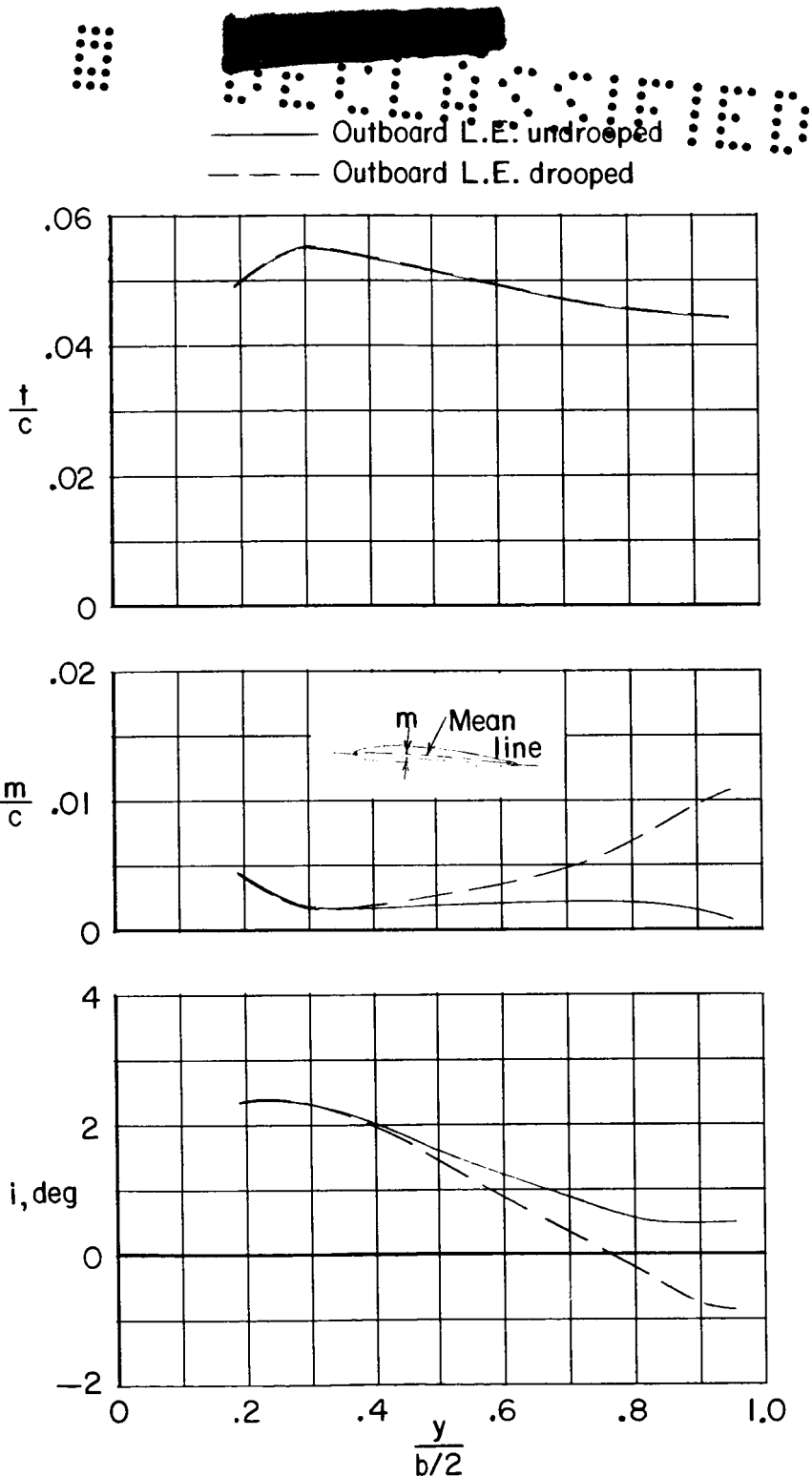
(e) Spanwise variations of local thickness ratio, maximum camber, and incidence for wing with and without leading-edge droop.

Figure 1.- Concluded.

Figure 2.- Longitudinal developments of normal cross-sectional area for several configurations.

Nacelle base areas extended rearward
Basic tunnel model
Model with small fuselage
Airplane with small fuselage
Nacelle base areas not extended rearward
Basic airplane
Airplane with small fuselage

Area, sq in.

Station, in.
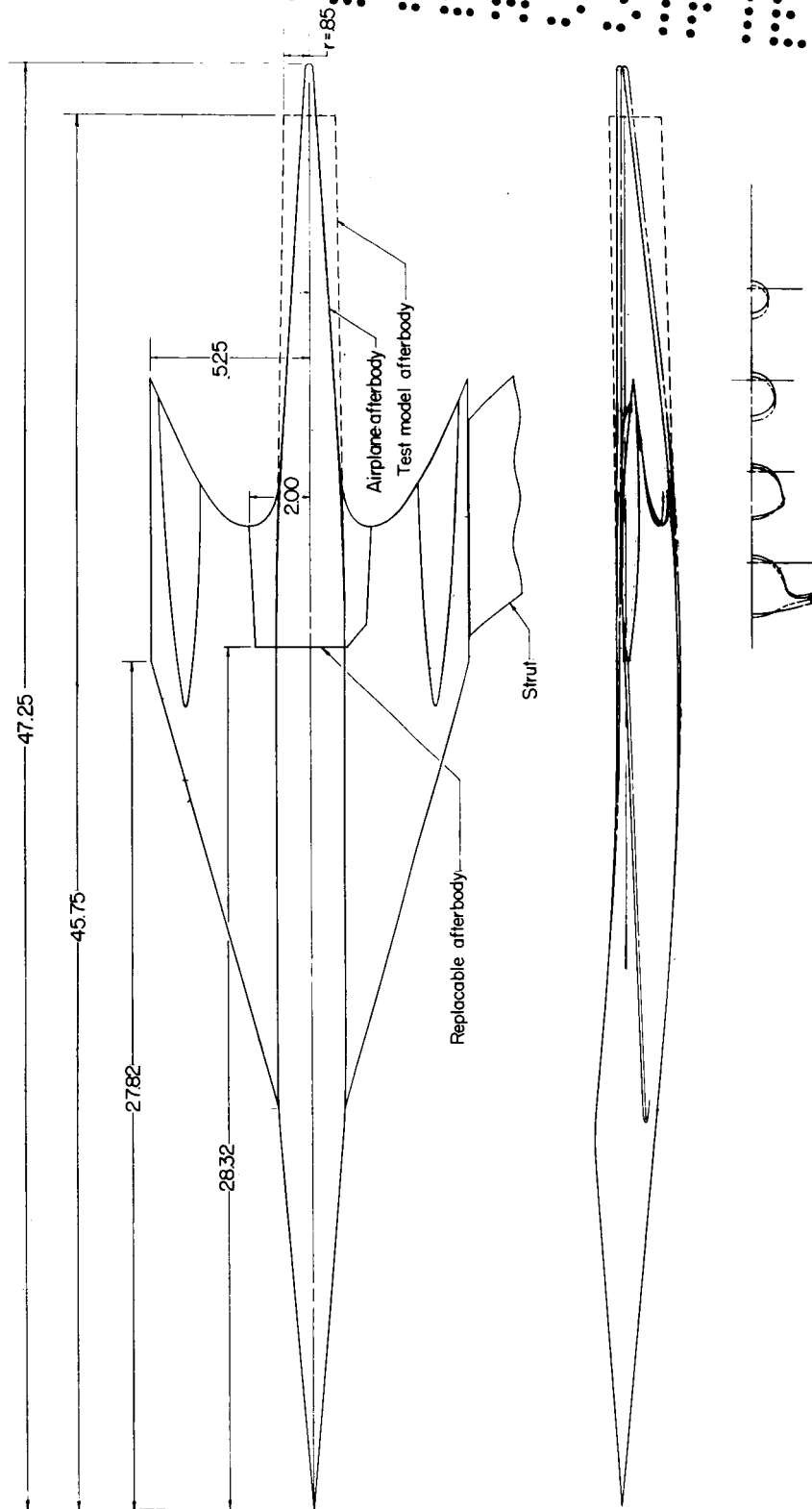
(a) Fuselage-truncated-wing configurations.

Figure 3.- Models used to evaluate effect of afterbody closure. All dimensions are in inches unless otherwise noted.

r=.75

r=.30

31.75

12.00

6.5°

Diameter=2.00
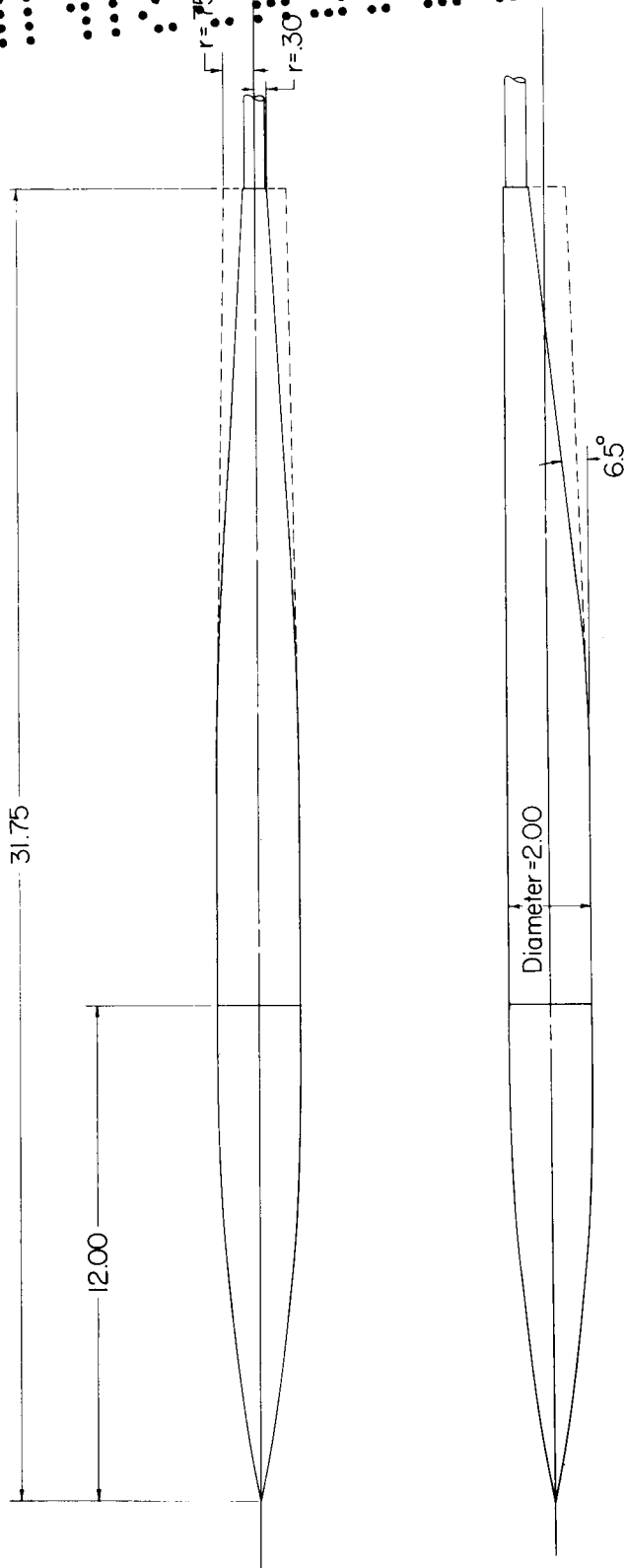
(b) Fuselage alone.

Figure 3.- Concluded.
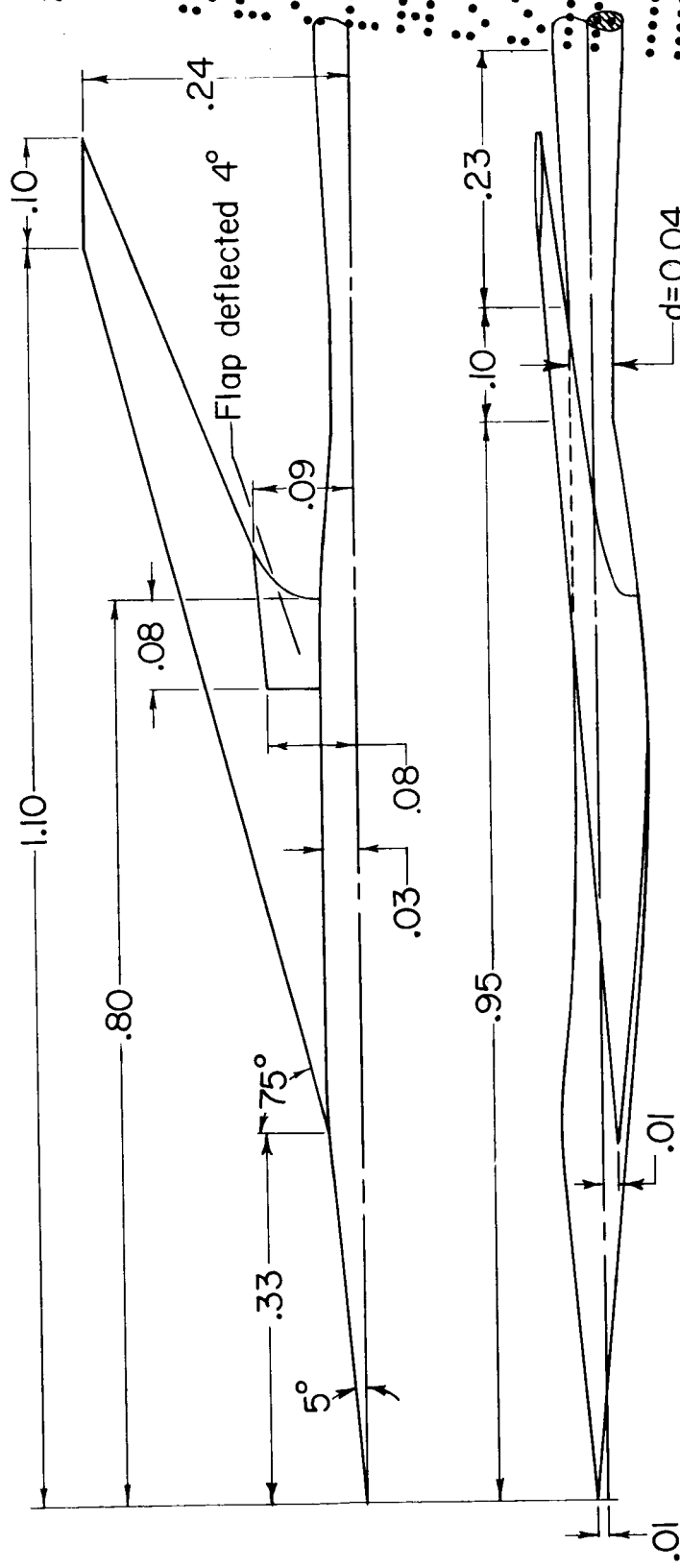
Figure 4.- Model used in sonic-boom investigation. All dimensions are in inches unless otherwise noted.

Flap deflected 4°

.24

.10

.09

.08

.08

.03

1.10

.80

75°

.33

5°

.23

.10

d=0.04

.95

.01

.01
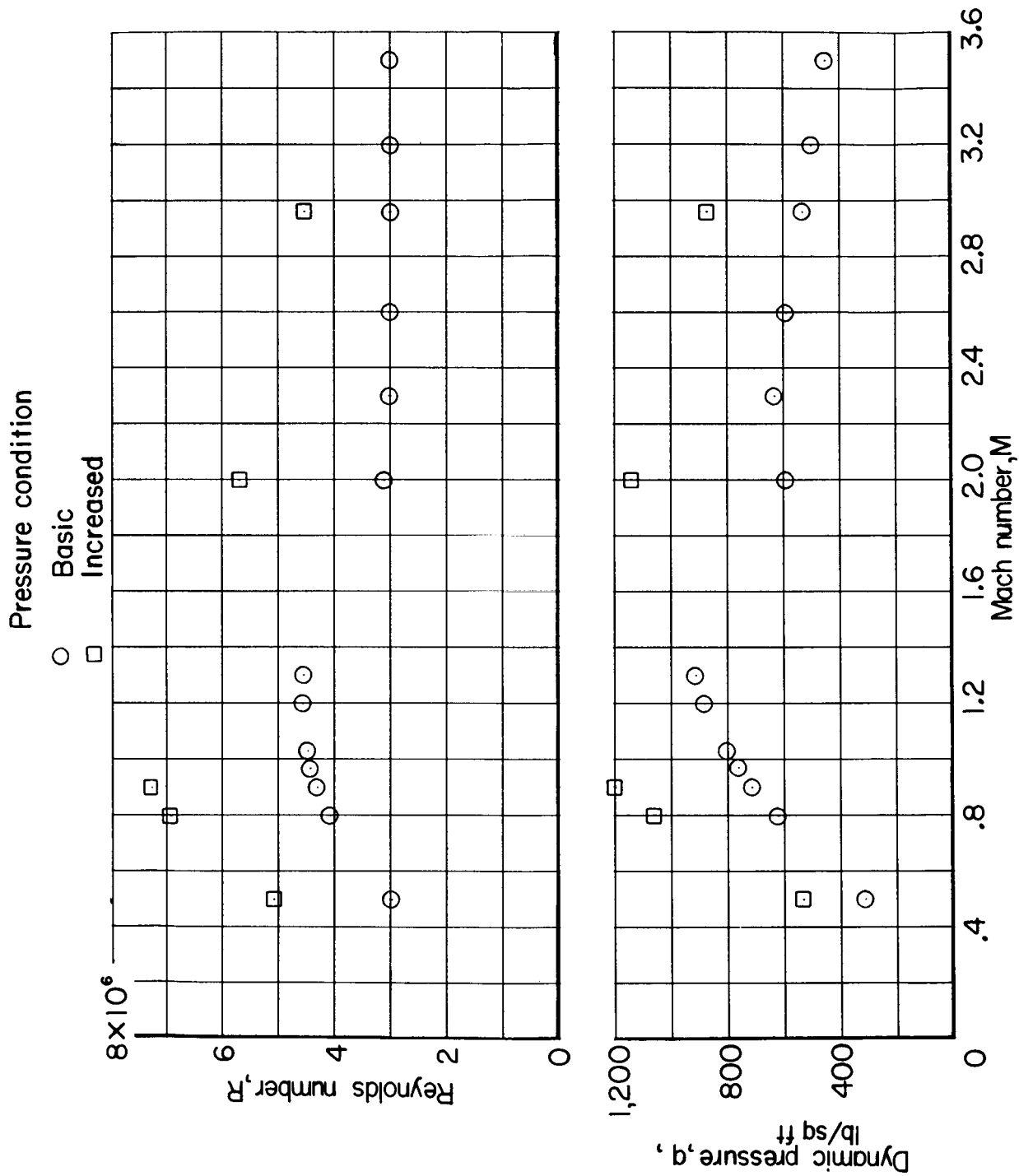
Figure 5.- Variation of test Reynolds numbers and dynamic pressures with Mach number.
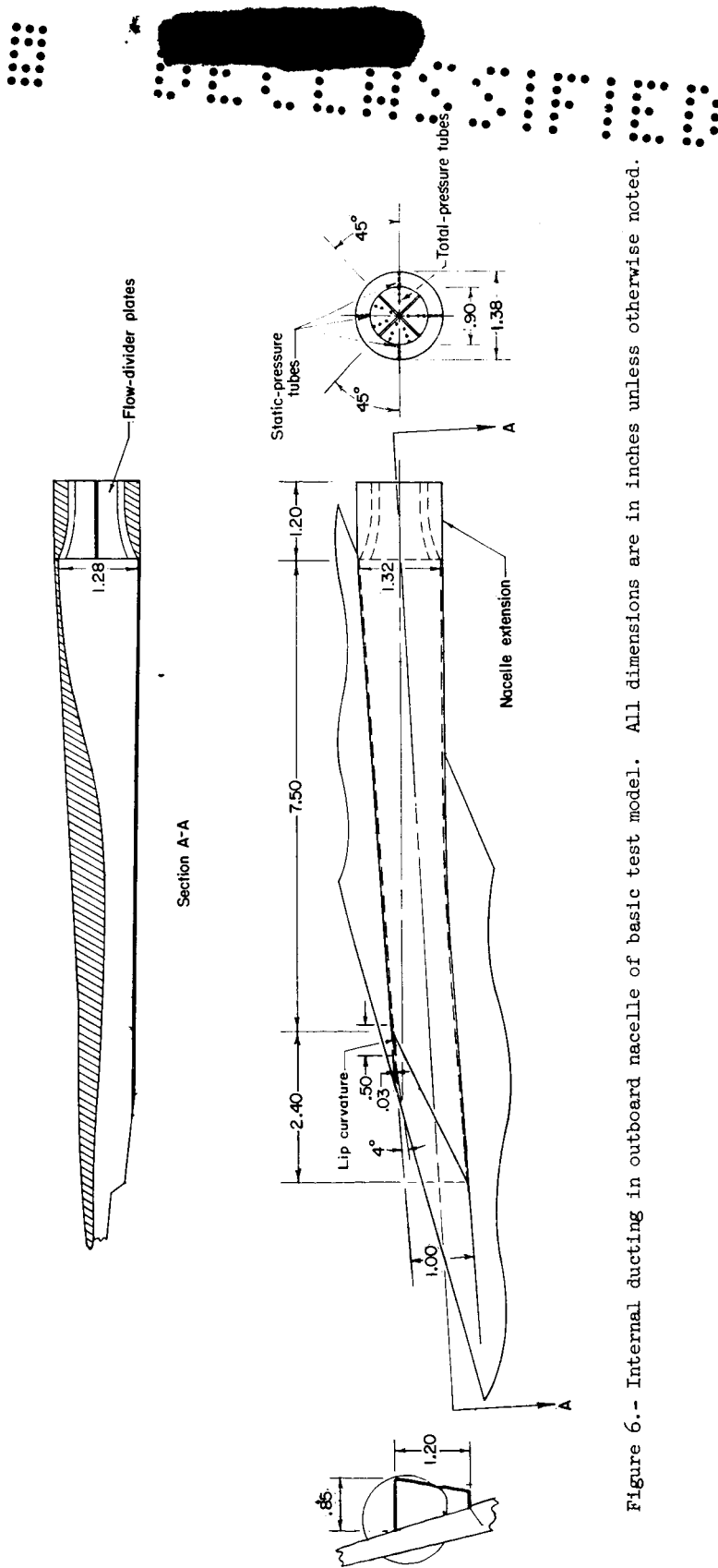
Figure 6.- Internal ducting in outboard nacelle of basic test model. All dimensions are in inches unless otherwise noted.
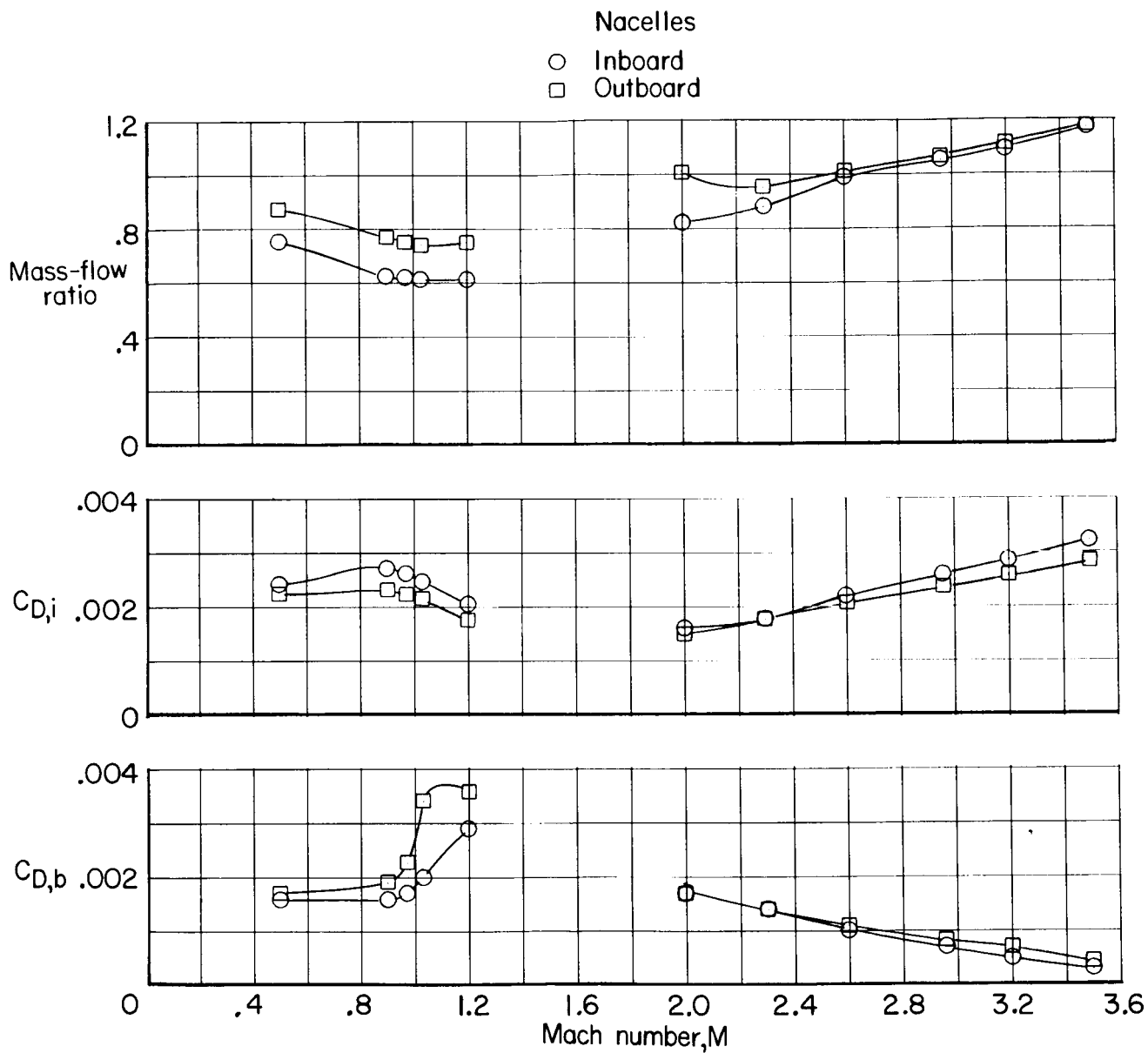
Figure 7.- Variation with Mach number of nacelle mass-flow ratio and internal drag and base drag coefficients.
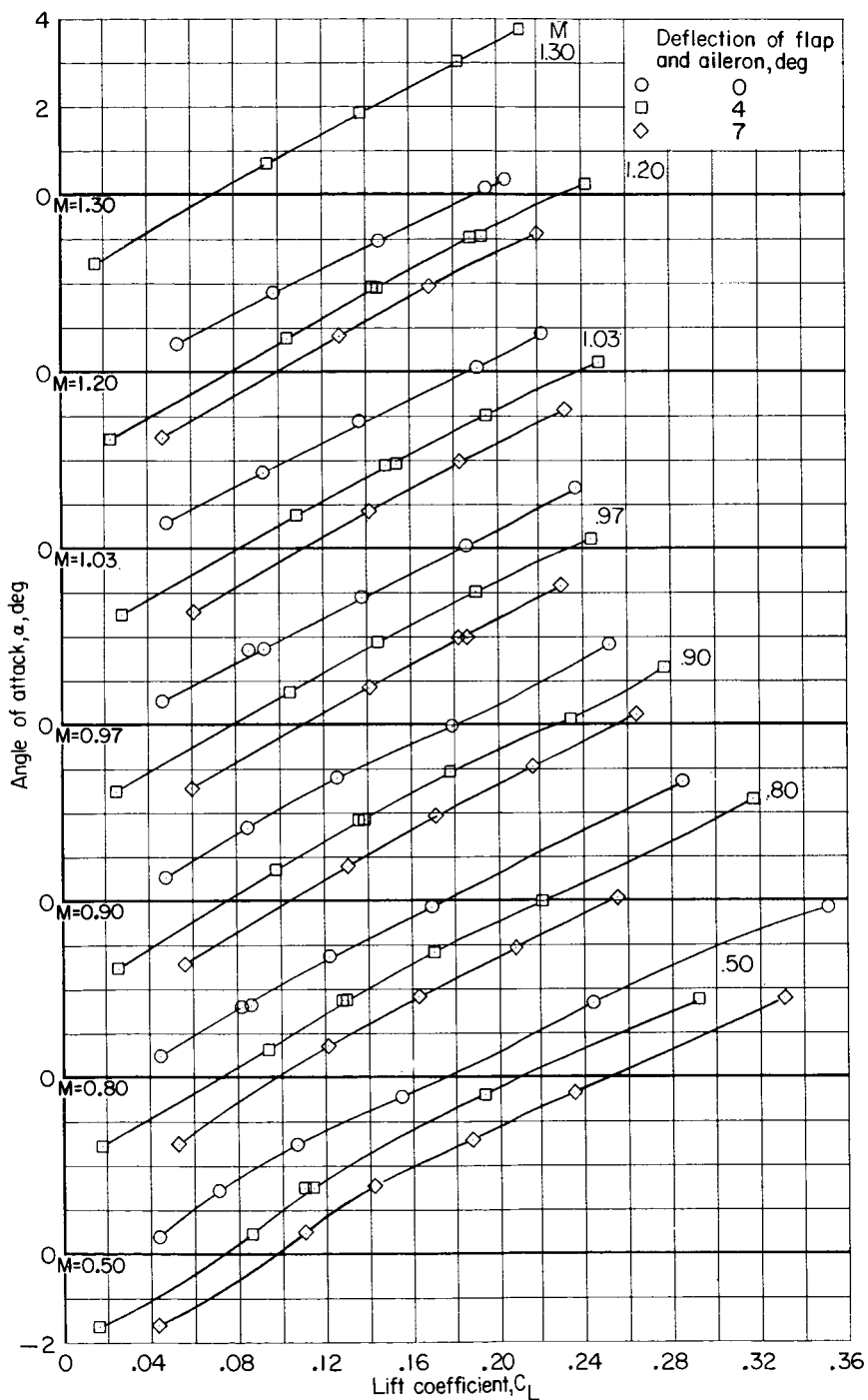
(a) α against C_L.

Figure 8.- Effect of trailing-edge flap deflection on the high subsonic and transonic longitudinal aerodynamic characteristics. Wing outboard leading edge undrooped; $\delta_e = 0°$; $p_t = 1$ atm.
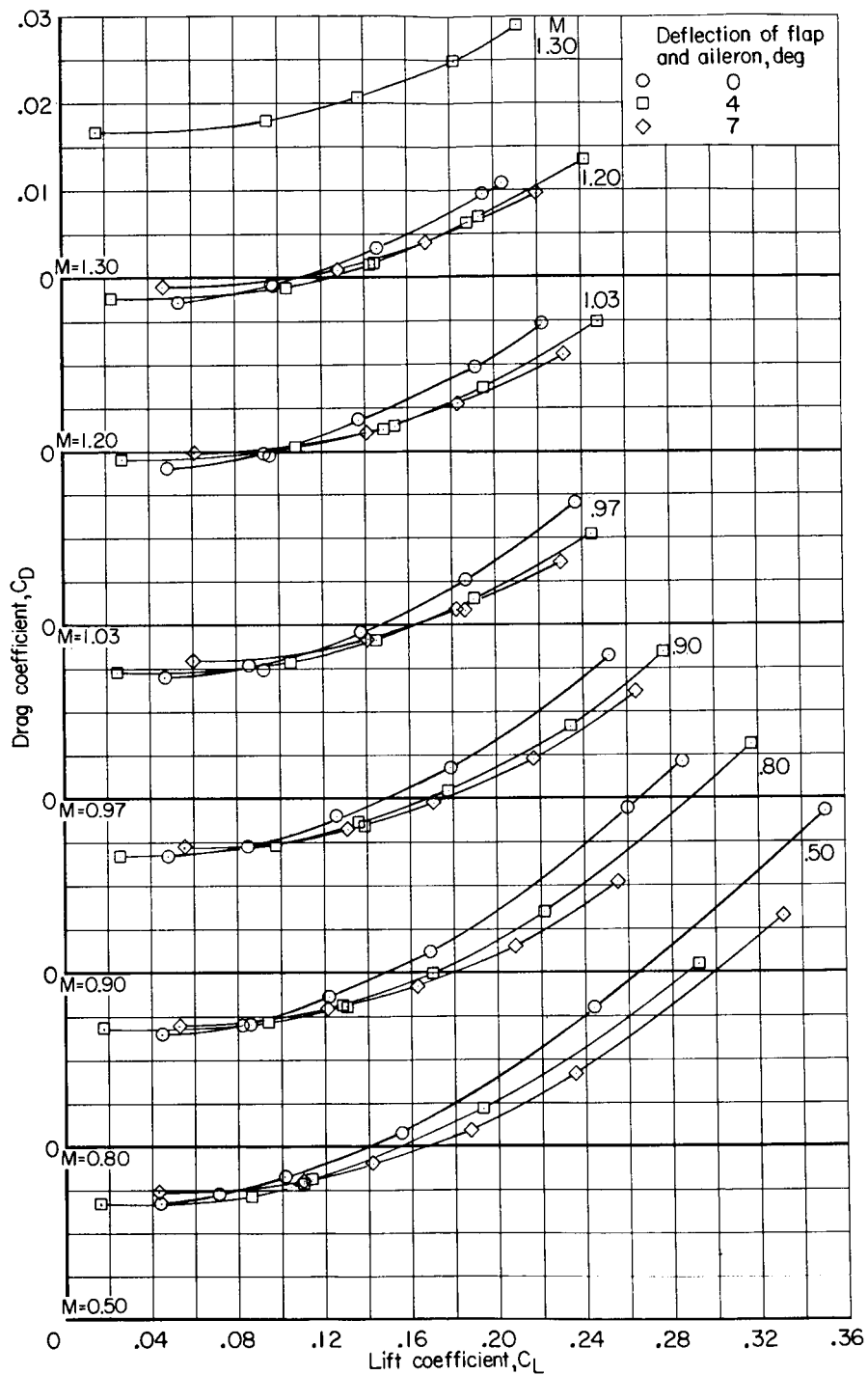
(b) C_D against C_L.

Figure 8.- Continued.
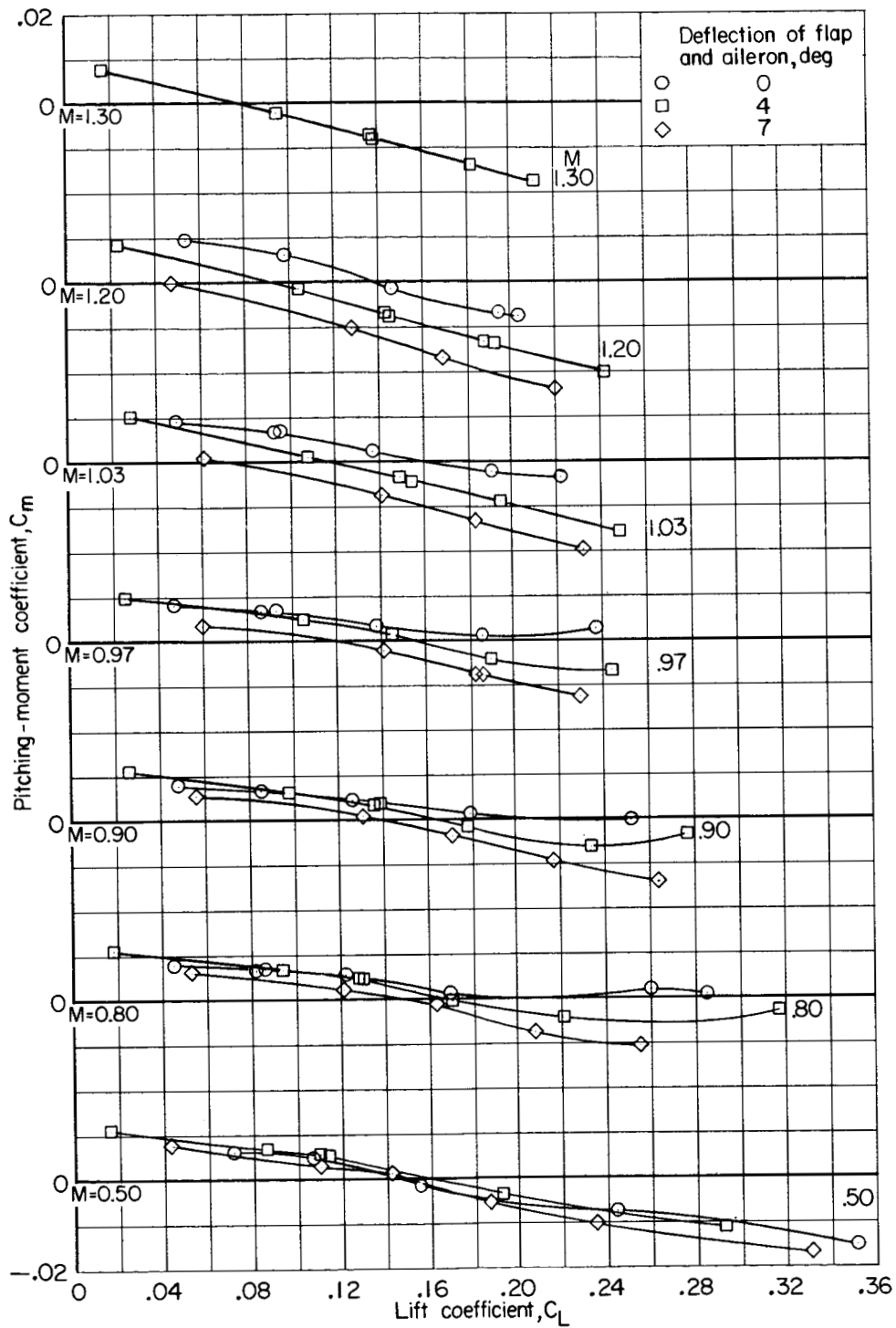
(c) C_m against C_L.

Figure 8.- Concluded.

Configuration

		Deflection of flap and aileron, deg
○	Outboard L.E. undrooped	4
□	Outboard L.E. drooped	4
◇	Outboard L.E. drooped	7
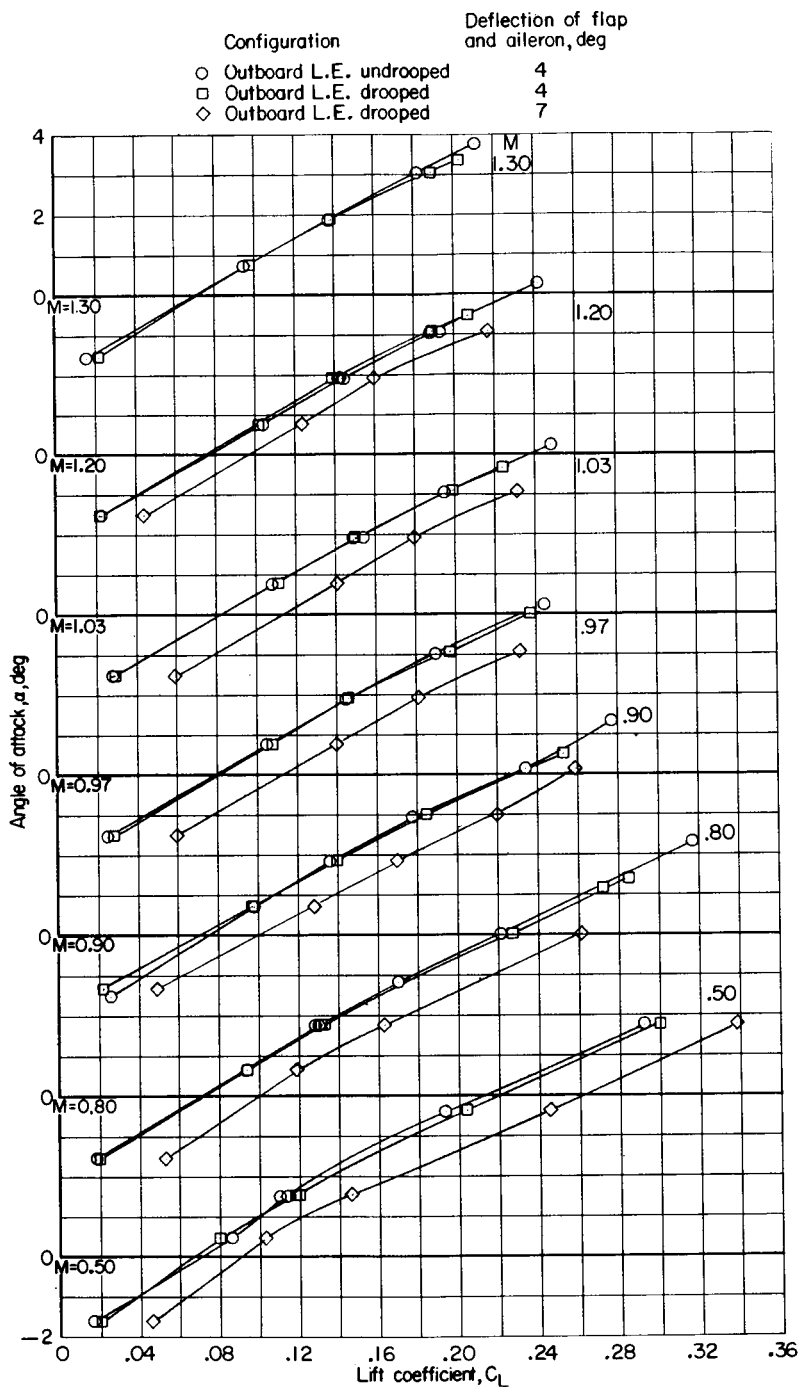
(a) α against C_L.

Figure 9.- Effect of wing outboard leading-edge droop on the high subsonic and transonic longitudinal aerodynamic characteristics. Wing outboard leading edge drooped; $\delta_e = 0^\circ$; $p_t = 1$ atm.
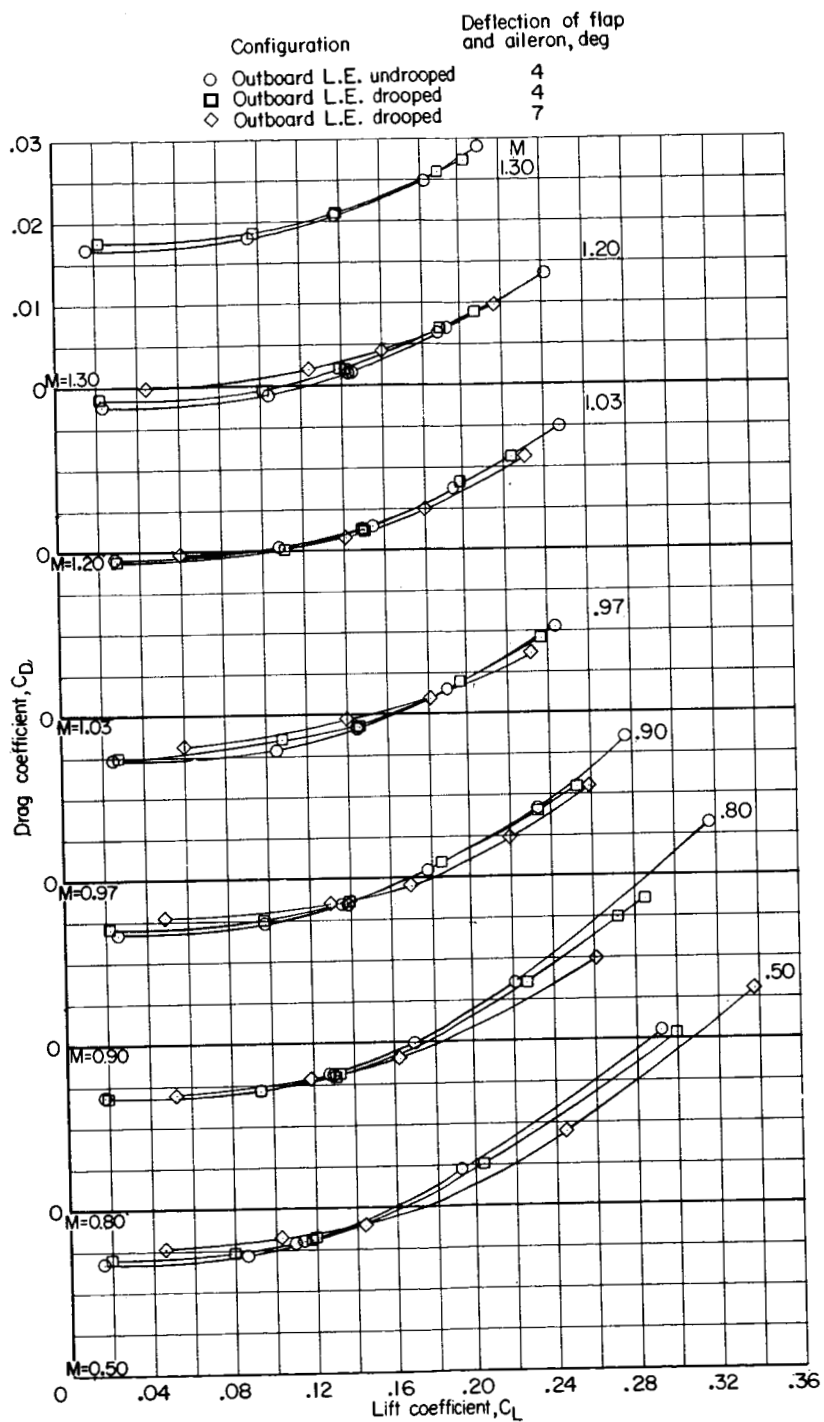
(b) C_D against C_L.

Figure 9.- Continued.

Configuration

Deflection of flap
and aileron, deg

○ Outboard L.E. undrooped   4
□ Outboard L.E. drooped   4
◇ Outboard L.E. drooped   7

(c) C_m against C_L.

Figure 9.- Concluded.
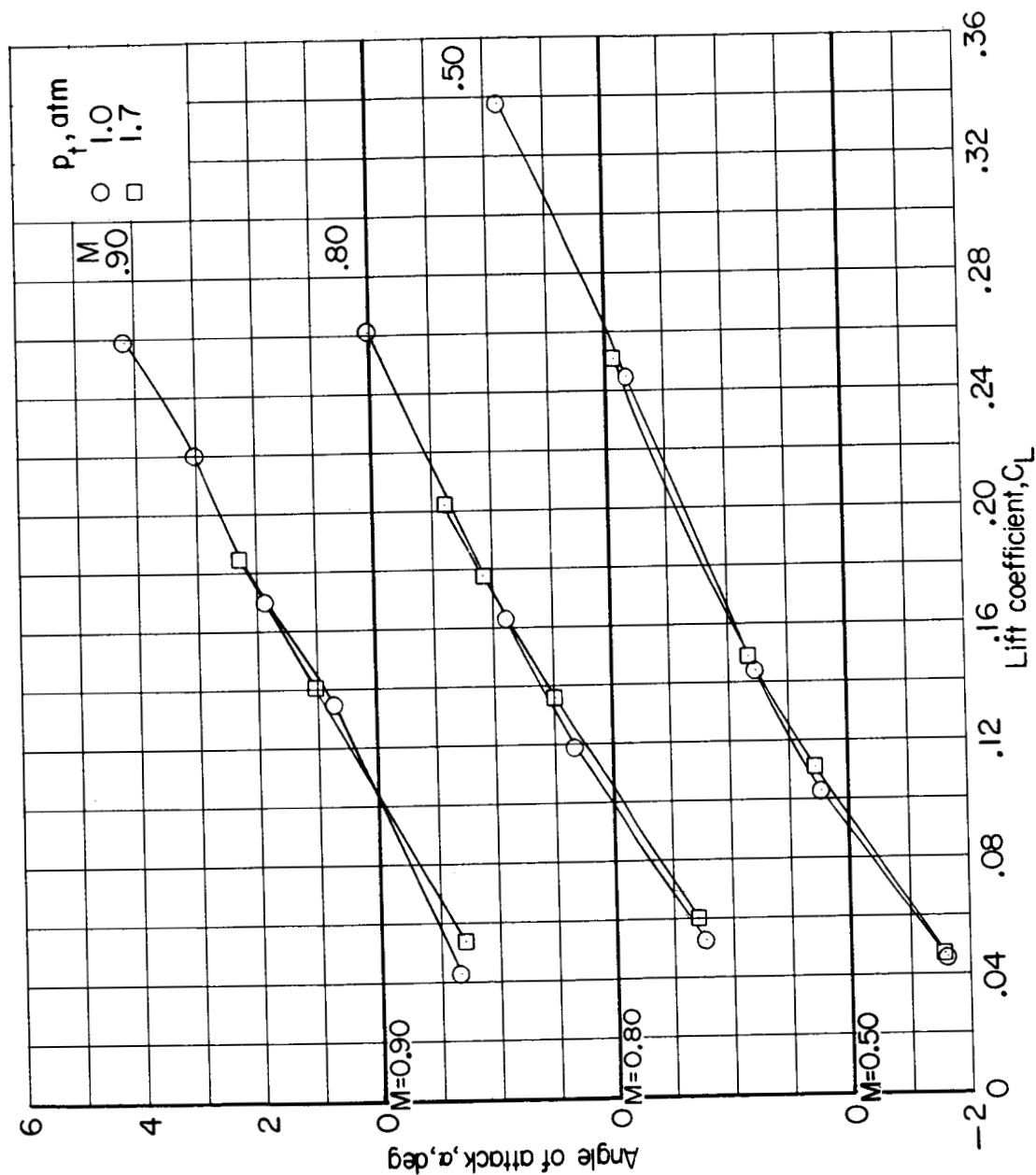
(a) α against C_L.

Figure 10.- Effect of Reynolds number on the high subsonic and transonic longitudinal aerodynamic characteristics. Wing outboard leading edge drooped; $\delta_f = 4°$; $\delta_a = 4°$; $\delta_e = 0°$.
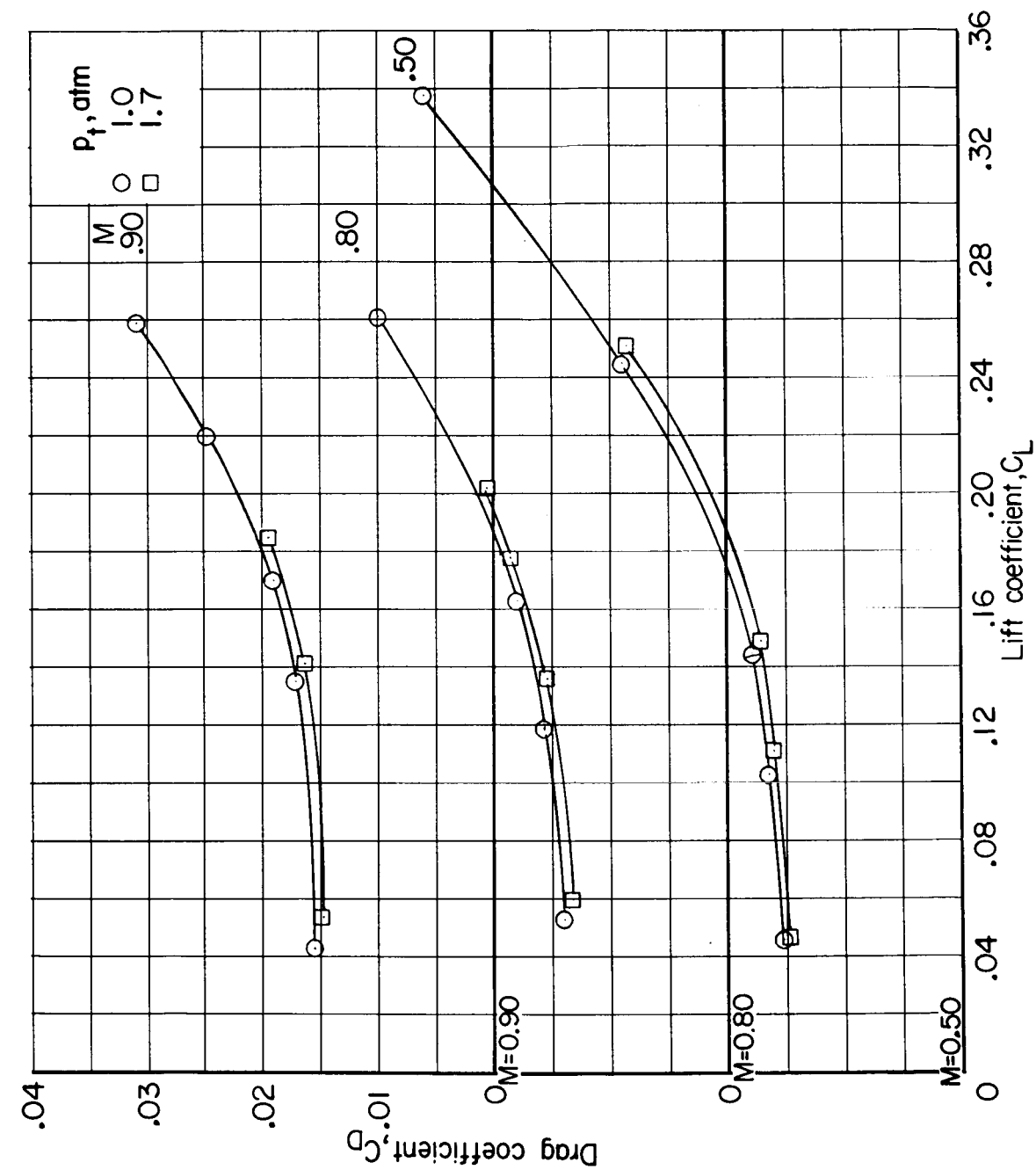
(b) C_D against C_L.

Figure 10.- Continued.
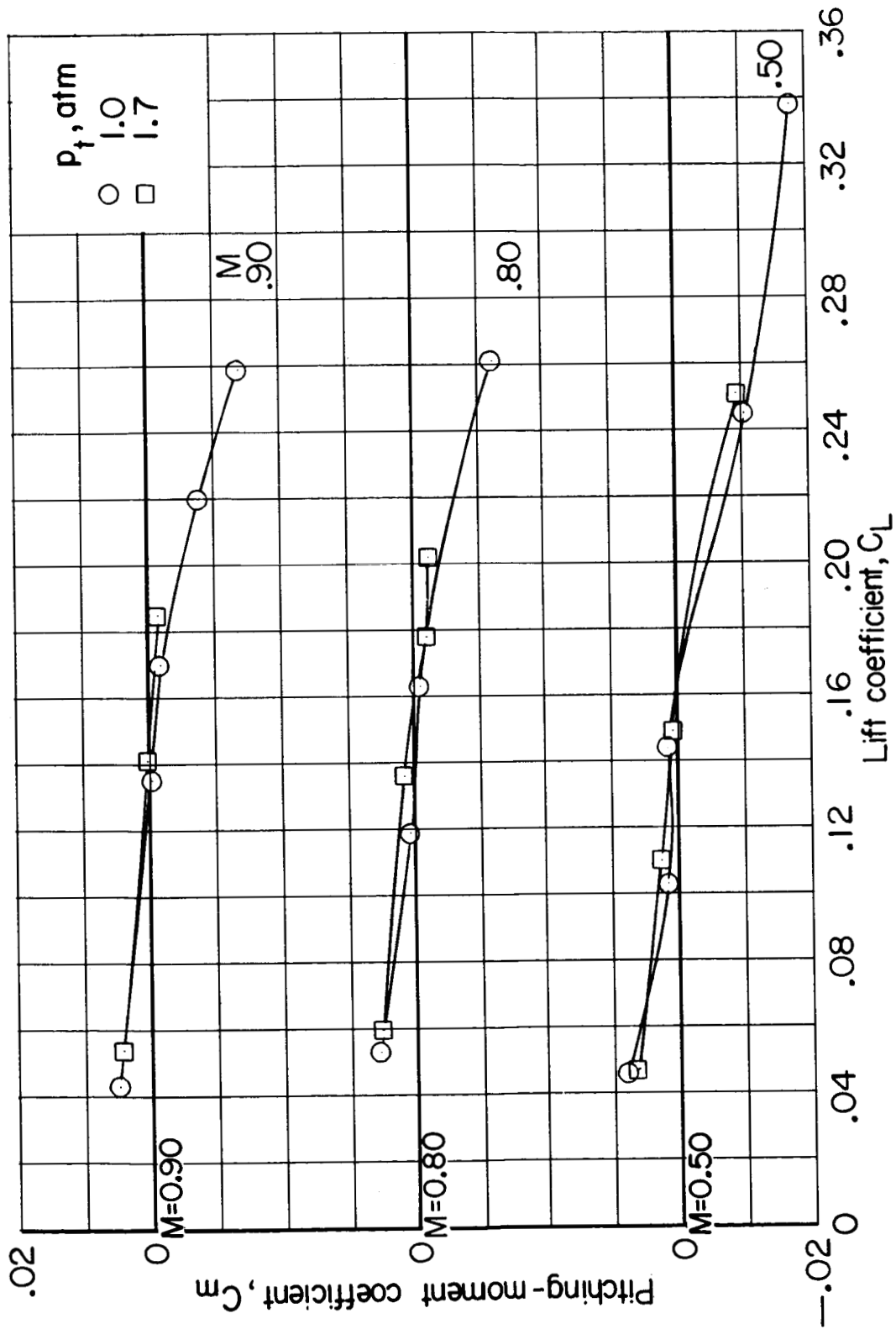
(c) C_m against C_L.

Figure 10.- Concluded.
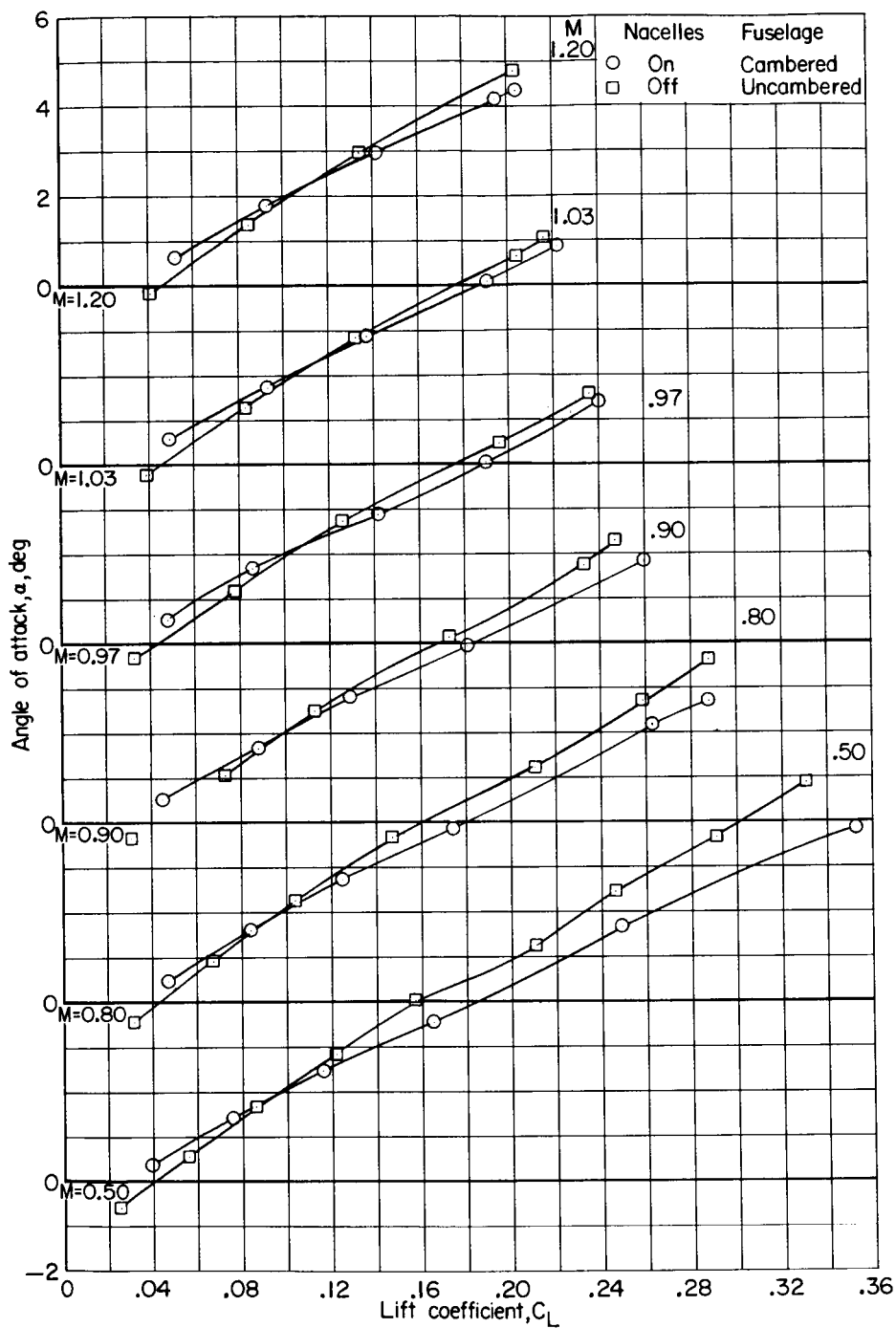
(a) α against C_L.

Figure 11.- Effect of nacelles and fuselage camber on the high subsonic and transonic aerodynamic characteristics. Wing outboard leading edge drooped; $\delta_f = 0^\circ$; $\delta_a = 0^\circ$; $\delta_e = 0^\circ$; $p_t = 1$ atm.
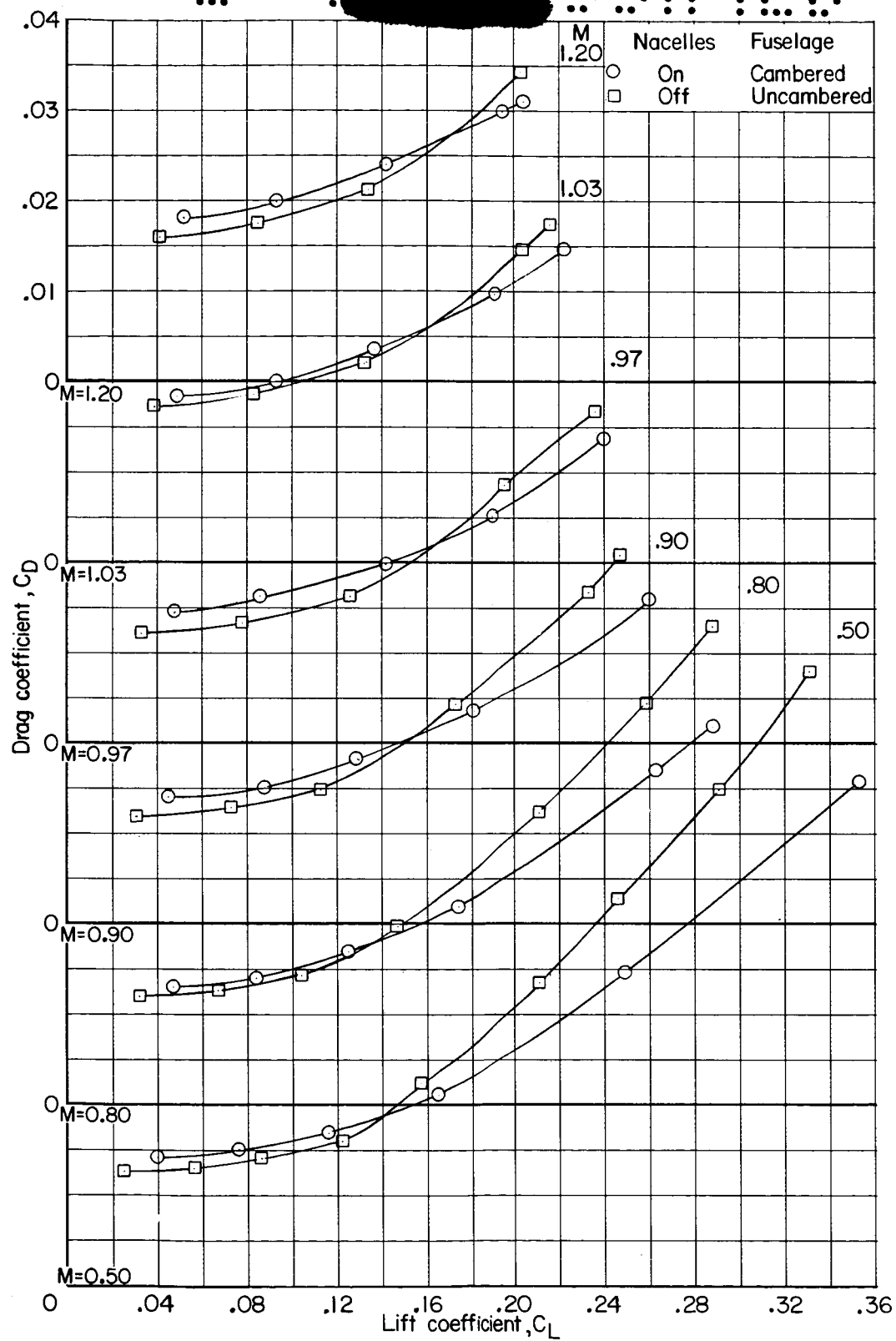
(b) C_D against C_L.

Figure 11.- Continued.
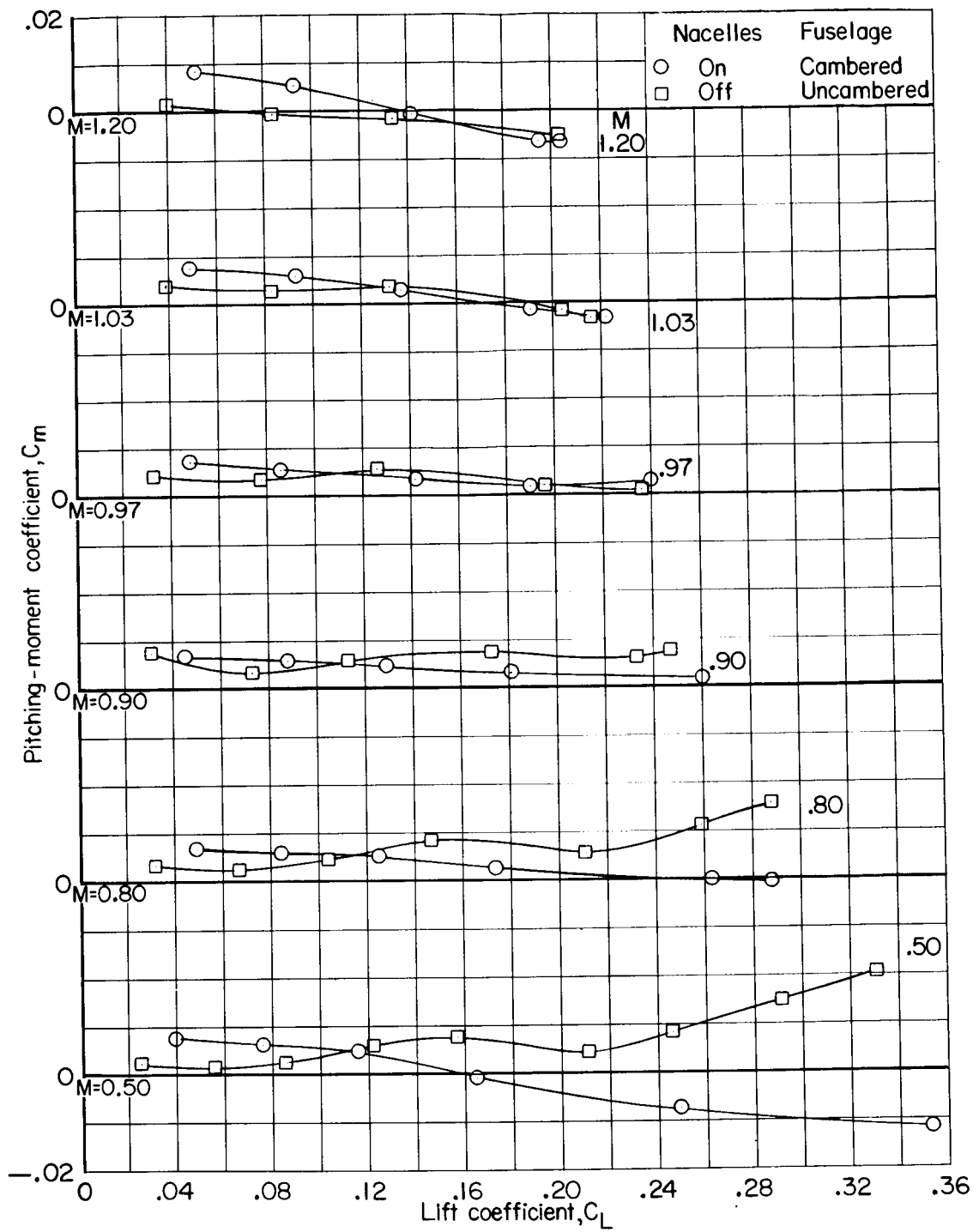
(c) C_m against C_L.

Figure 11.- Concluded.

Experiments with nacelles and fuselage camber deleted
- ○ Basic
- □ Reduced fuselage size and dihedral

(a) α against C_L.
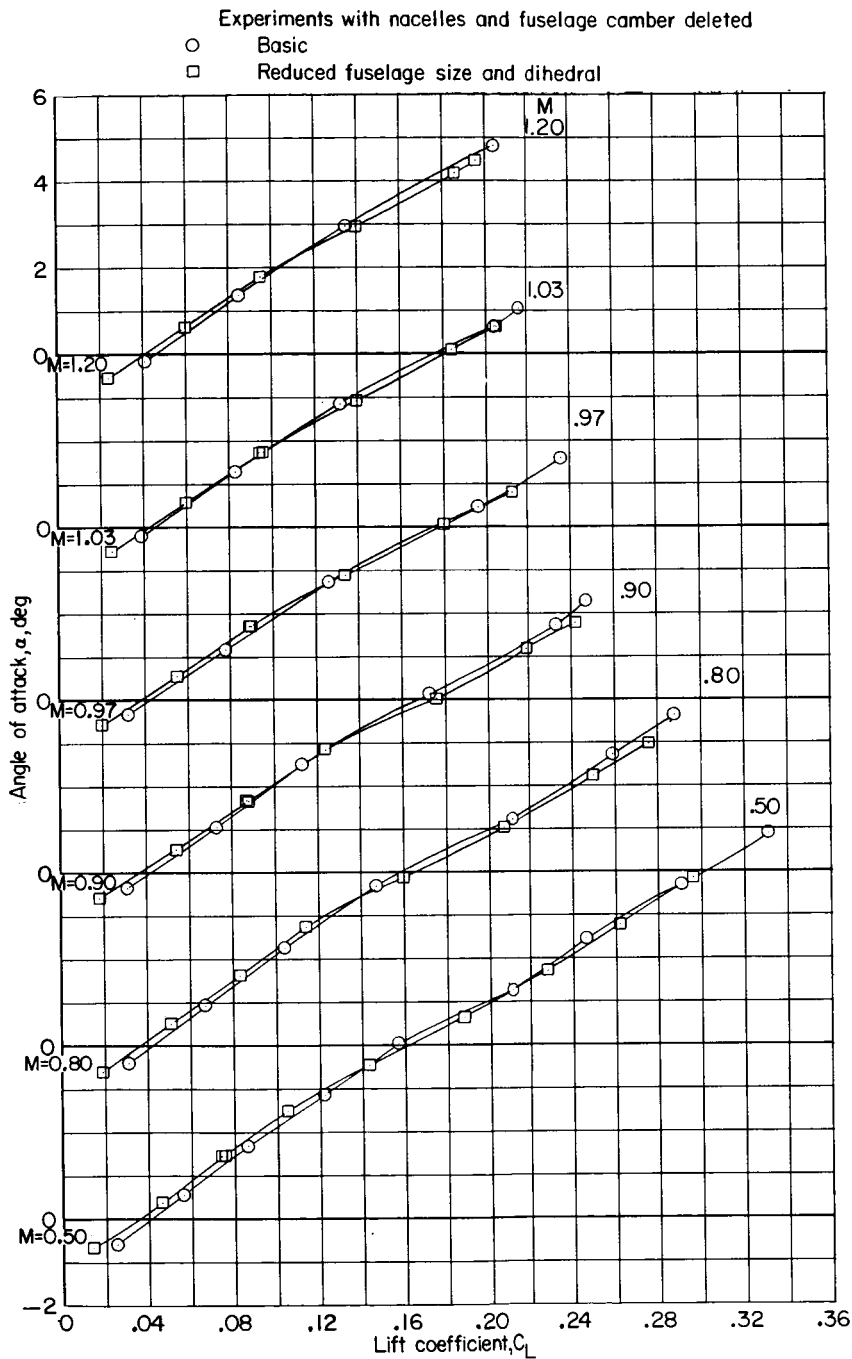
Figure 12.- Effect of reducing fuselage size and wing dihedral on high subsonic and transonic longitudinal characteristics. Nacelles off; fuselage uncambered; $\delta_f = 0^\circ$; $\delta_a = 0^\circ$; $\delta_e = 0^\circ$; leading edge drooped.

Experiments with nacelles and fuselage camber deleted
○ Basic
□ Reduced fuselage size and dihedral
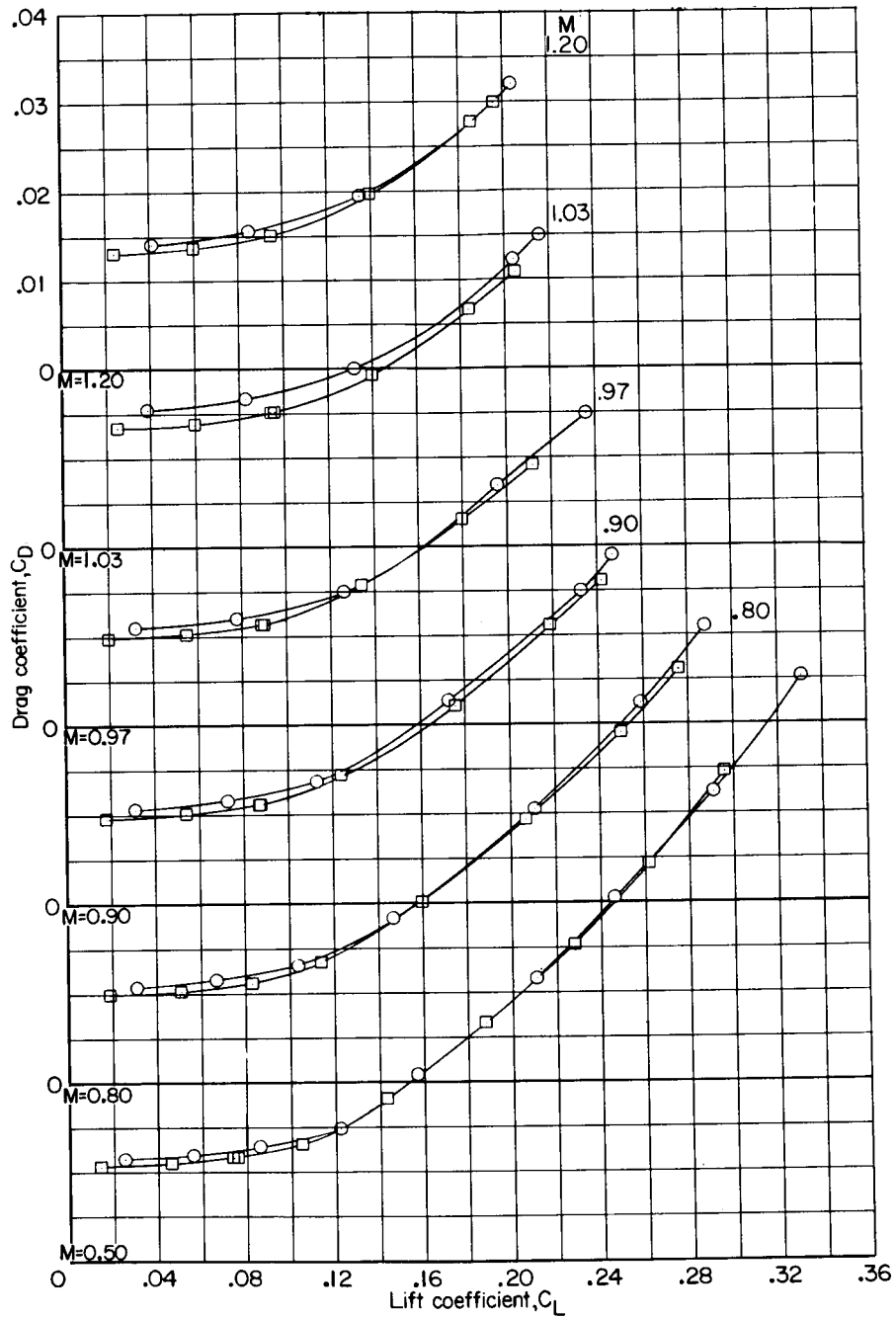
(b) C_D against C_L.

Figure 12.- Continued.

Experiments with nacelles and fuselage camber deleted

○   Basic

□   Reduced fuselage size and dihedral
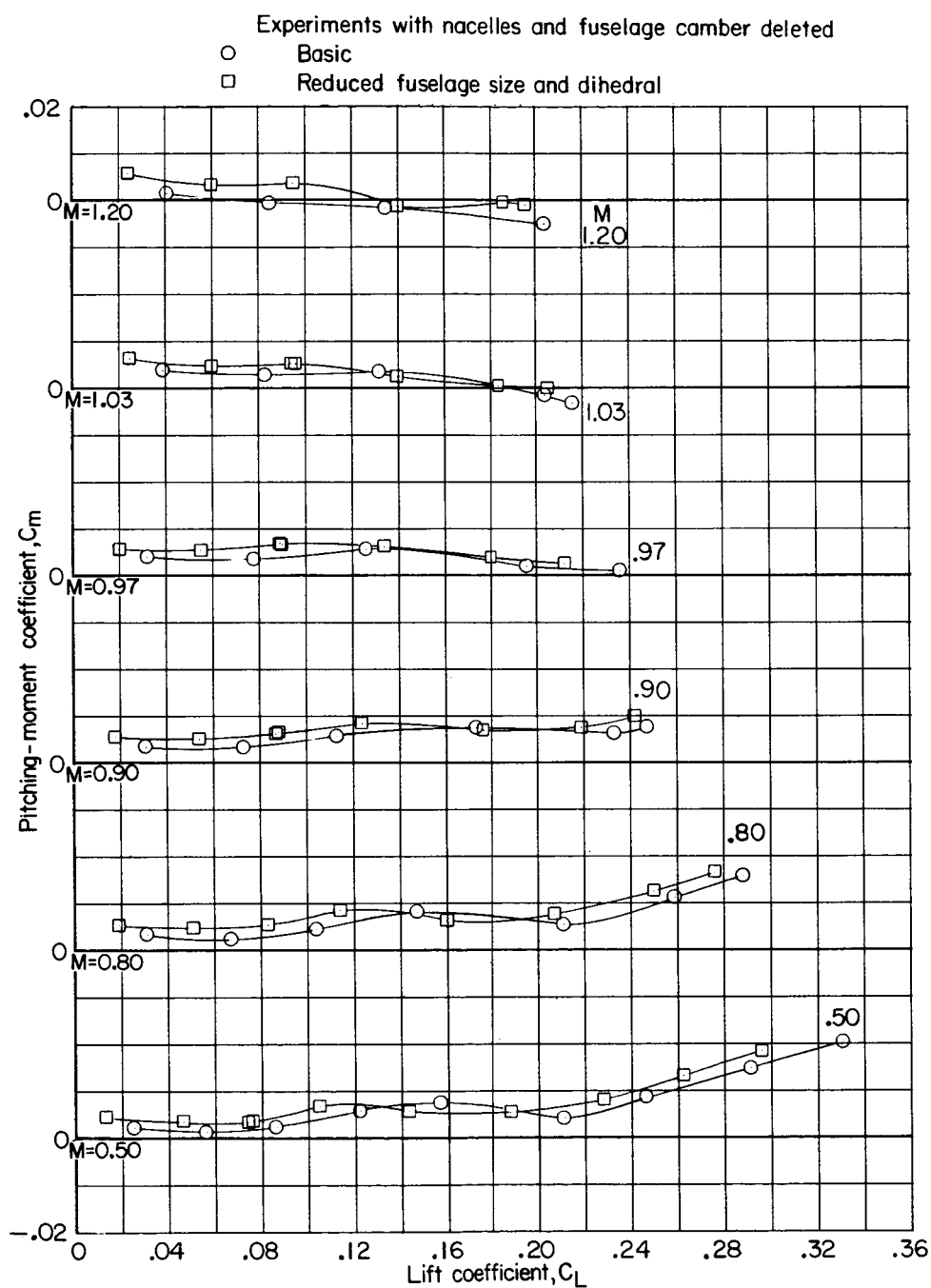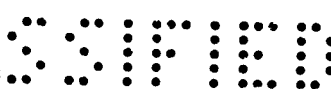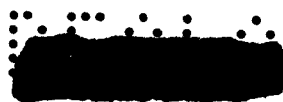
(c) C_m against C_L.

Figure 12.- Concluded.
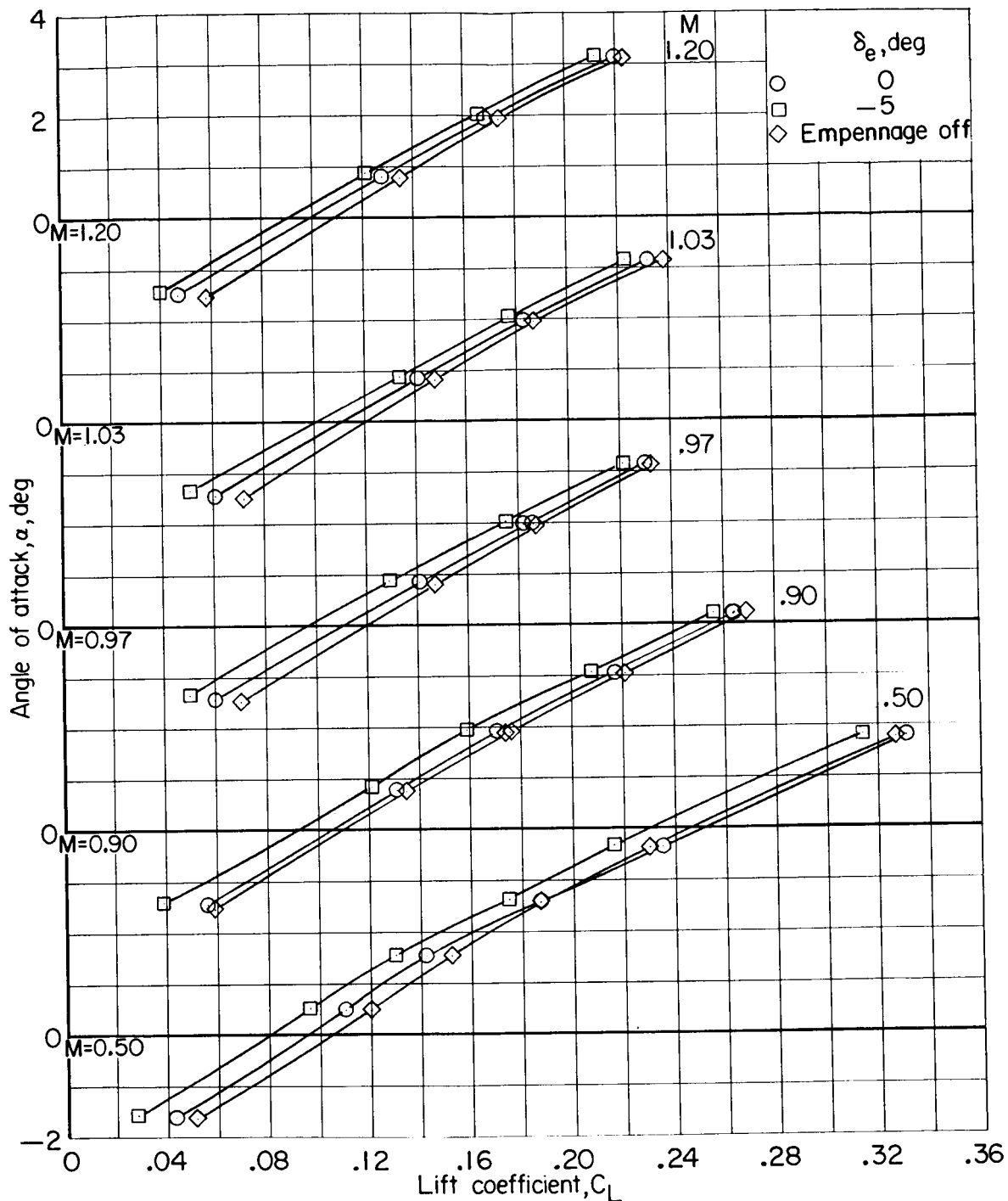
(a) α against C_L.

Figure 13.- Effect of elevator deflection and empennage on the high subsonic and transonic longitudinal aerodynamic characteristics. Wing outboard leading edge undrooped; $\delta_f = 7°$; $\delta_a = 7°$; $p_t = 1$ atm.
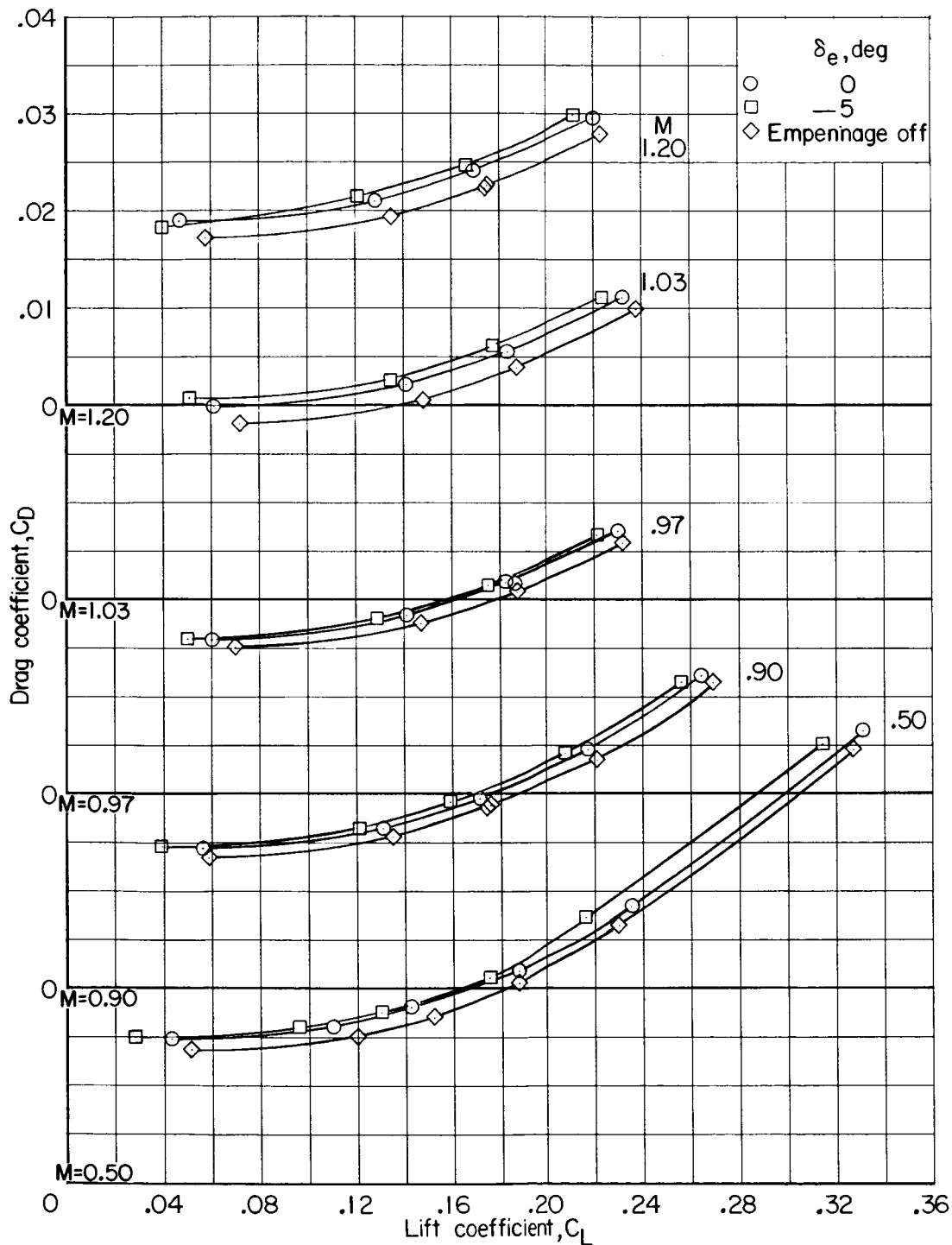
(b) C_D against C_L.

Figure 13.- Continued.
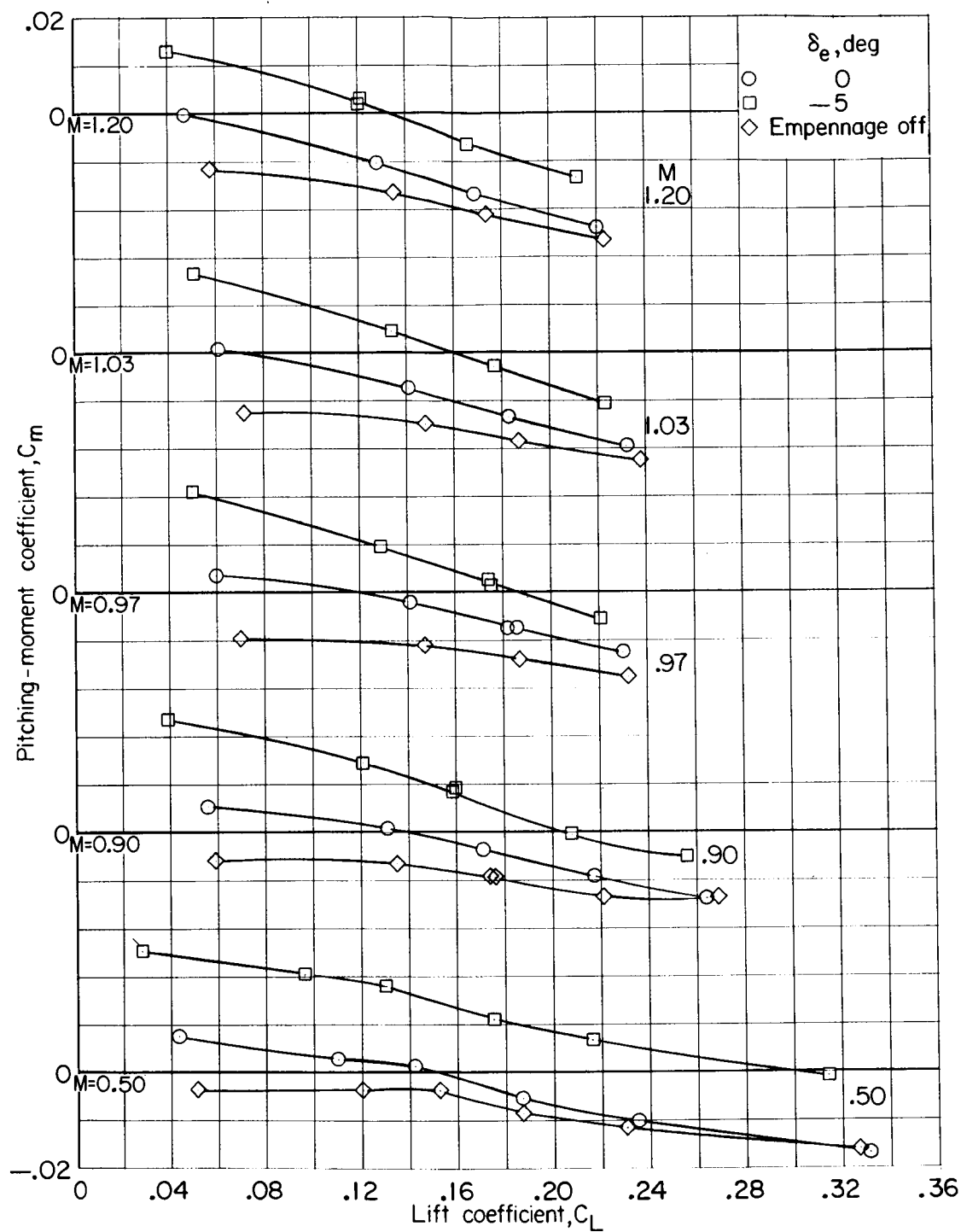
(c) C_m against C_L.

Figure 13.- Concluded.
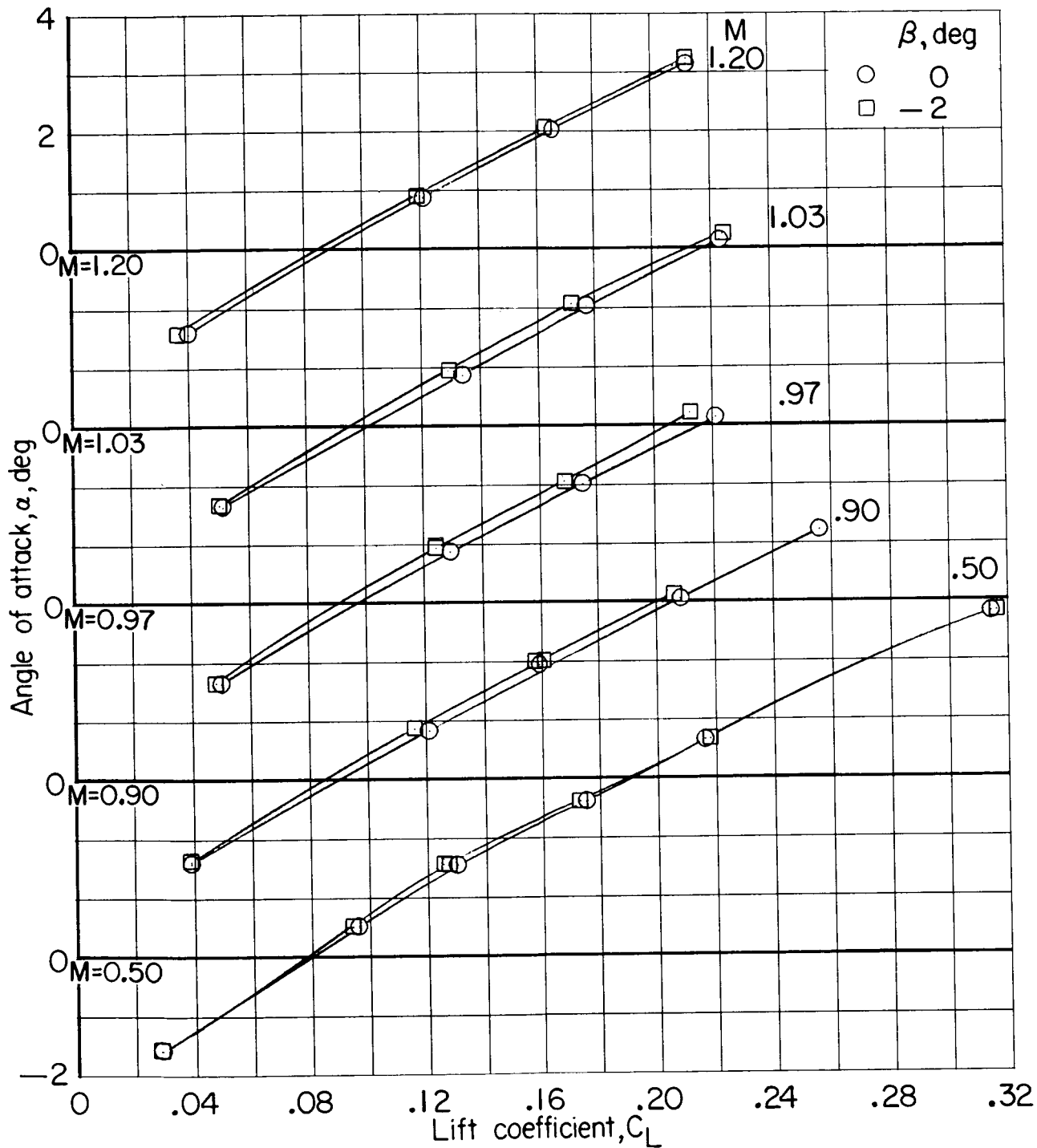
(a) α against C_L.

Figure 14.- Effect of sideslip on the high subsonic and transonic aerodynamic characteristics. Wing outboard leading edge undrooped; $\delta_f = 7^\circ$; $\delta_a = 7^\circ$; $\delta_e = -5^\circ$; $p_t = 1$ atm.
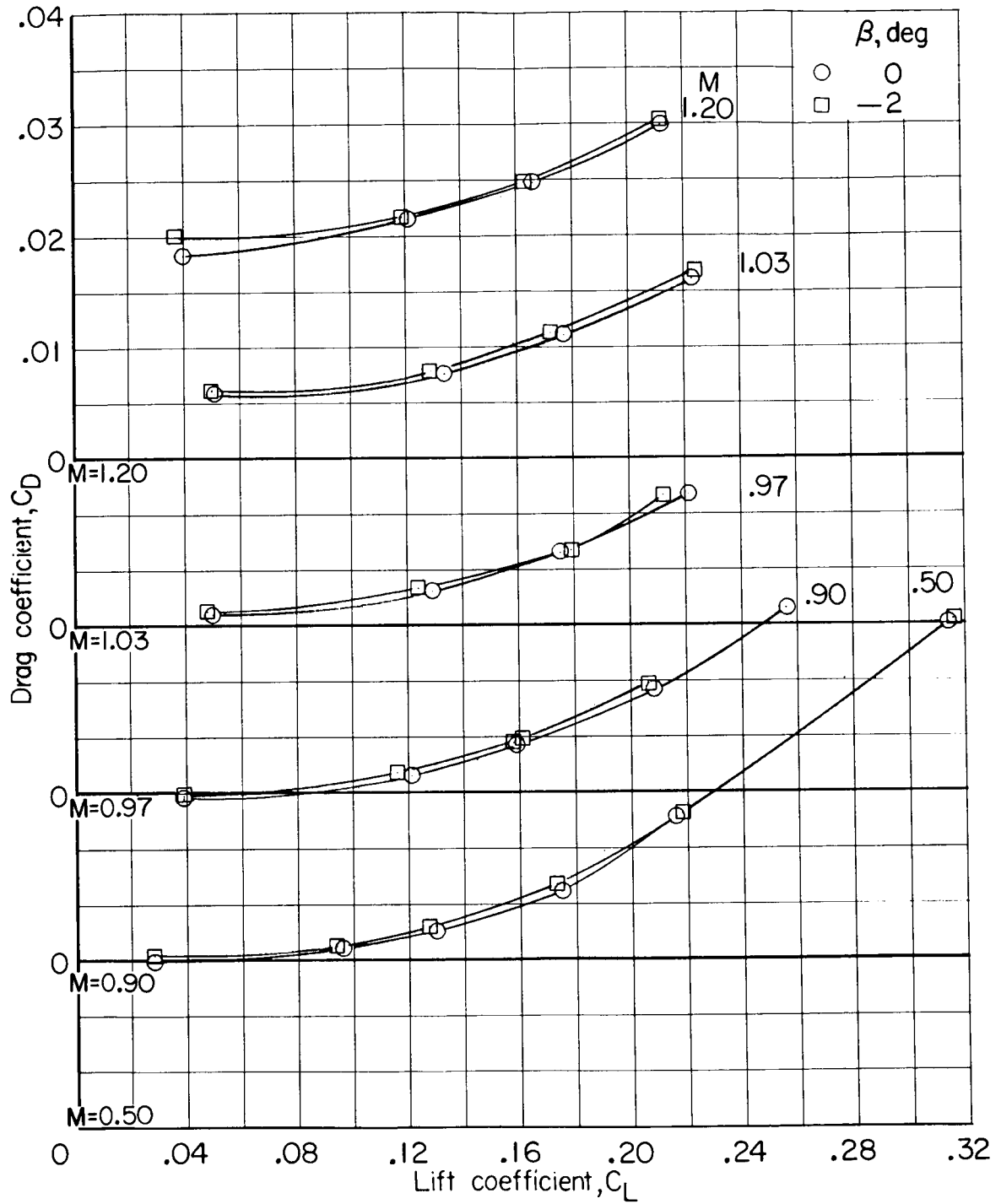
(b) C_D against C_L.

Figure 14.- Continued.

(c) C_m against C_L.
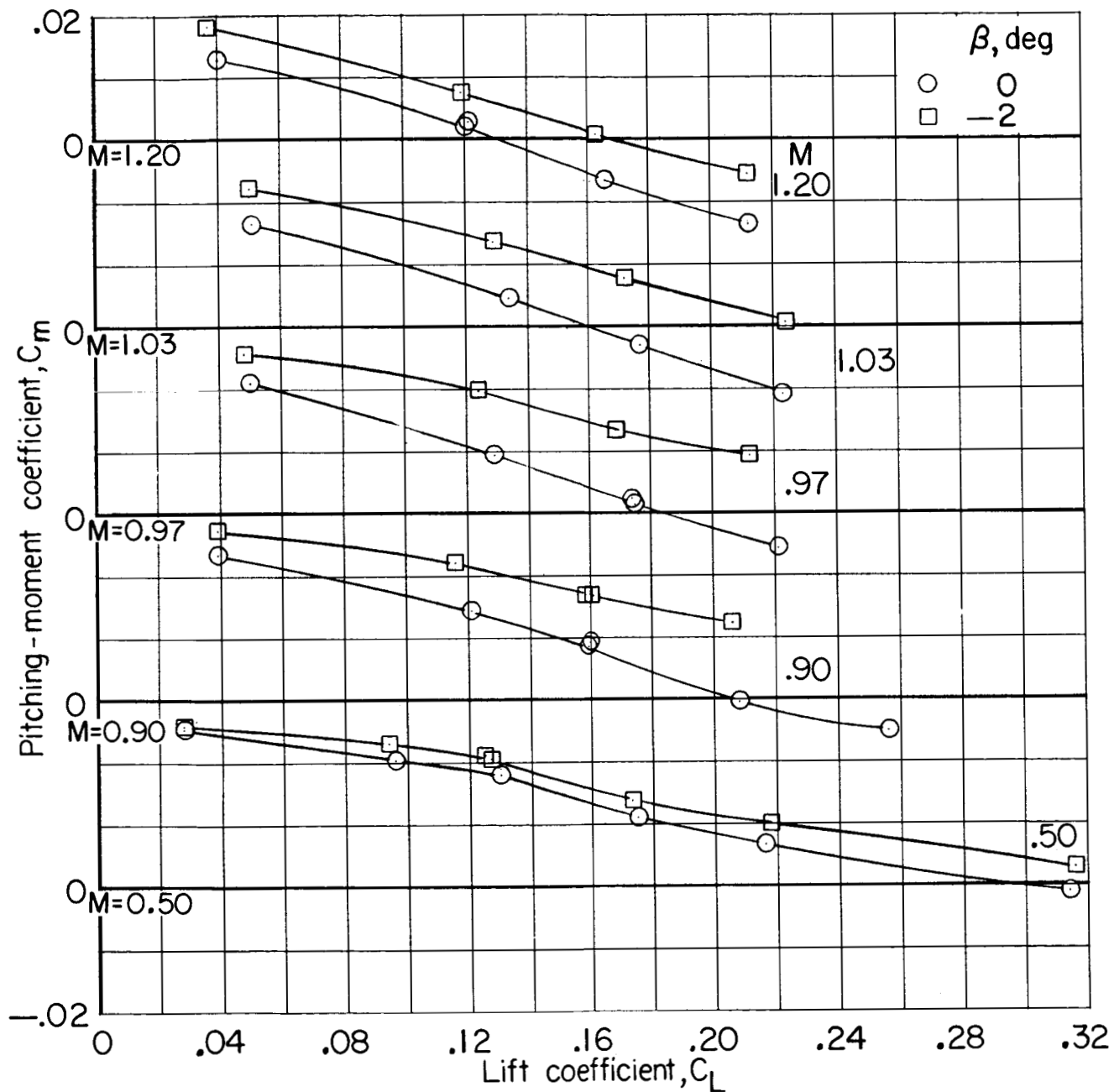
Figure 14.- Continued.
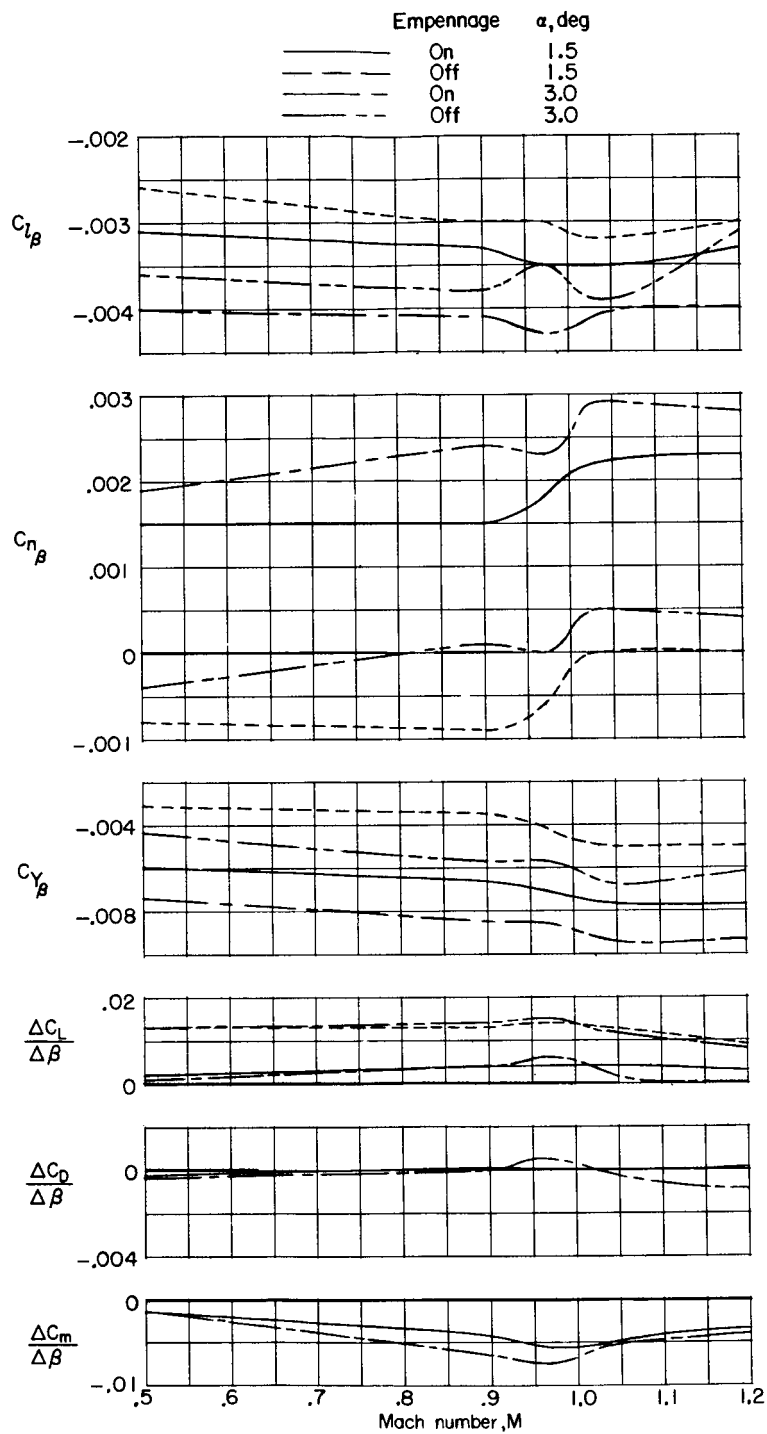
(d) Lateral stability derivatives and longitudinal increments due to sideslip.

Figure 14.- Concluded.
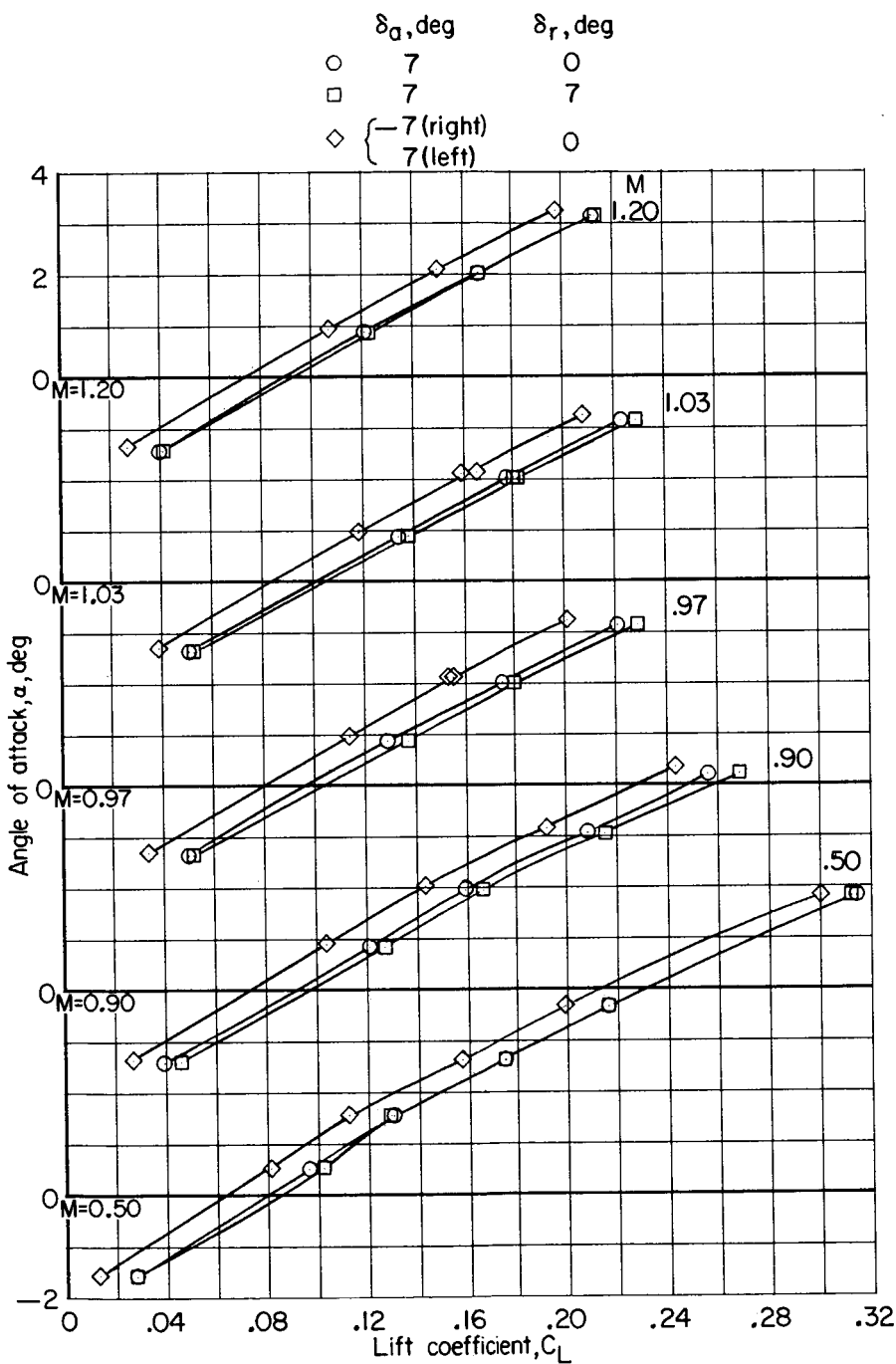
(a) α against C_L.

Figure 15.- Effect of rudder and aileron deflection on the high subsonic and transonic longitudinal aerodynamic characteristics. Wing outboard leading edge undrooped; $\delta_f = 7^\circ$; $\delta_a = 7^\circ$; $\delta_e = -5^\circ$; $p_t = 1$ atm.
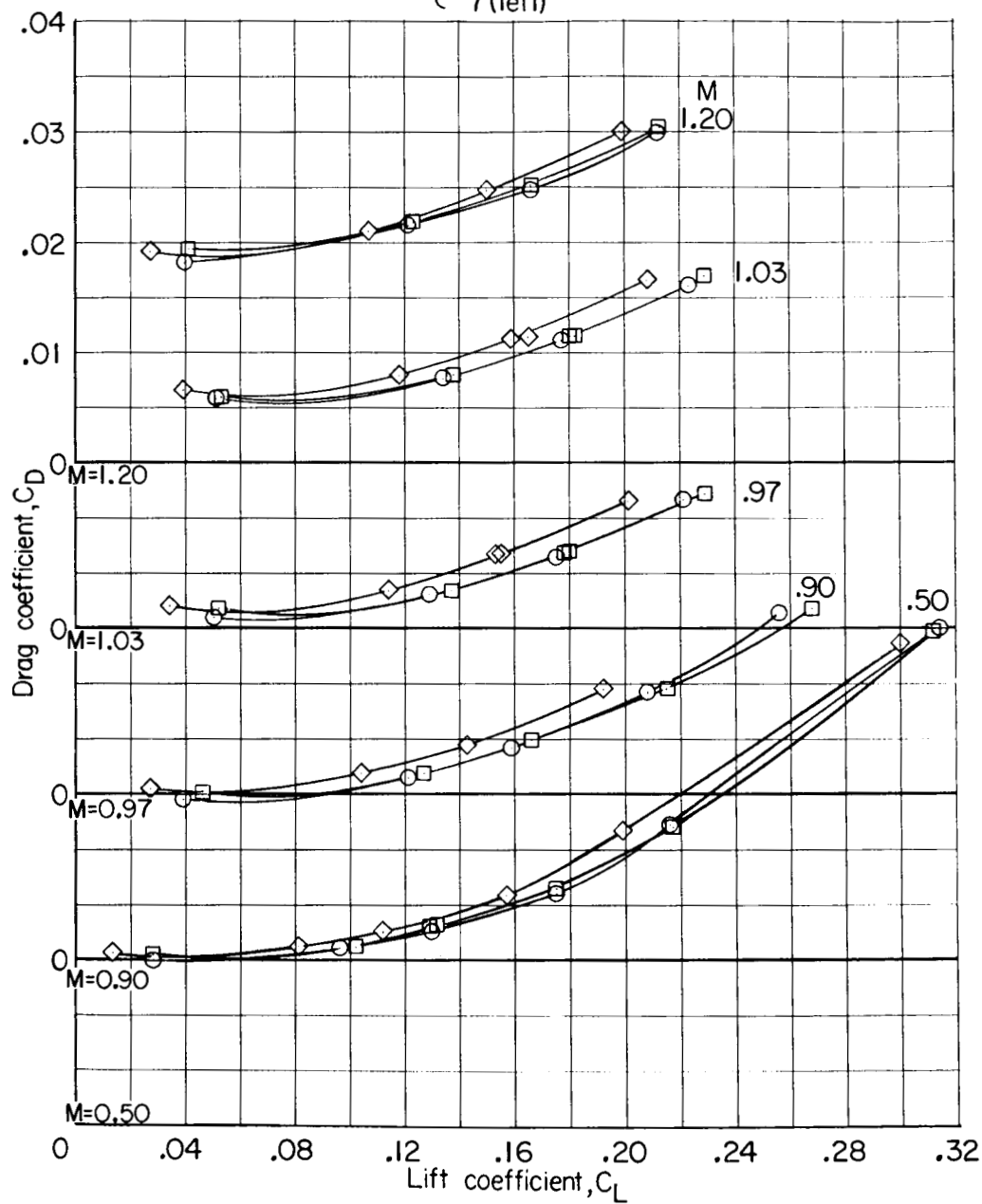
(b) C_D against C_L.

Figure 15.- Continued.
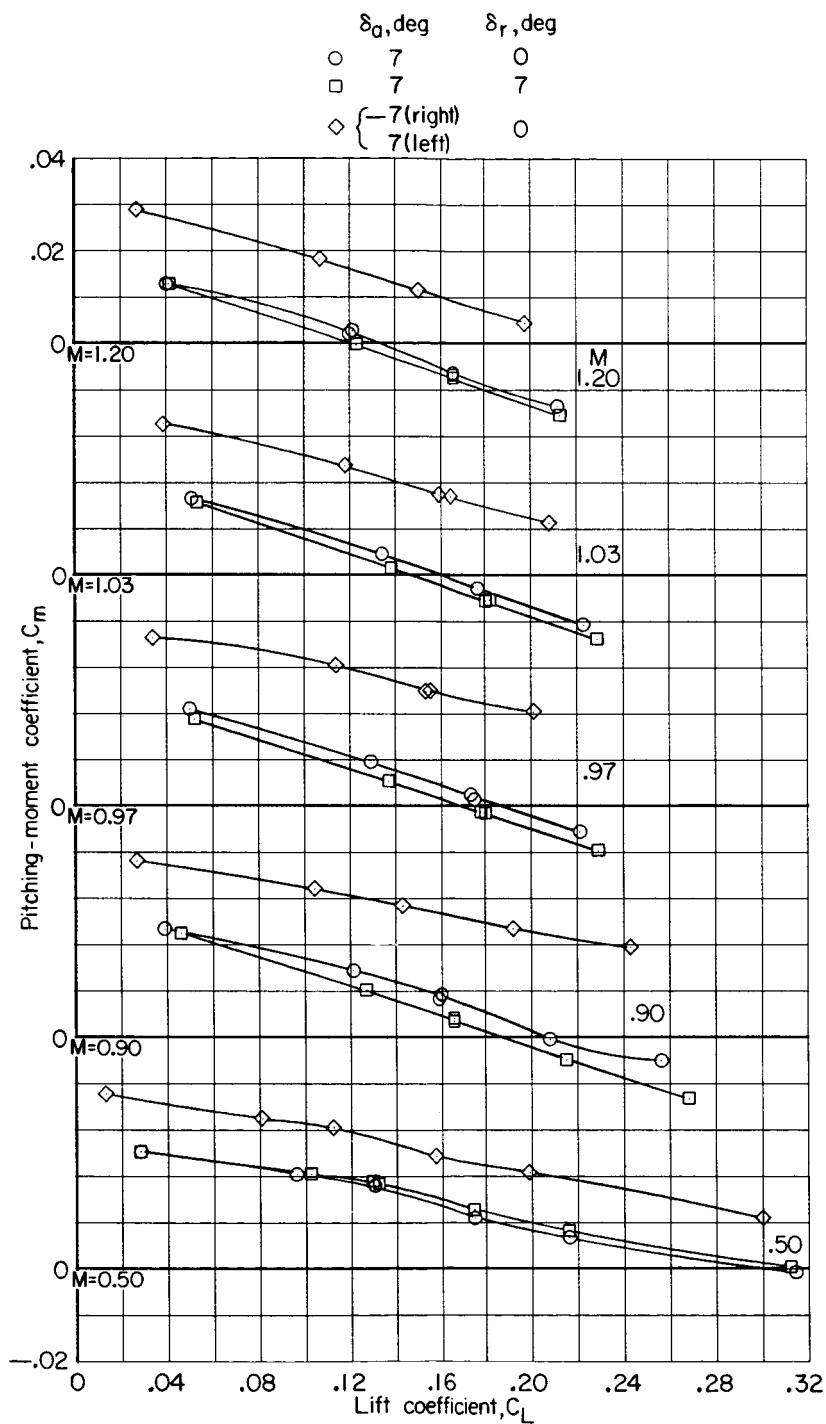
(c) C_m against C_L.

Figure 15.- Continued.
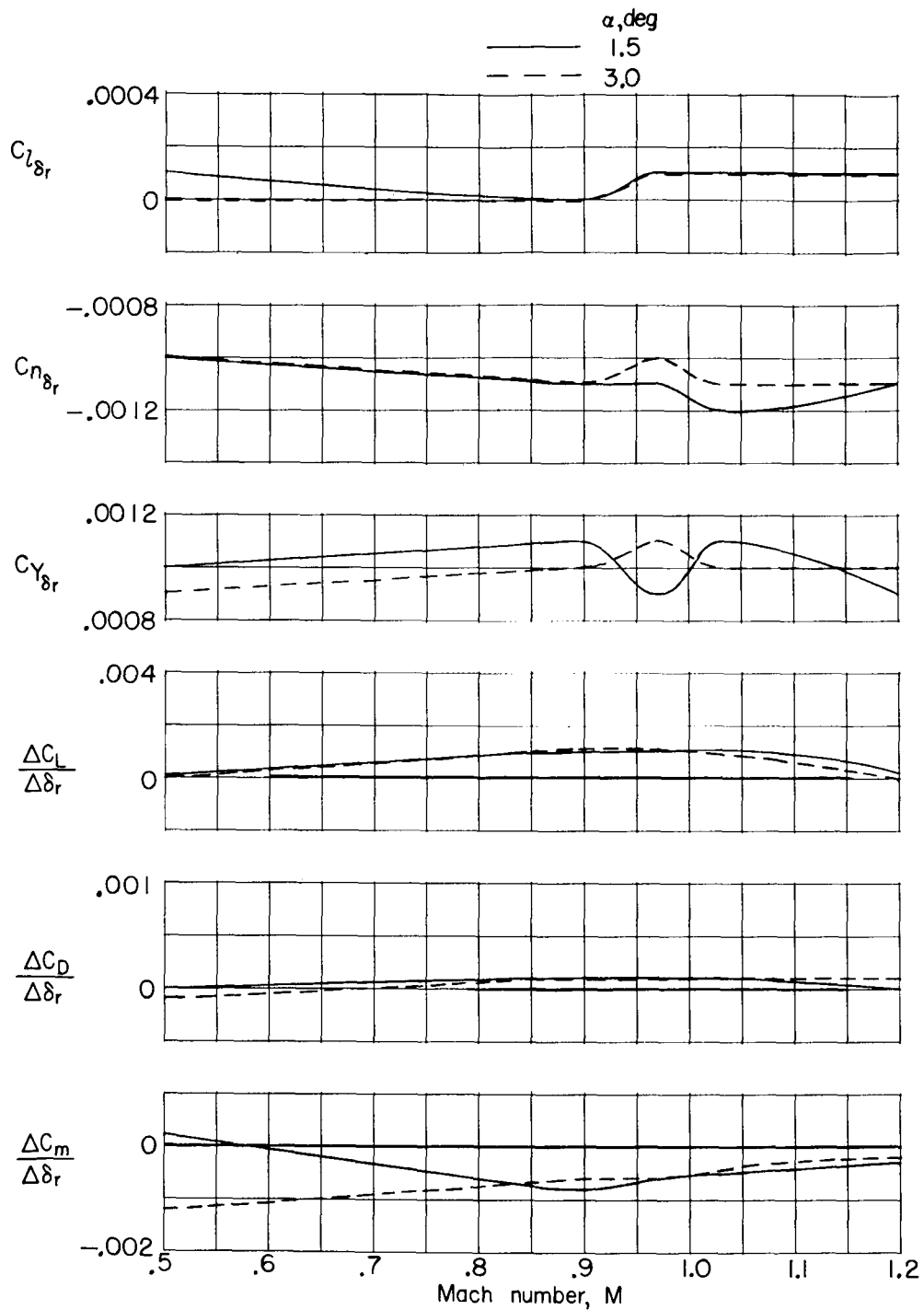
(d) Lateral stability derivatives and longitudinal increments due to rudder deflection.

Figure 15.- Continued.
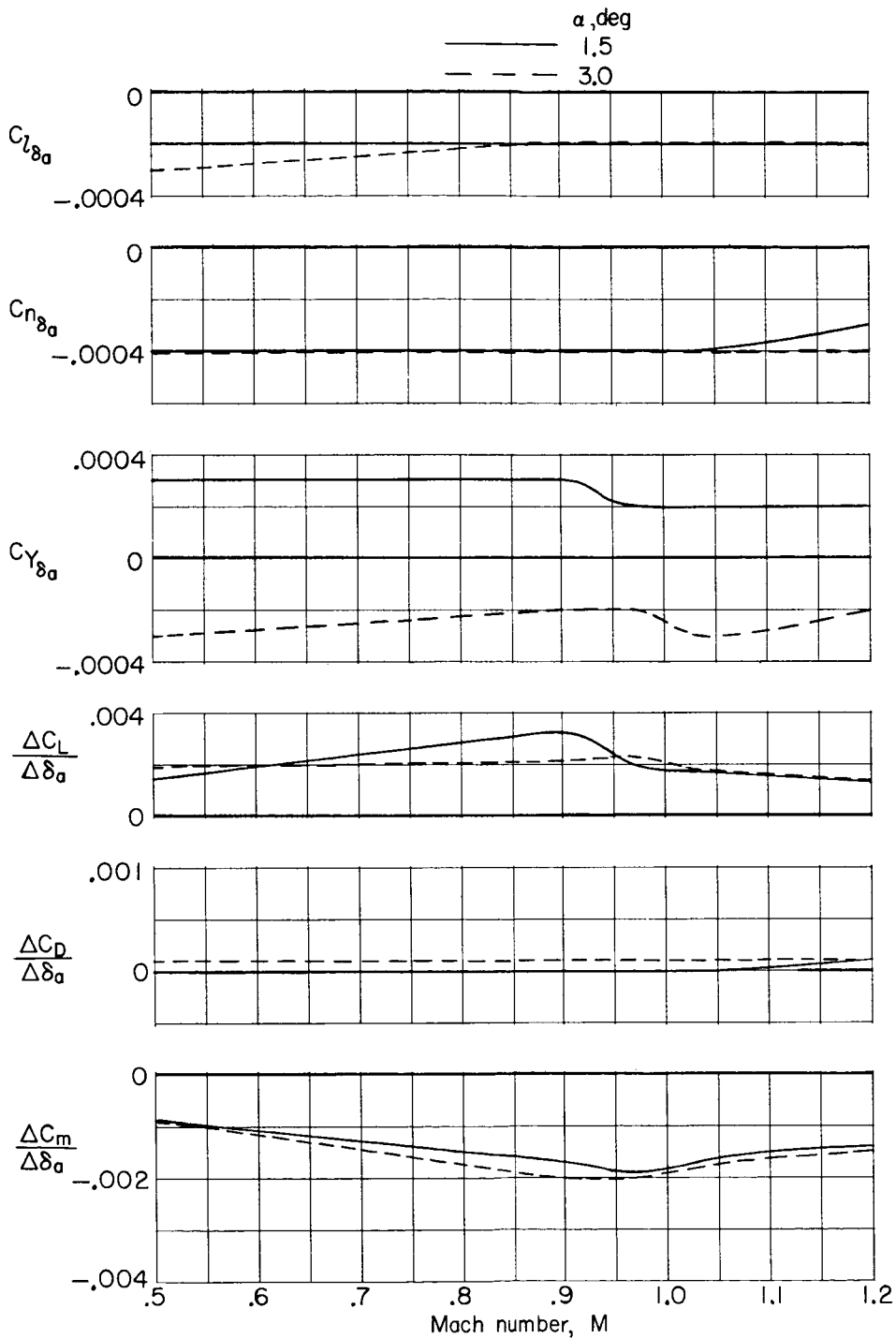
(e) Lateral stability derivatives and longitudinal increments due to aileron deflection.

Figure 15.- Concluded.

M = 0.97; C_L = 0.187.
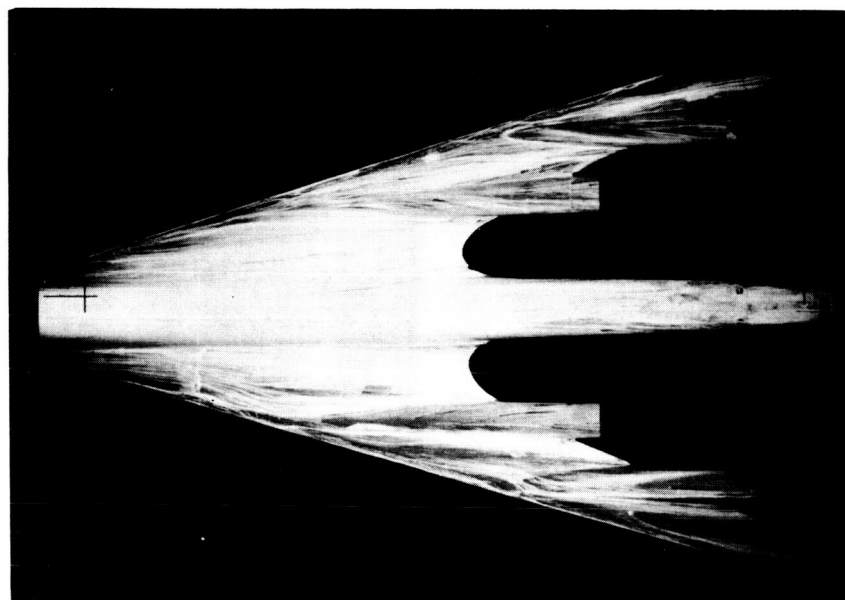
M = 0.90; C_L = 0.176.   L-63-5

Figure 16.- Fluorescent-oil film photographs of the boundary-layer flow patterns. Wing outboard
leading edge undrooped; δ_f = 7°; δ_a = 7°; empennage off.

Reynolds number, R   Transition-strip density, grains/in.

○	3.10×10^6	100
□	5.69×10^6	100
◇	3.10×10^6	20
△	5.69×10^6	20
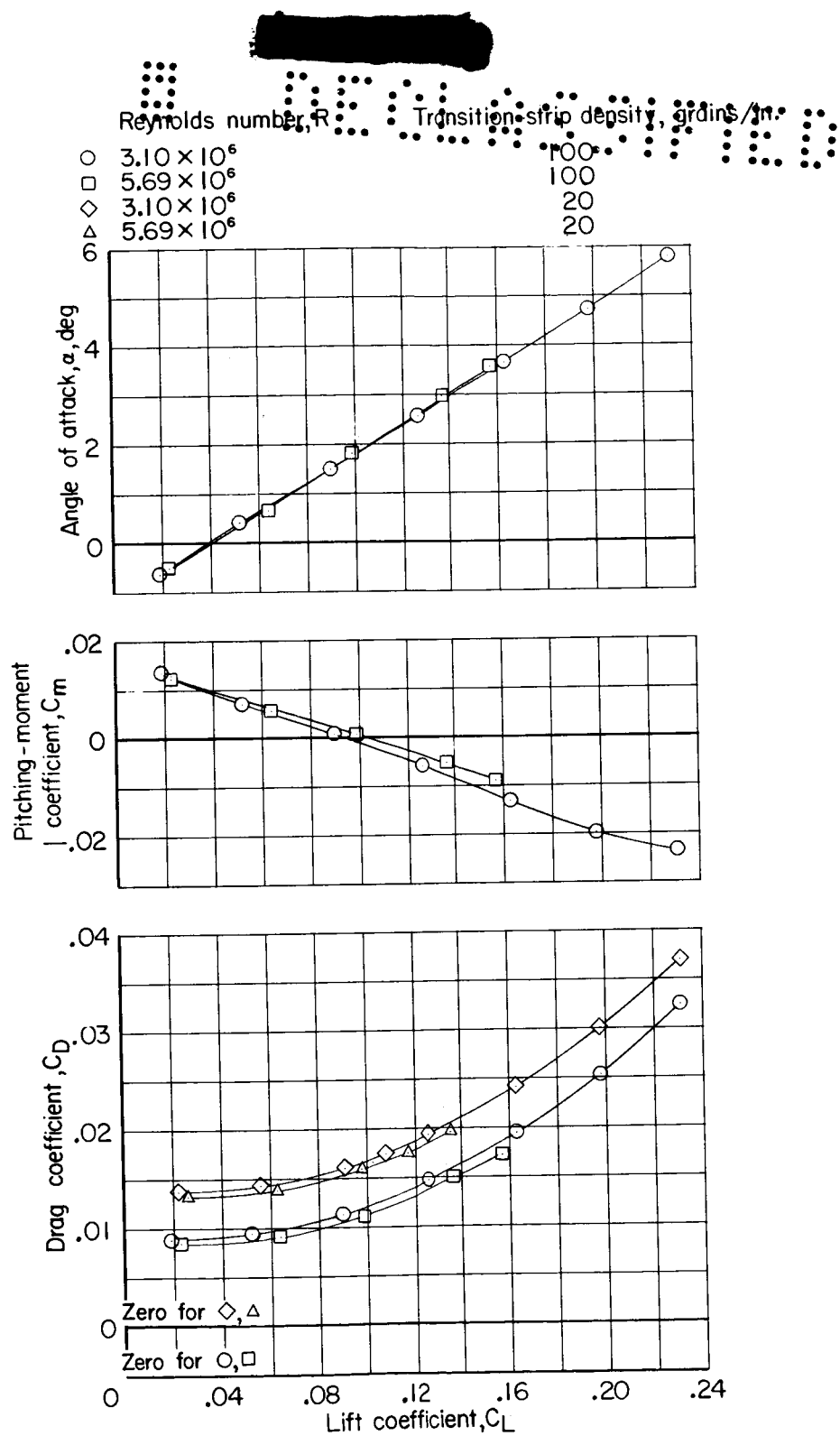
Figure 17.- Effects of transition-strip density and Reynolds number variation at M = 2.01. $\delta_f = 4^\circ$; $\delta_a = 4^\circ$; $\delta_e = 1.75^\circ$; leading edge drooped.

○ Outboard L.E. undrooped

□ Outboard L.E. drooped
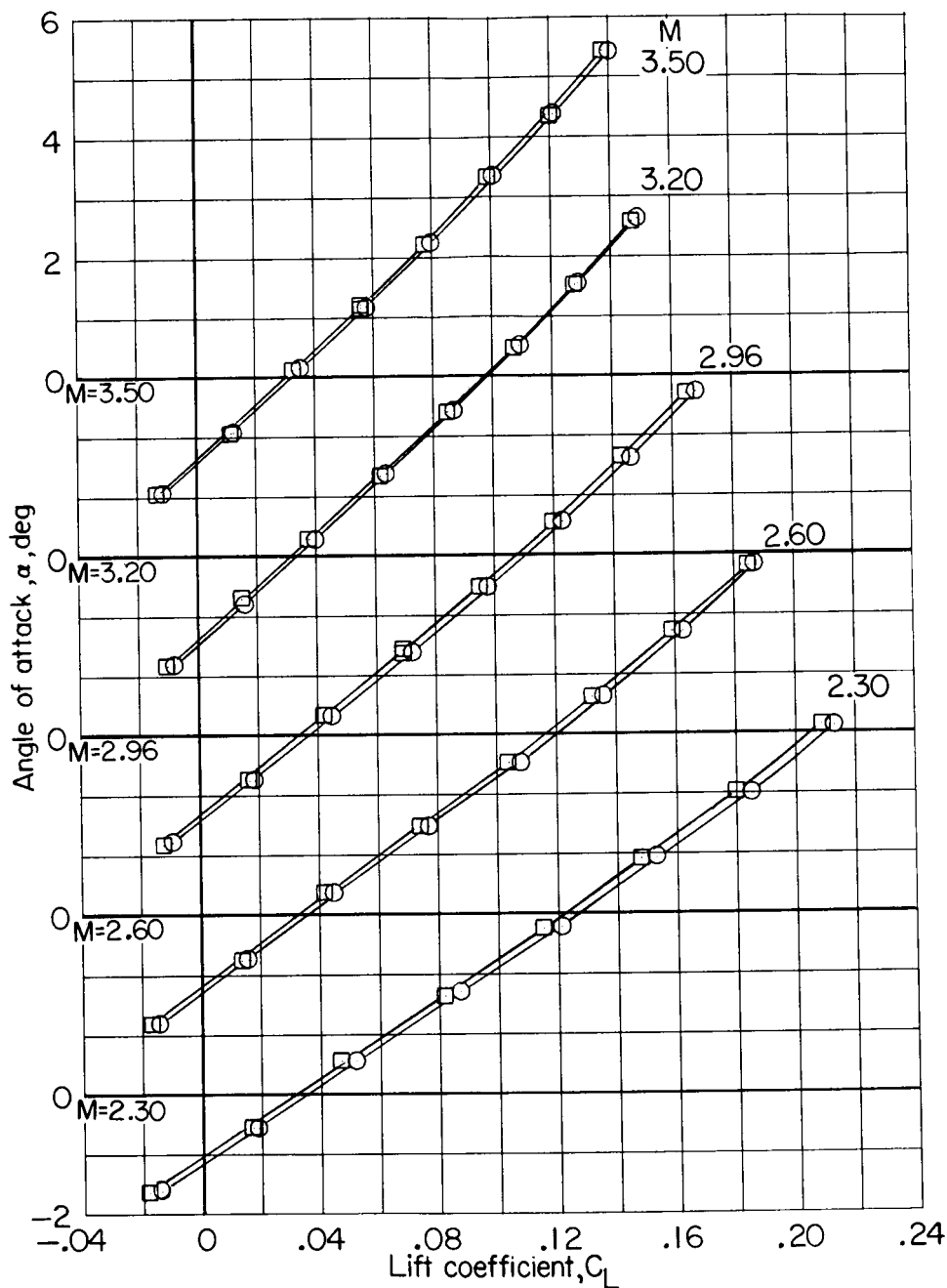
(a) α against C_L.

Figure 18.- Effect of wing outboard leading-edge droop on supersonic longitudinal aerodynamic characteristics. Basic fuselage; $\delta_f = 0°$; $\delta_a = 0°$; $\delta_e = 1.75°$.

○ Outboard L.E. undrooped
□ Outboard L.E. drooped
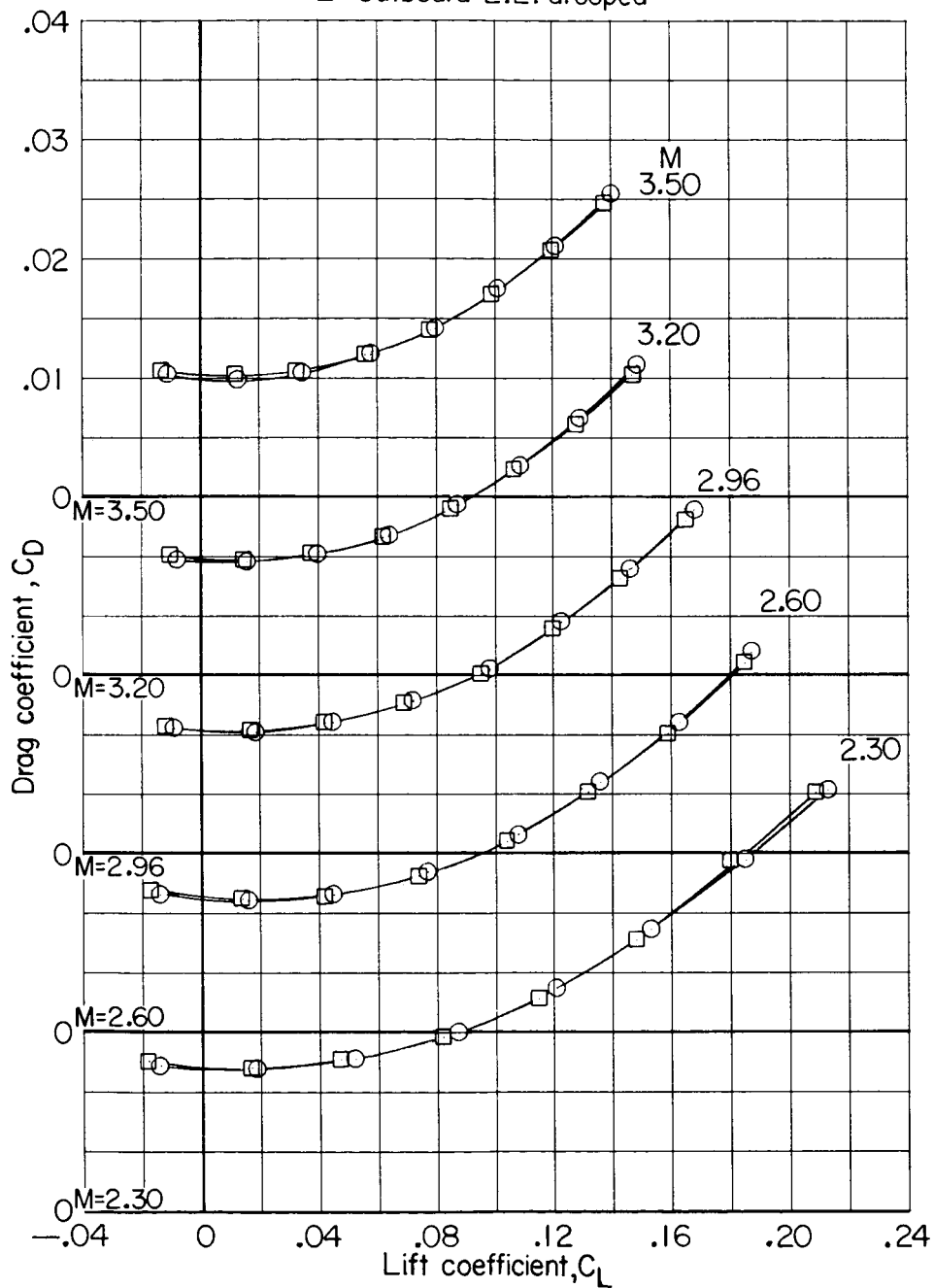
(b) C_D against C_L.

Figure 18.- Continued.

○ Outboard L.E. undrooped
□ Outboard L.E. drooped
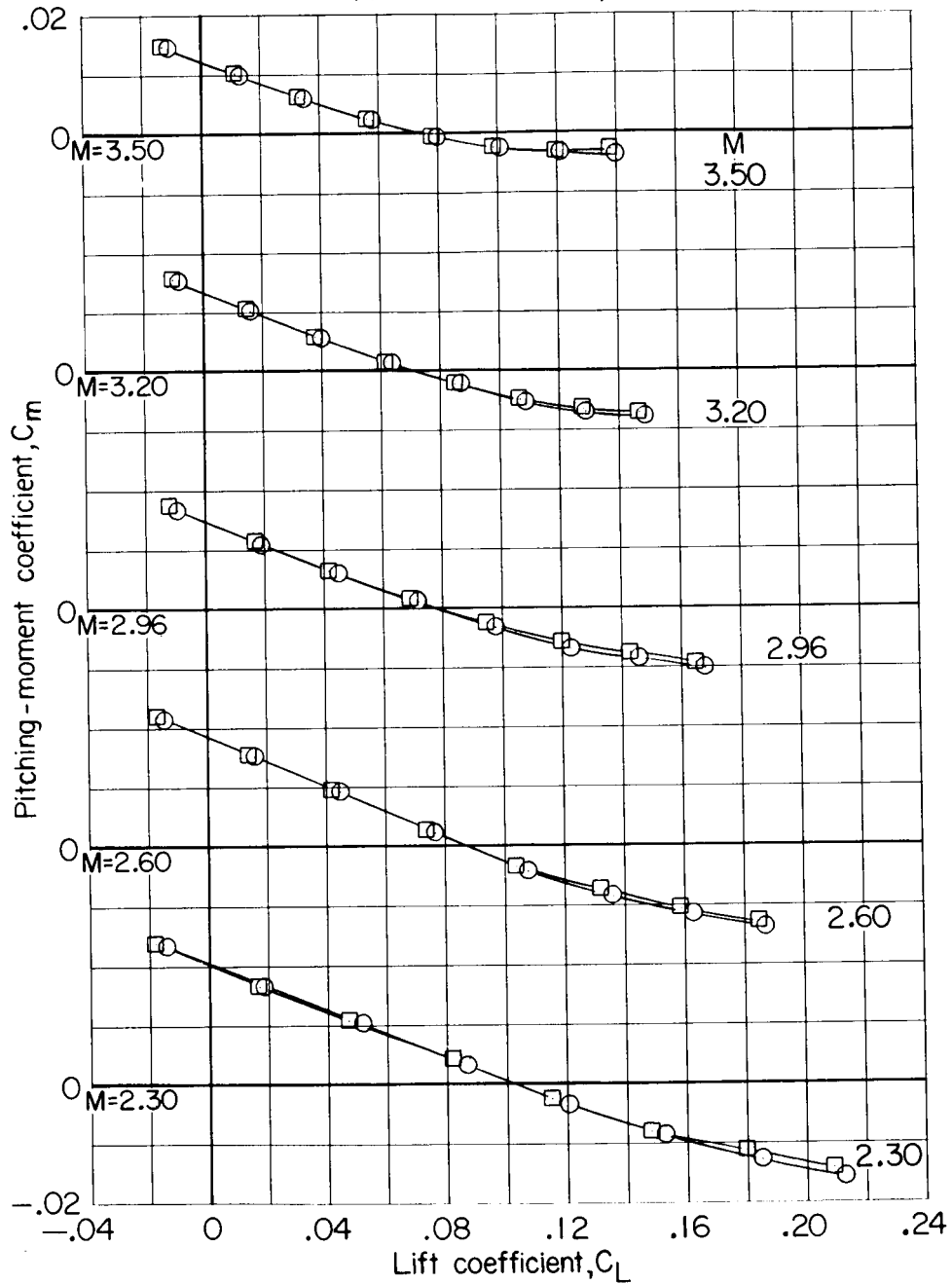
(c) C_m against C_L.

Figure 18.- Concluded.
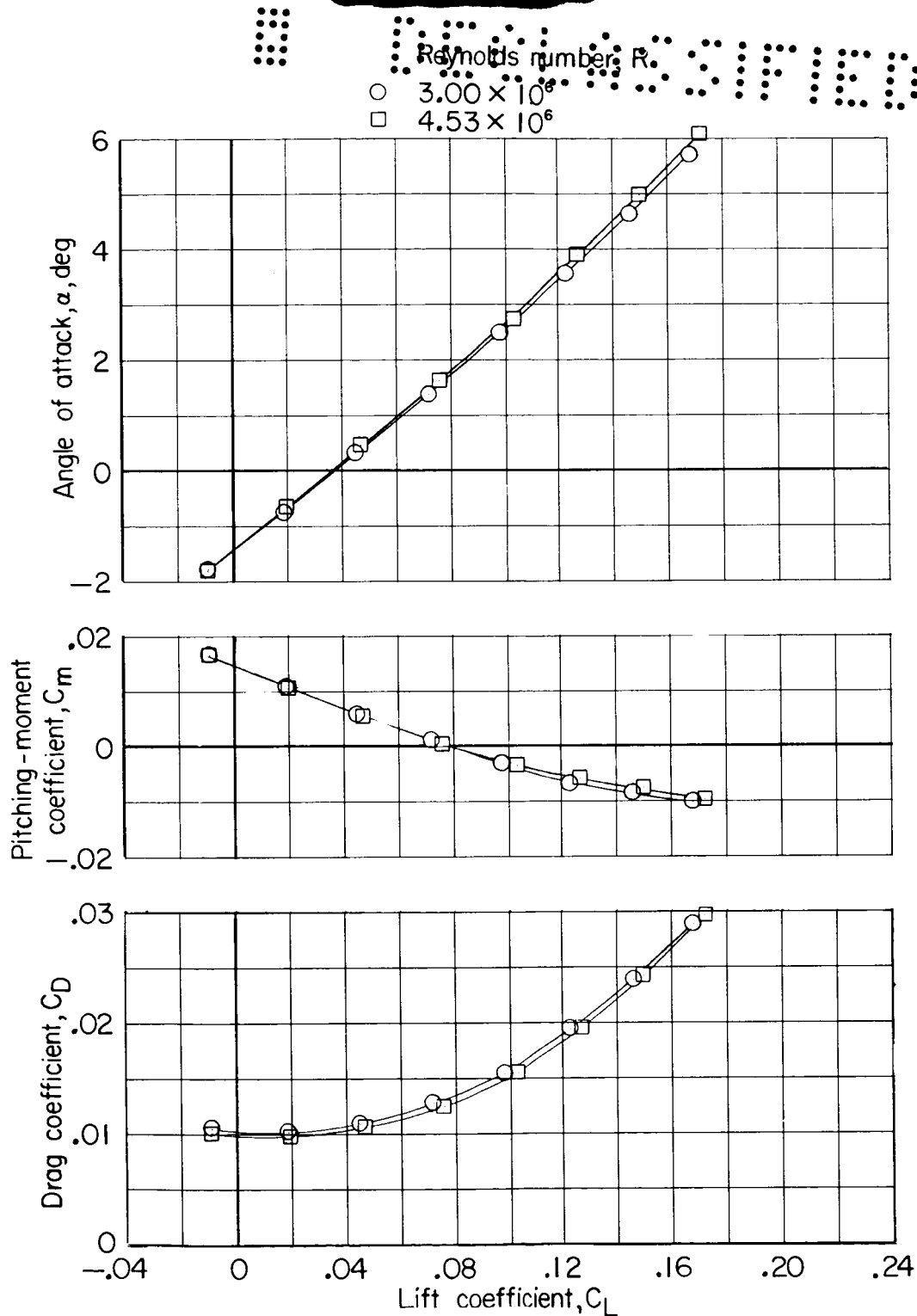
Figure 19.- Effects of Reynolds number variation at M = 2.96. $\delta_f = 0°$; $\delta_a = 0°$; $\delta_e = 1.75°$; leading edge undrooped.
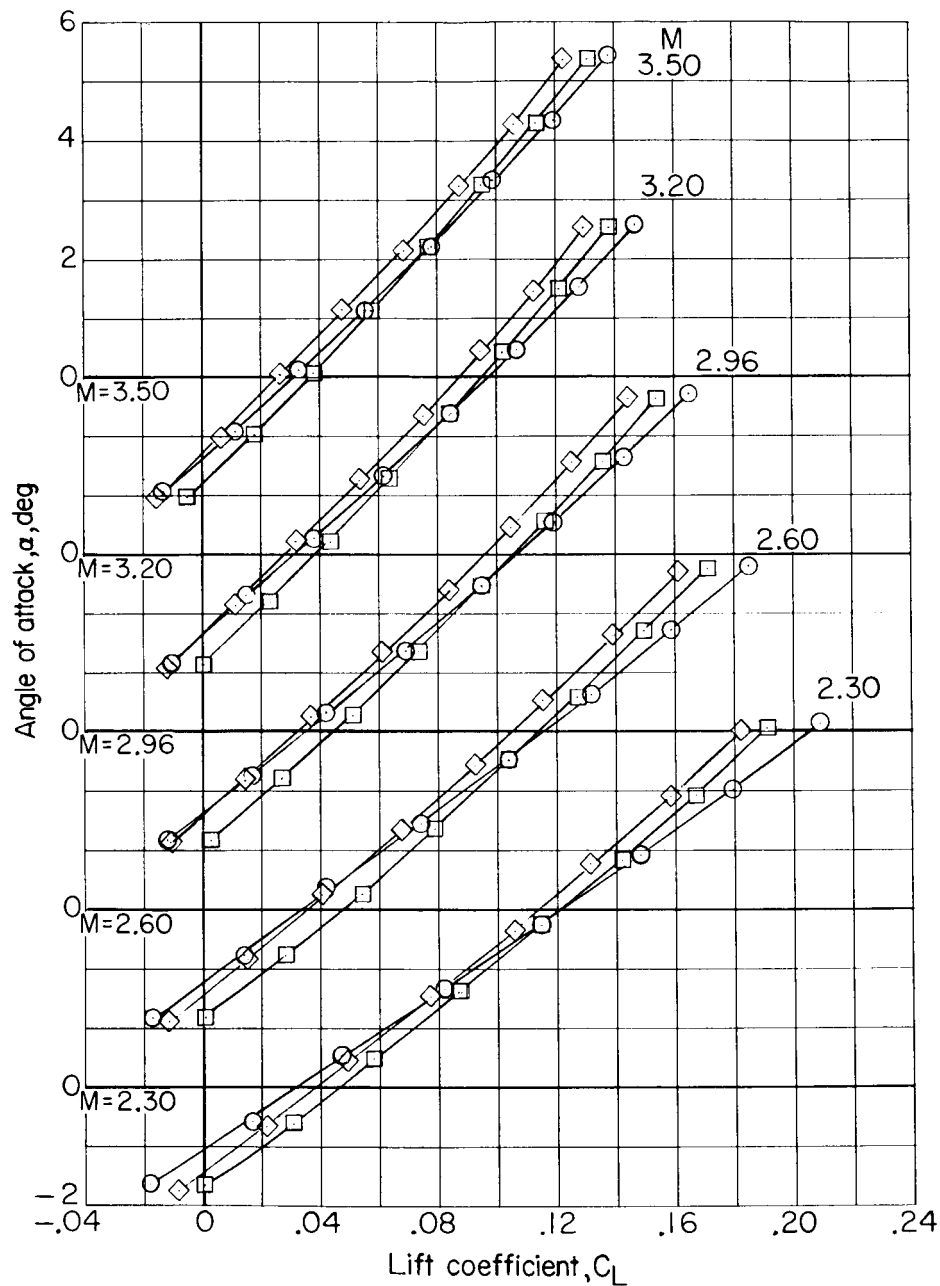
(a) α against C_L.

Figure 20.- Effects of nacelles and fuselage camber on supersonic longitudinal aerodynamic charac-
teristics. $\delta_f = 0°$; $\delta_a = 0°$; $\delta_e = 1.75°$; leading edge drooped.

Nacelles Fuselage
○ On Cambered
□ Off Cambered
◇ Off Uncambered
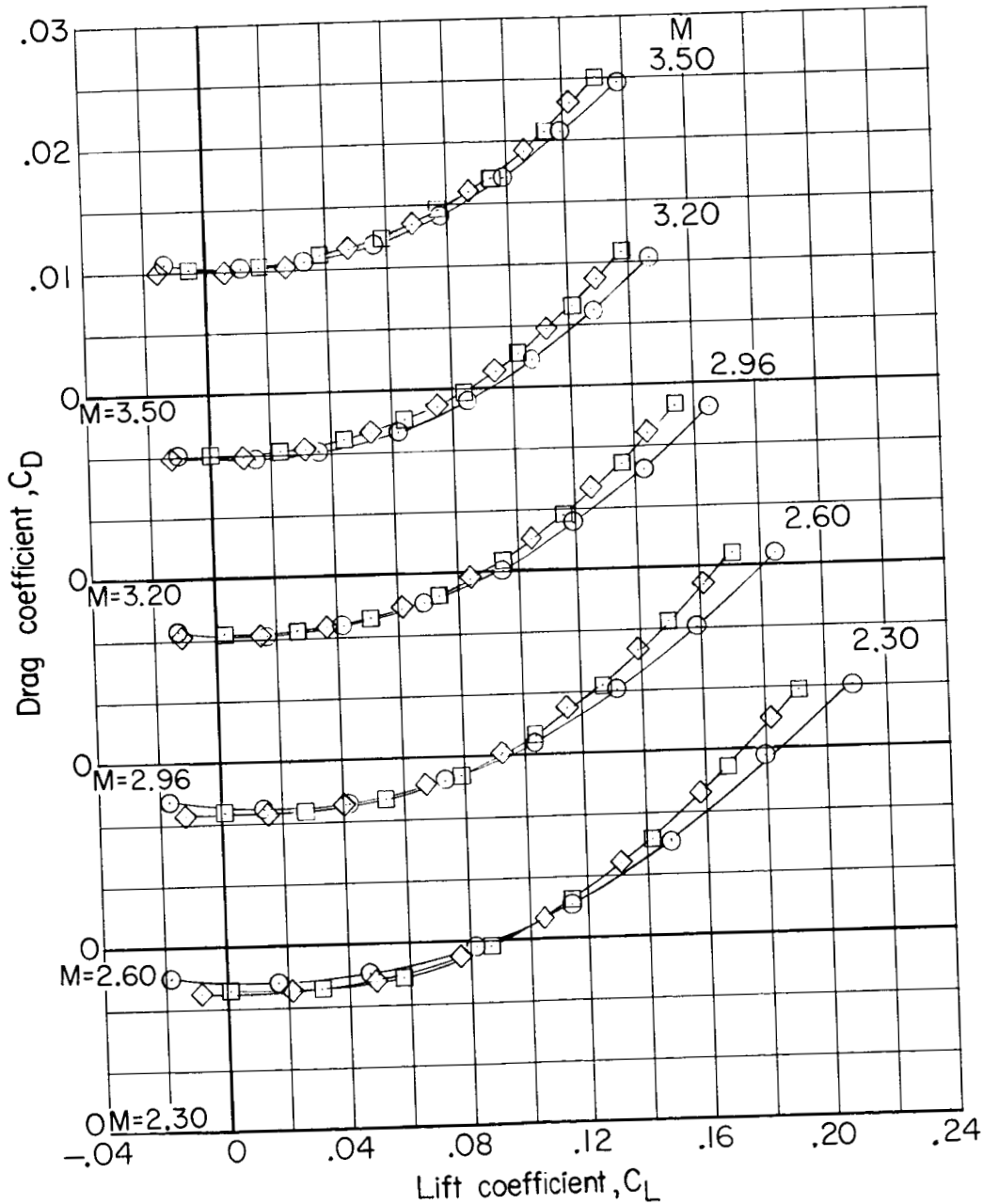
(b) C_D against C_L.

Figure 20.- Continued.

Nacelles		Fuselage
○	On	Cambered
□	Off	Cambered
◇	Off	Uncambered
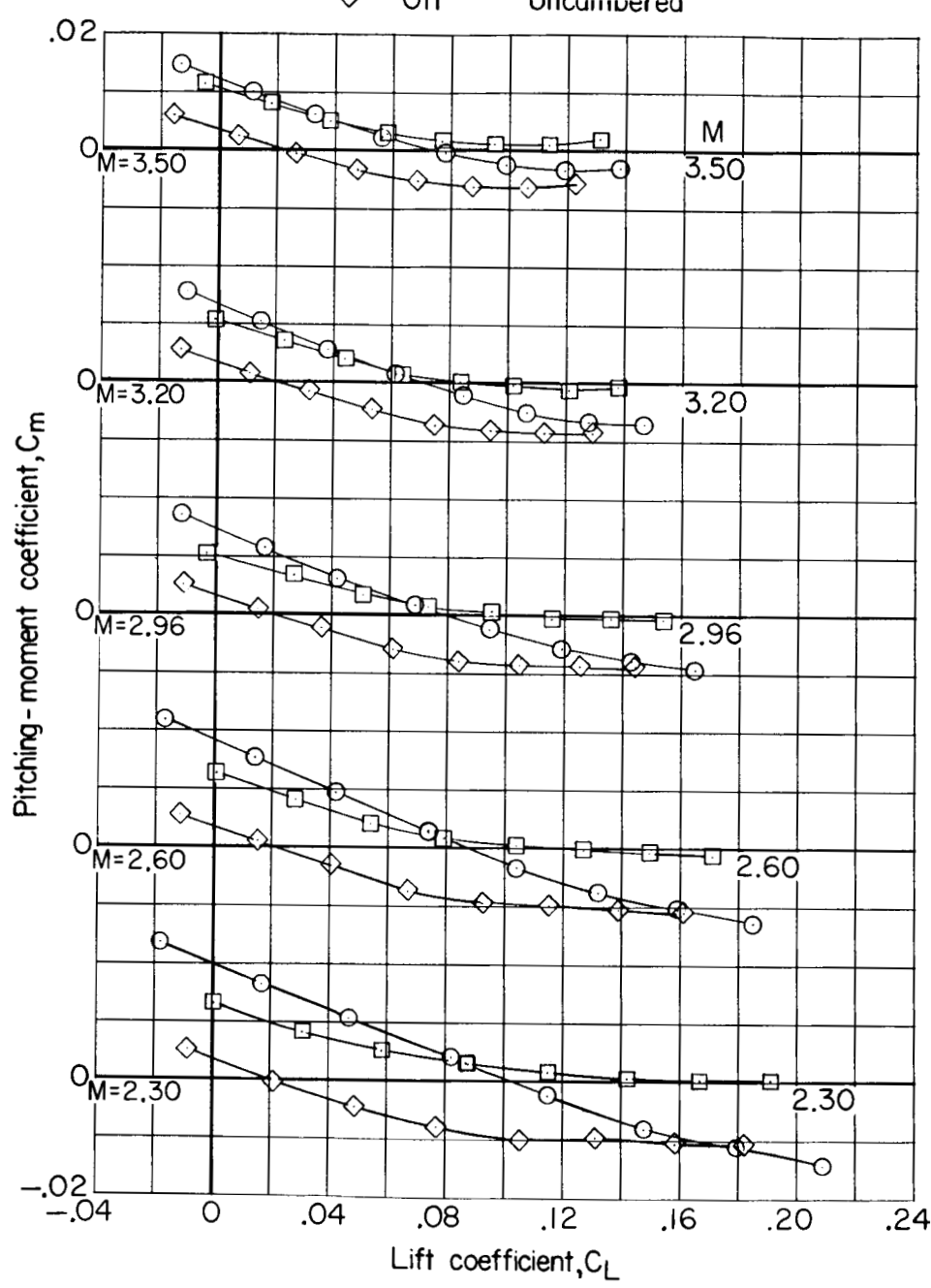
(c) C_m against C_L.

Figure 20.- Concluded.

	Nacelles	Fuselage	Dihedral
O	Off	Basic	Basic
□	Off	Small	Reduced
— — —	On	Small	Reduced (estimated)
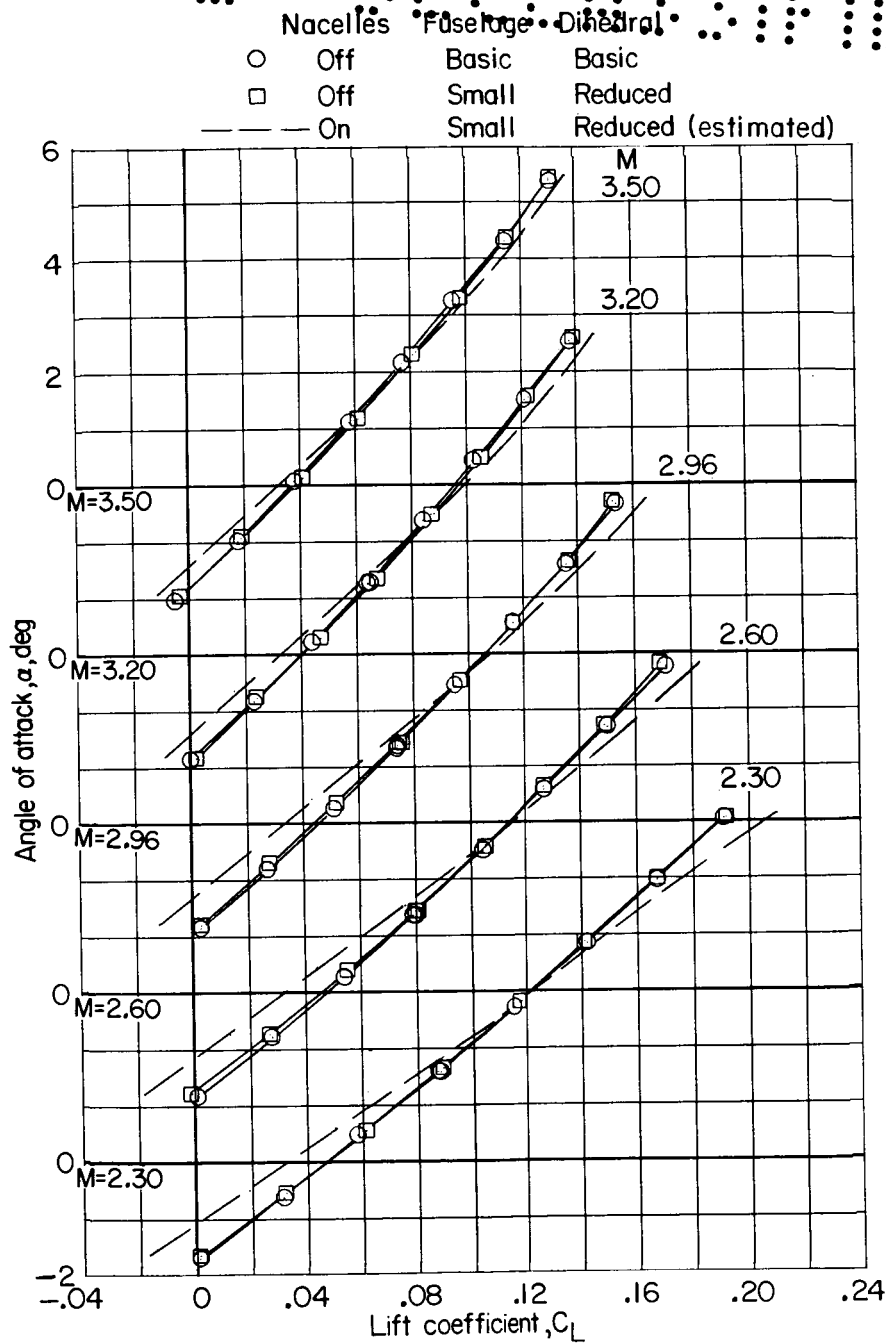
(a) α against C_L.

Figure 21.- Effects of reducing fuselage size and wing dihedral on supersonic longitudinal aerodynamic characteristics. Nacelles off; $\delta_f = 0°$; $\delta_a = 0°$; $\delta_e = 1.75°$; leading edge drooped. (Results for nacelles-on configuration have been estimated using nacelle increments determined from fig. 20.)
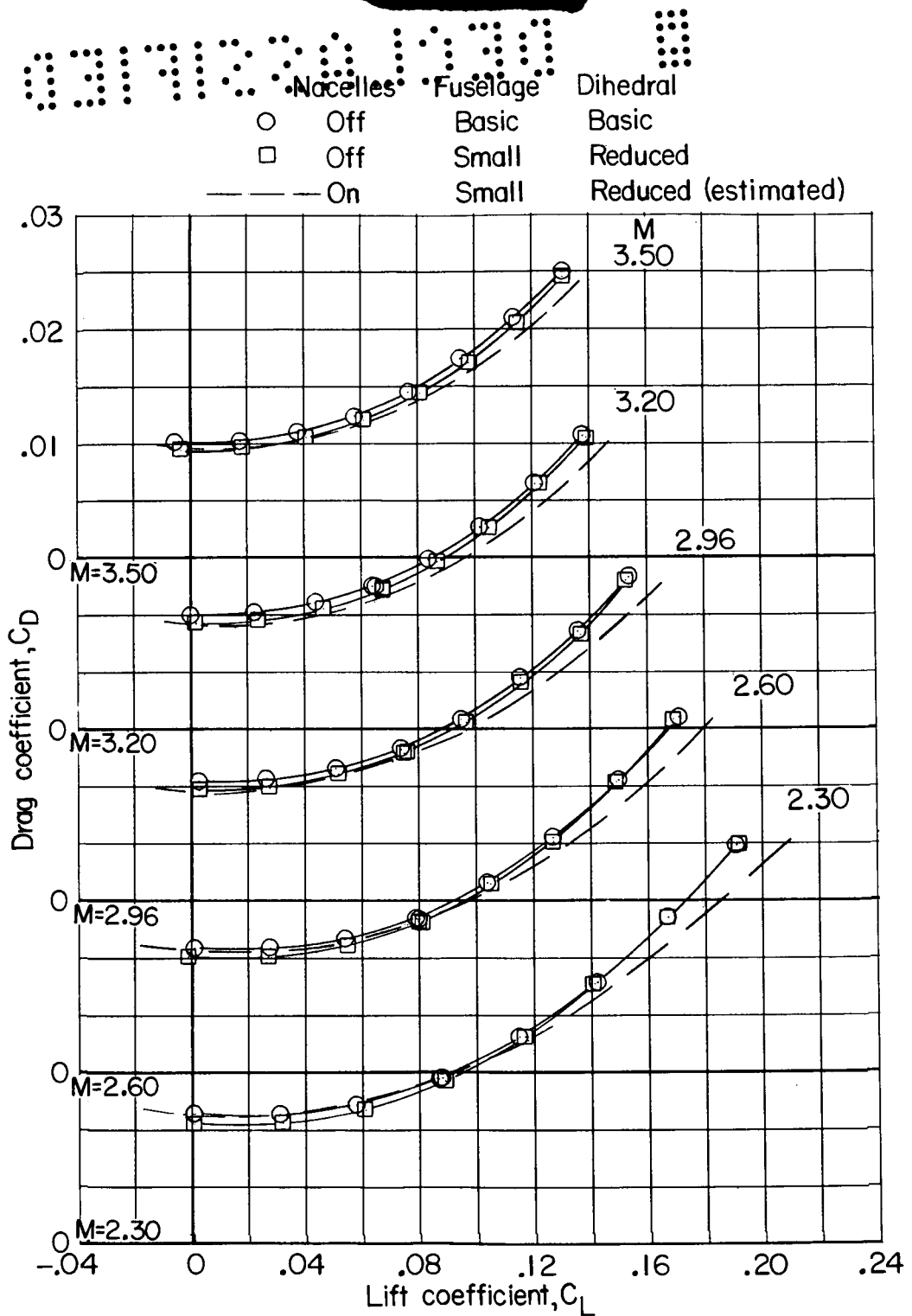
(b) C_D against C_L.

Figure 21.- Continued.

Nacelles	Fuselage	Dihedral
○ Off	Basic	Basic
□ Off	Small	Reduced
——— On	Small	Reduced (estimated)
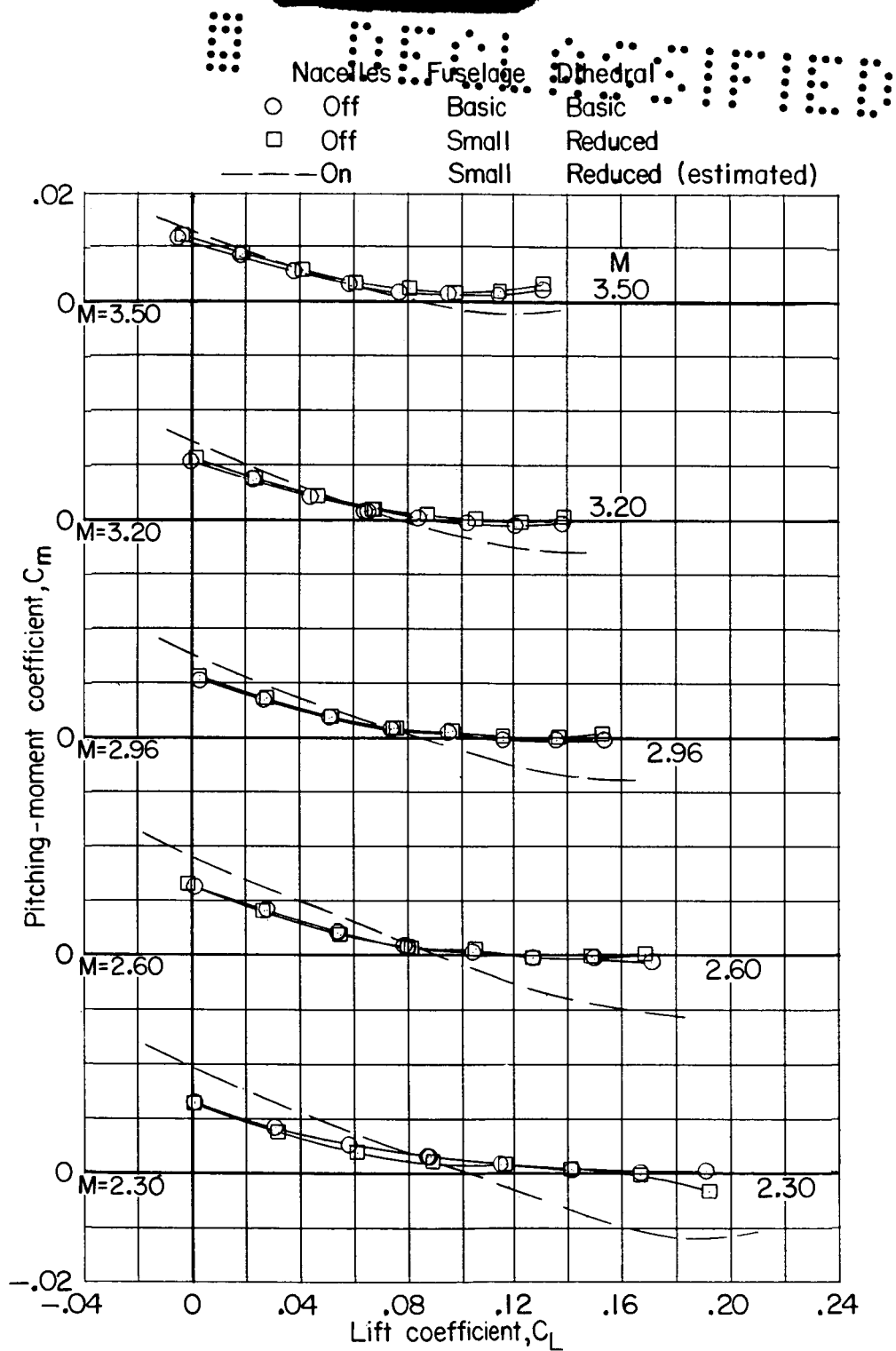
(c) C_m against C_L.

Figure 21.- Concluded.
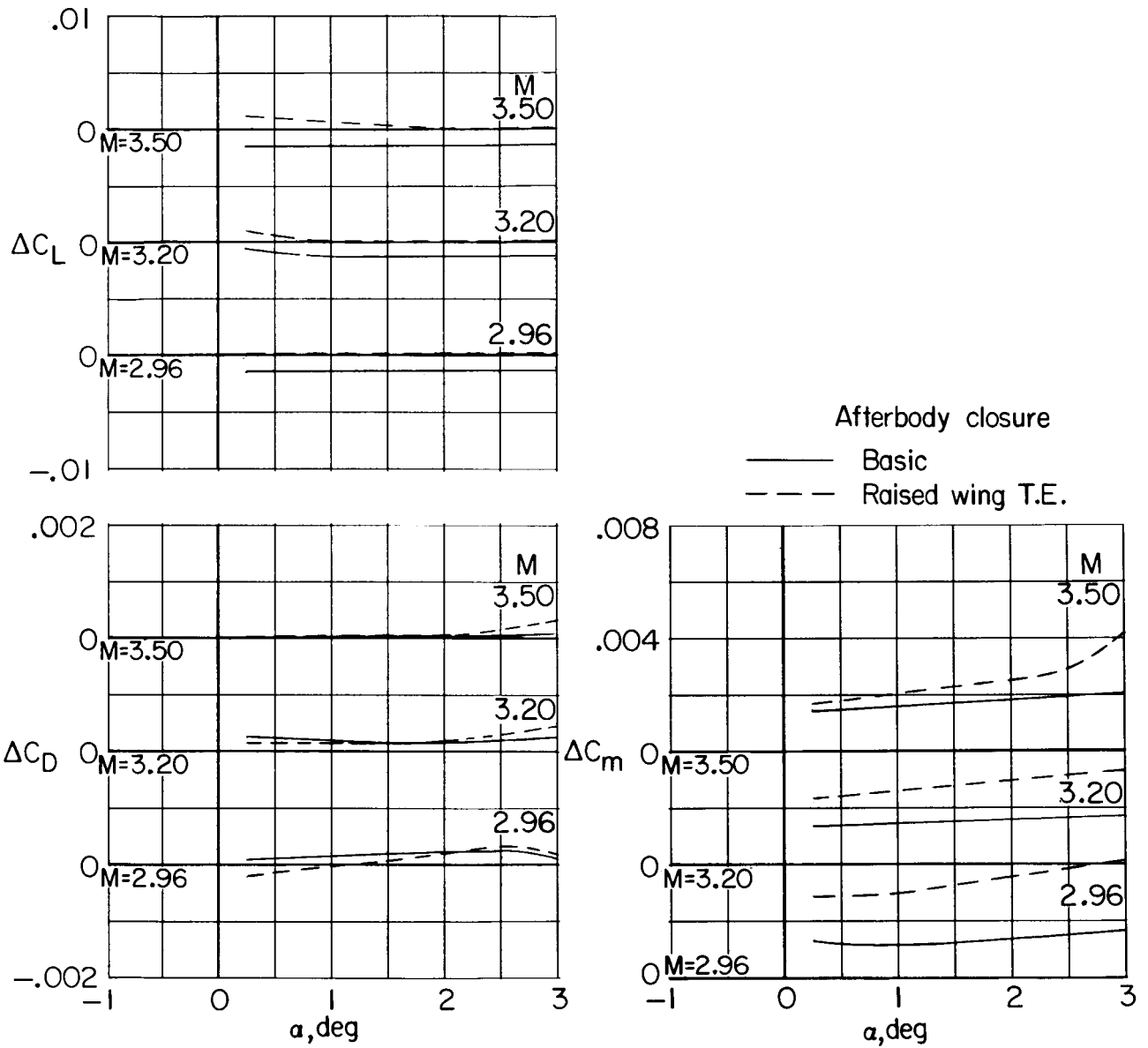
Figure 22.- Incremental effect of afterbody closure.

Empennage δ_e, deg
○   On   1.75
□   On   —2.25
◇   Off
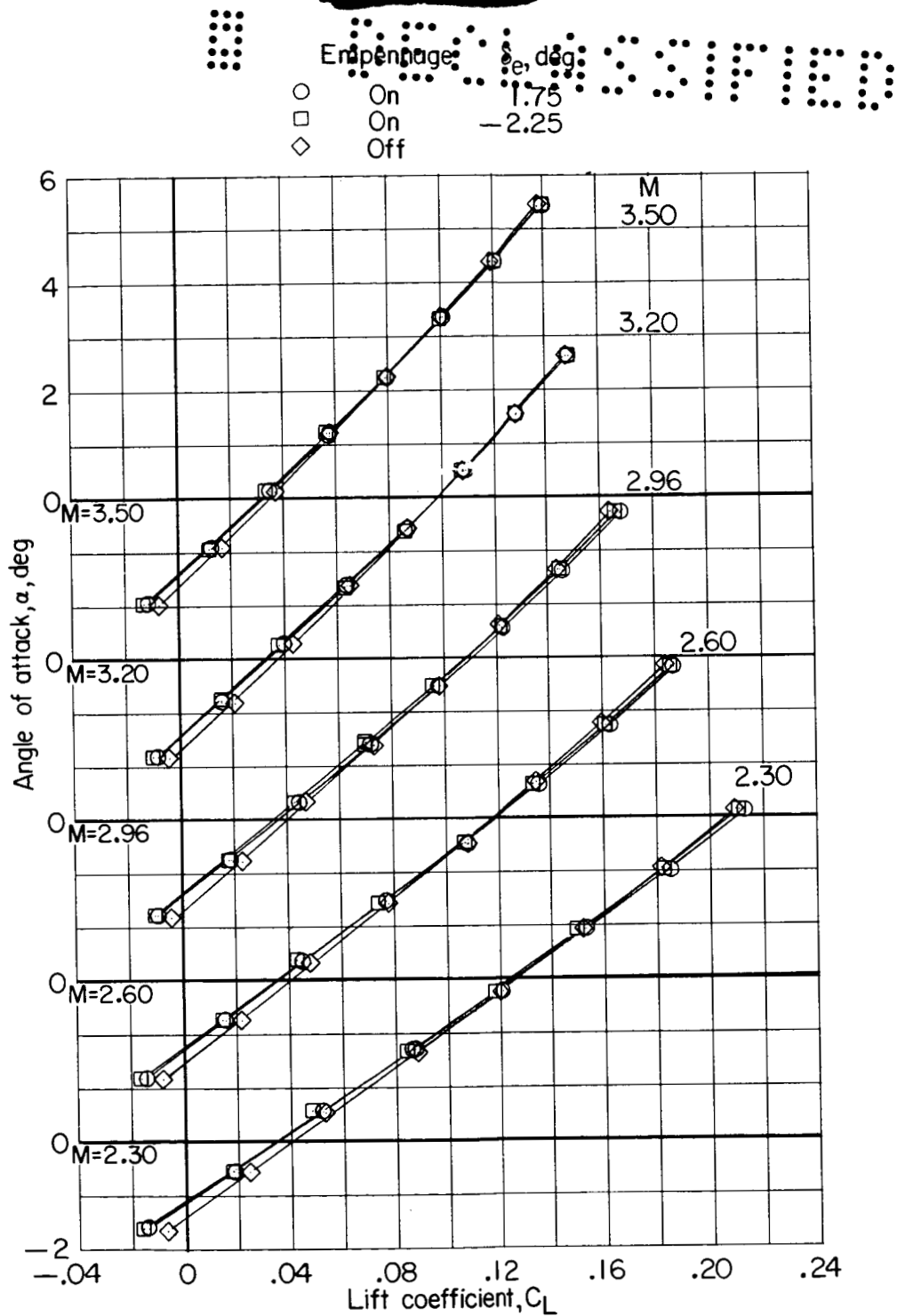
(a) α against C_L.

Figure 23.- Effect of elevator deflection and empennage on supersonic longitudinal aerodynamic characteristics. $\delta_f = 0°$; $\delta_a = 0°$; leading edge undrooped.
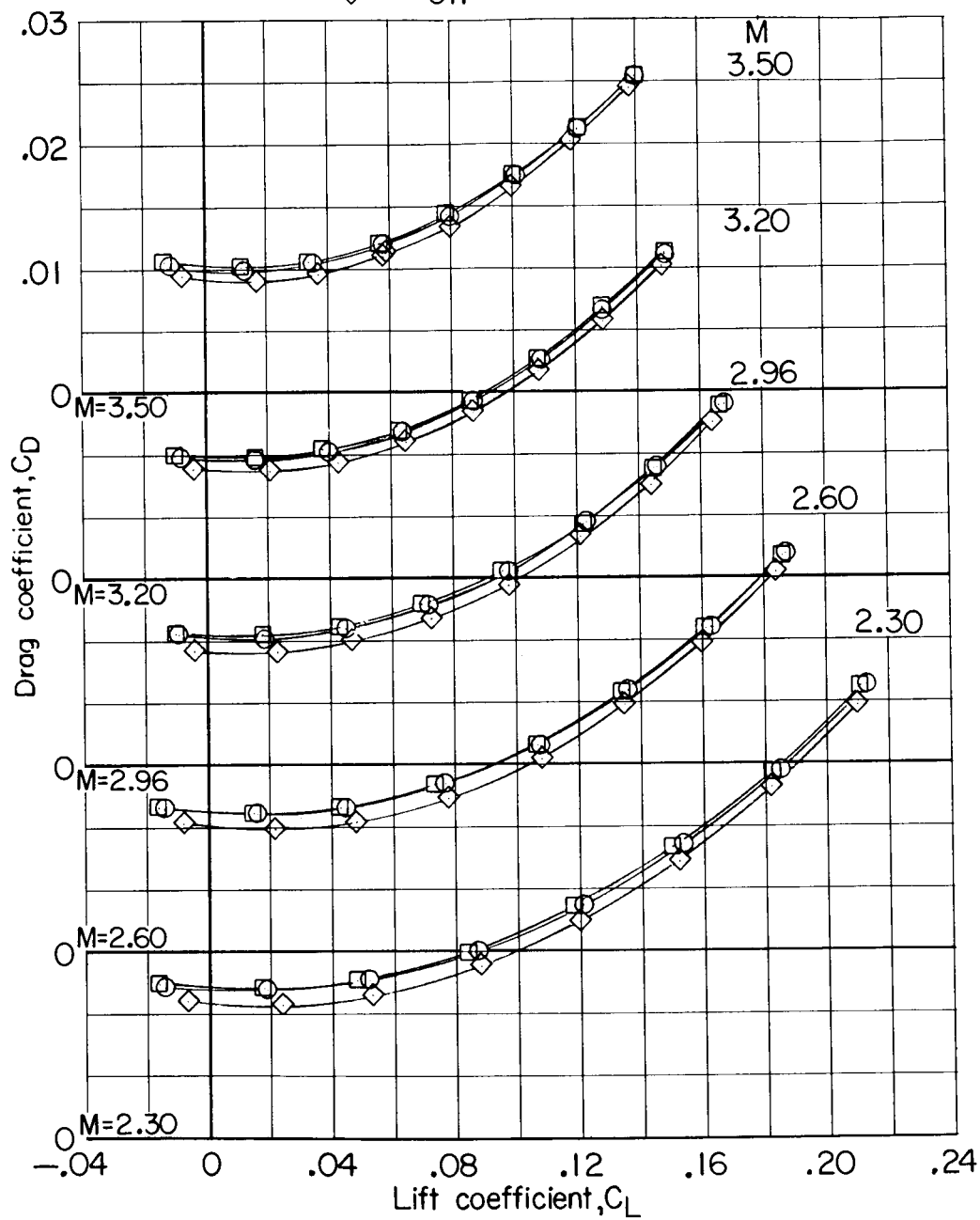
(b) C_D against C_L.

Figure 23.- Continued.

Empennage	δ_p, deg
○ On	1.75
□ On	−2.25
◇ Off	
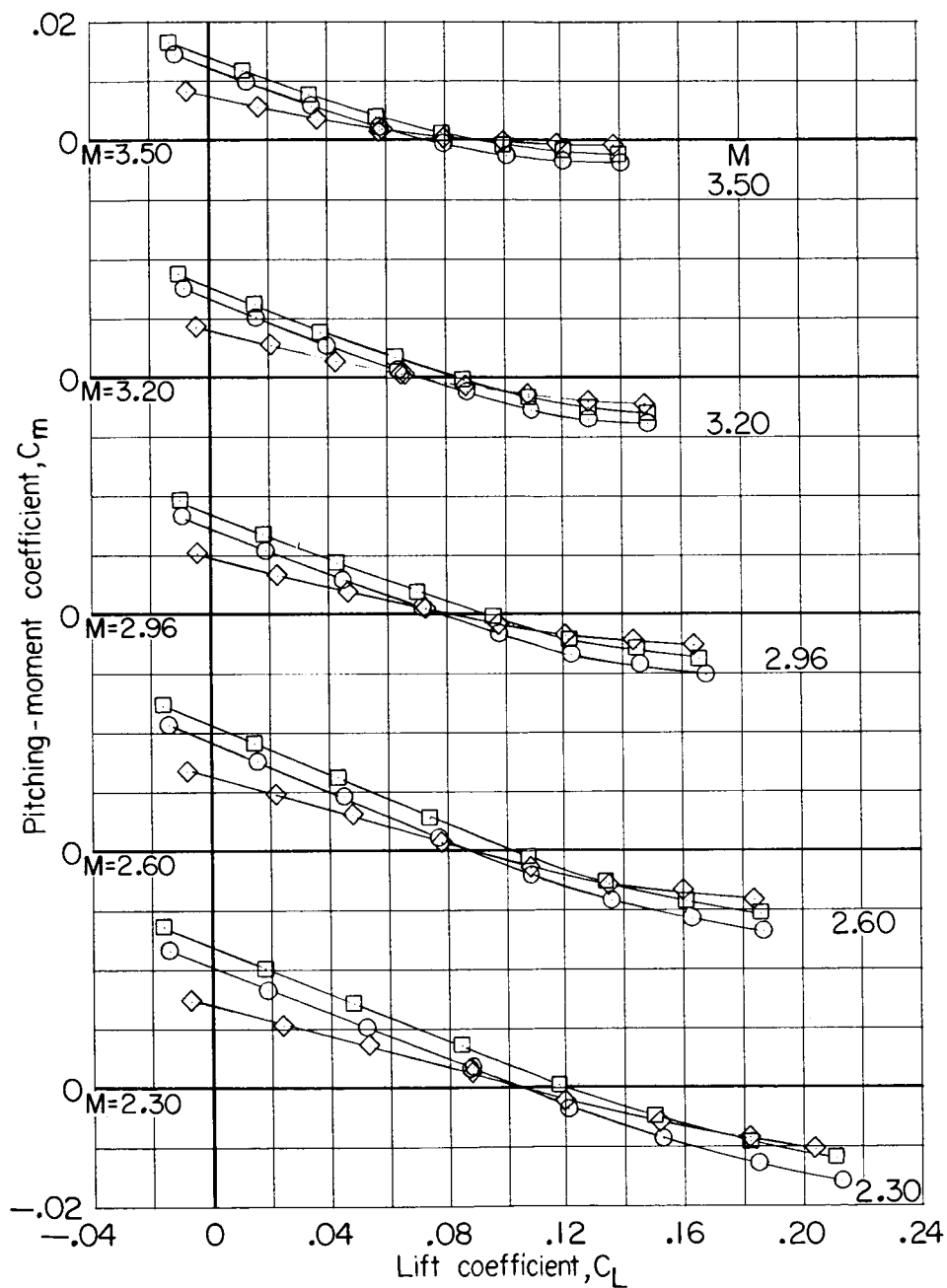
(c) C_m against C_L.

Figure 23.- Concluded.

Empennage	α, deg
On	2
Off	2
On	4
Off	4
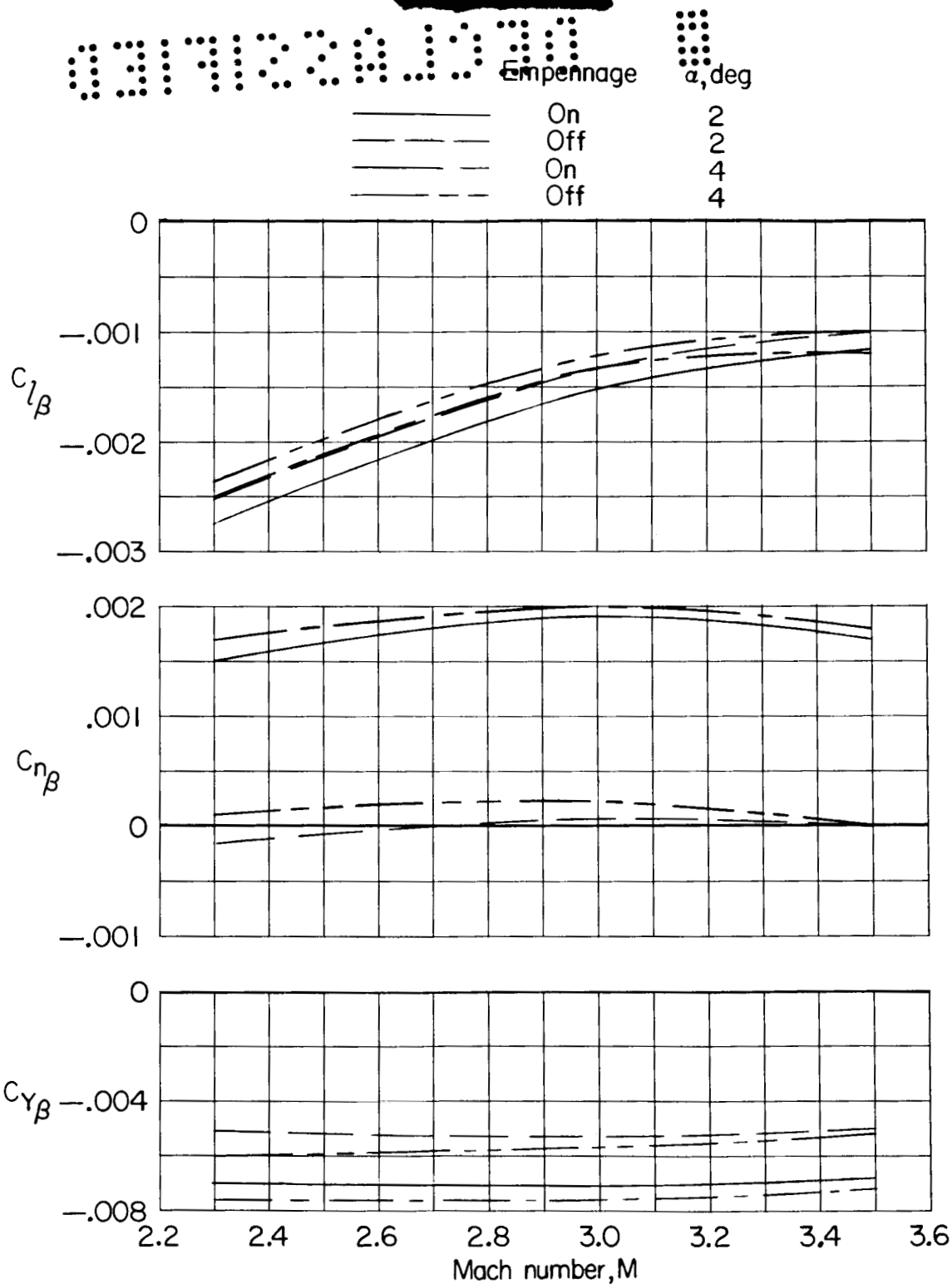
Figure 24.- Effect of empennage and angle of attack on lateral stability derivatives at super-sonic Mach numbers. $\delta_f = 0°$; $\delta_a = 0°$; δ_e (for empennage on) = $1.75°$; leading edge drooped.
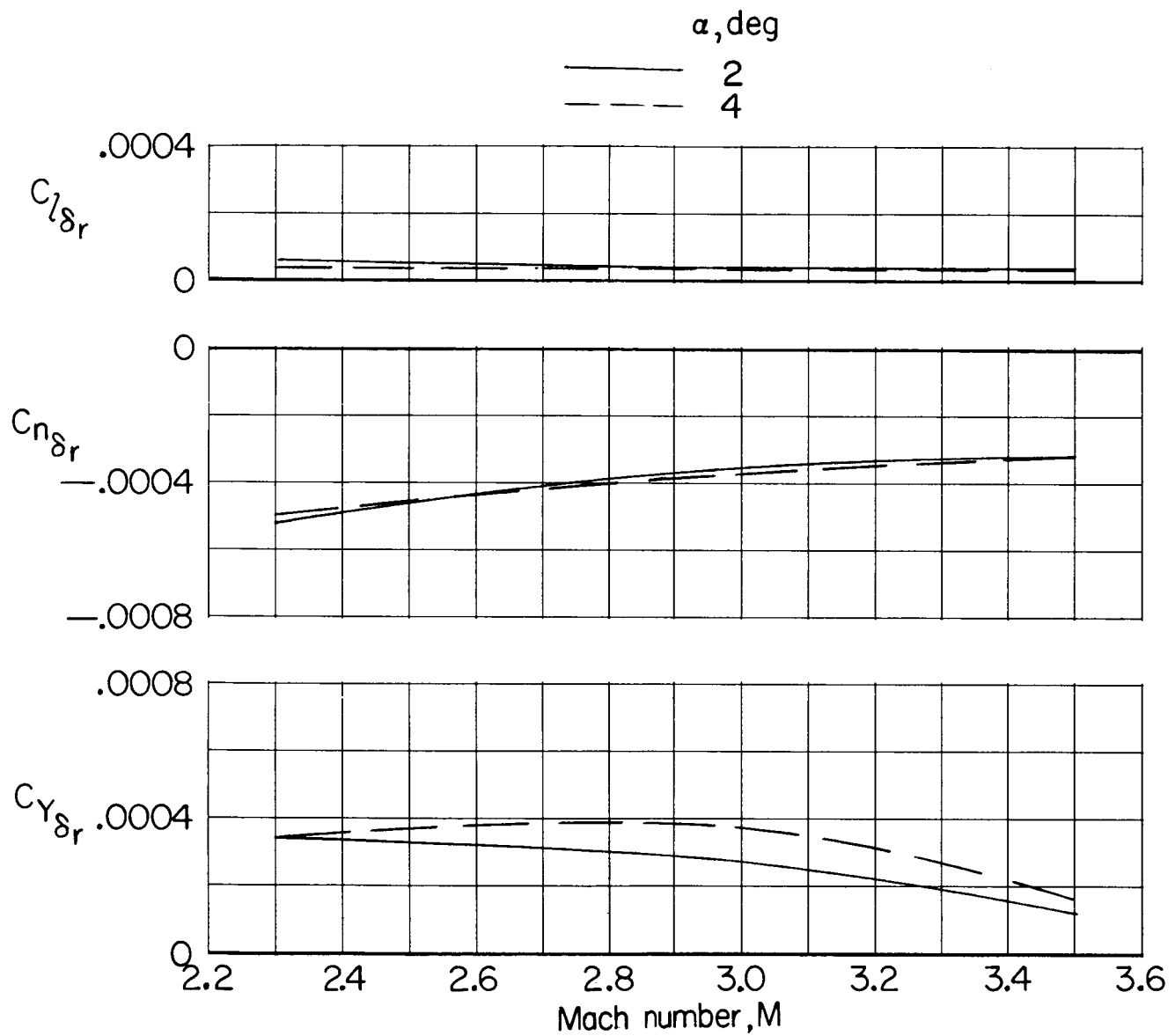
Figure 25.- Effects of rudder deflection on supersonic lateral aerodynamic characteristics. $\delta_f = 0°$; $\delta_a = 0°$; $\delta_e = 1.75°$; leading edge drooped.
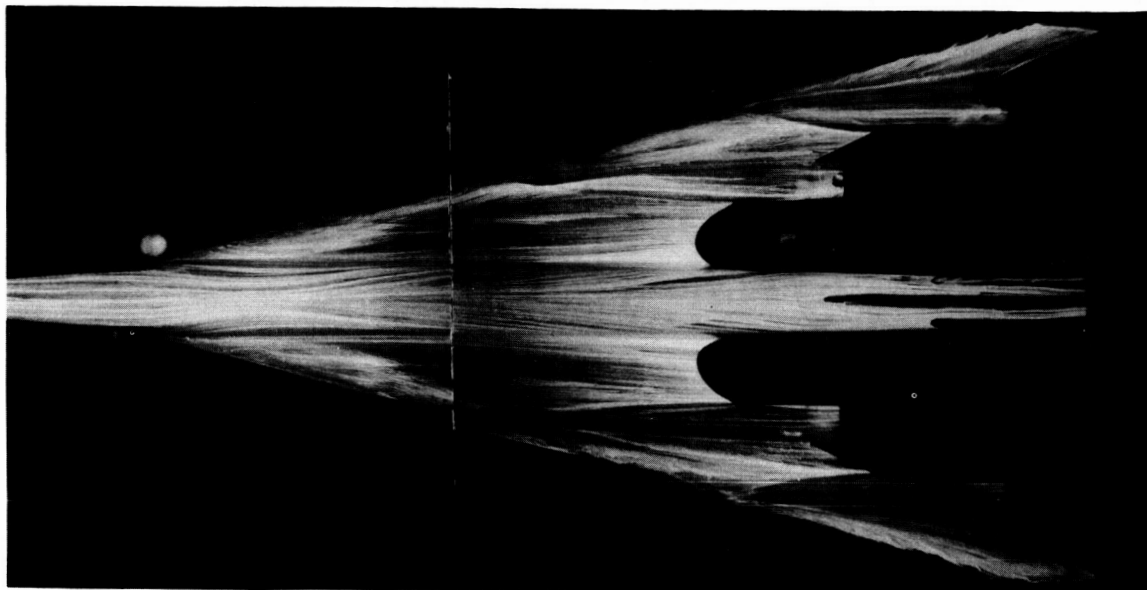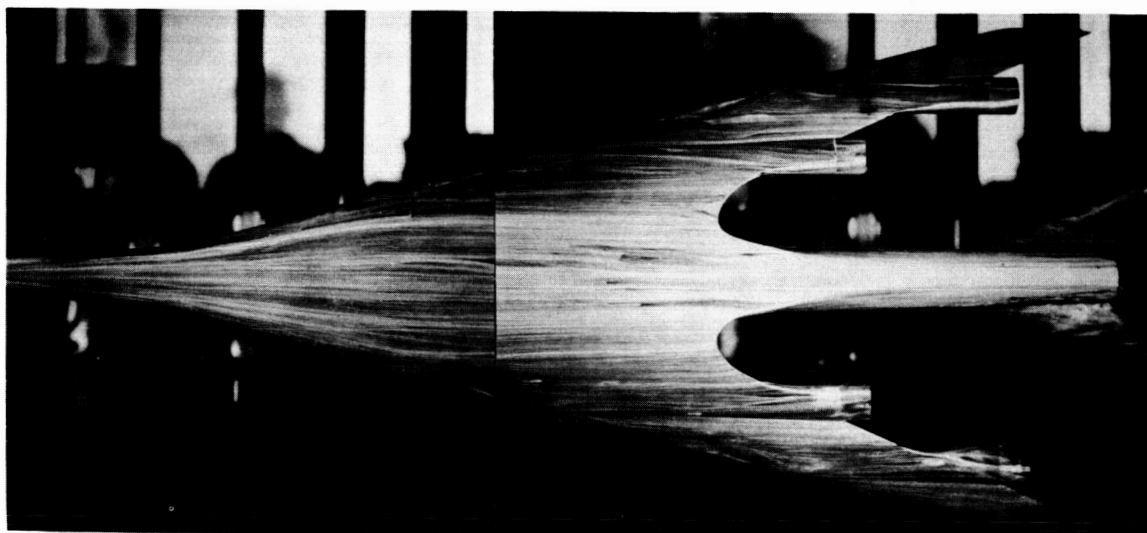
Upper surface

Lower surface

(a)   M = 2.60; C_L = 0.08.   L-63-6

Figure 26.- Fluorescent-oil film photographs of boundary-layer flow patterns. δ_f = 0°; δ_a = 0°; δ_e = 1.75°; leading edge drooped.
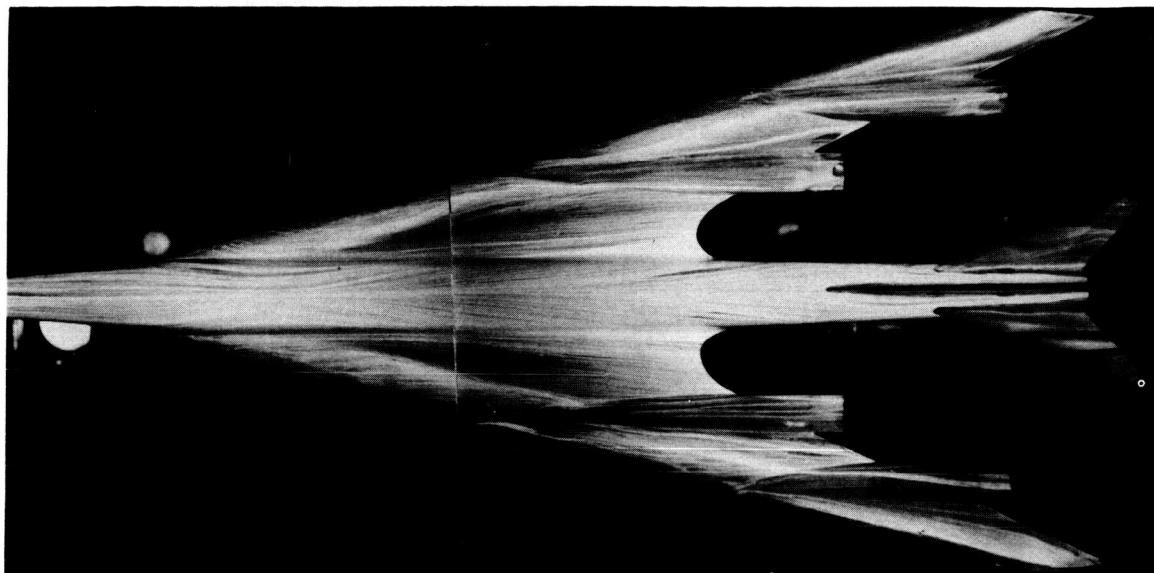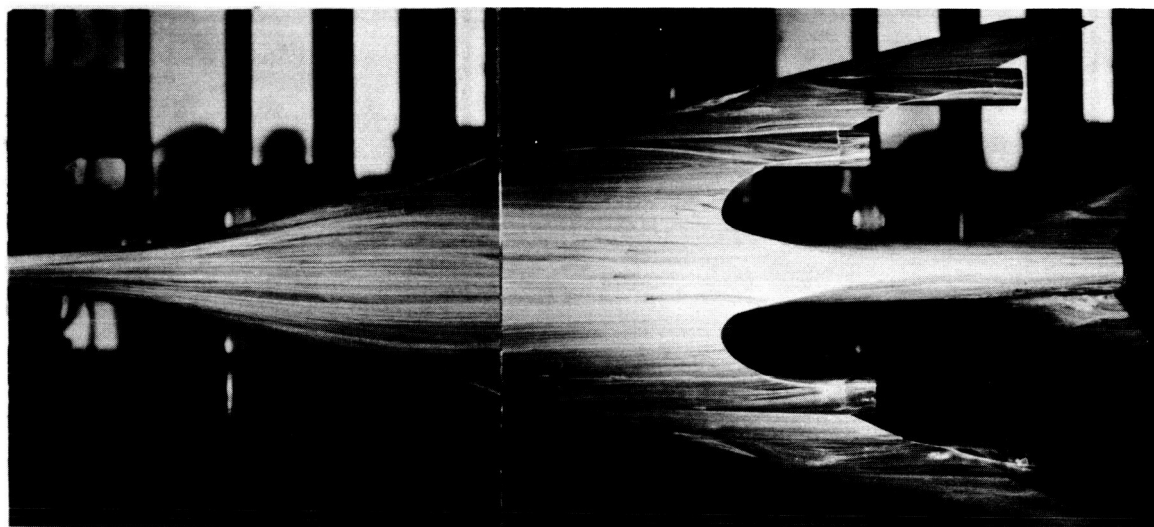
Upper surface

Lower surface

(b) M = 2.96; C_L = 0.07.   L-62-7063

Figure 26.- Concluded.
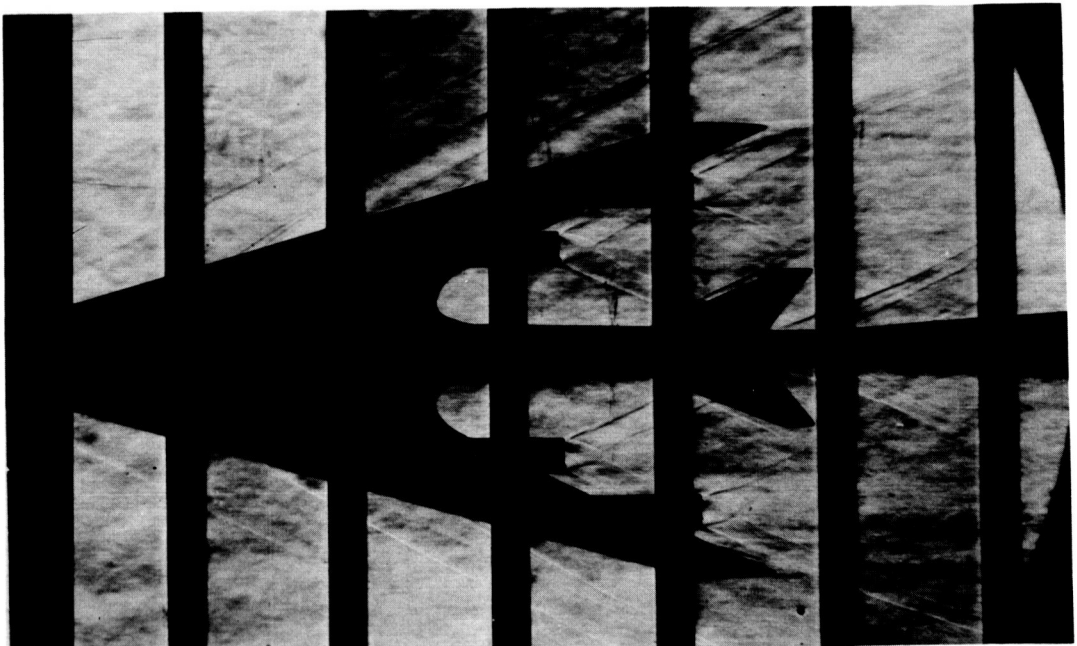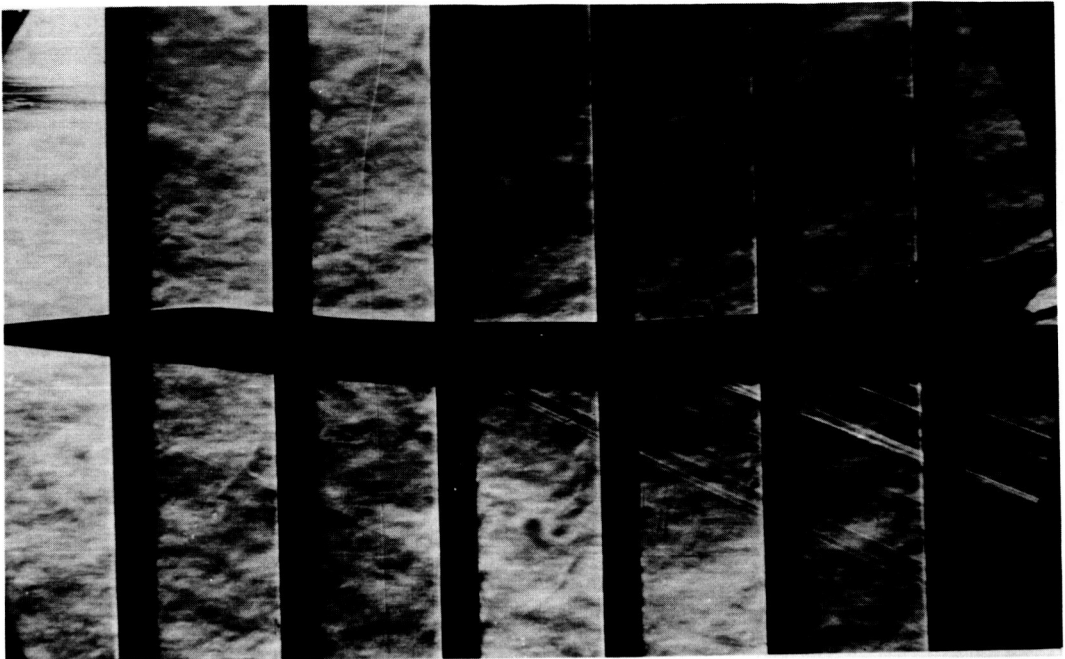
(a)   M = 2.60; α = 1.47°.   L-63-7

Figure 27.- Schlieren photographs.   Leading edge drooped; $\delta_f = 0°$; $\delta_a = 0°$; $\delta_e = 1.75°$.
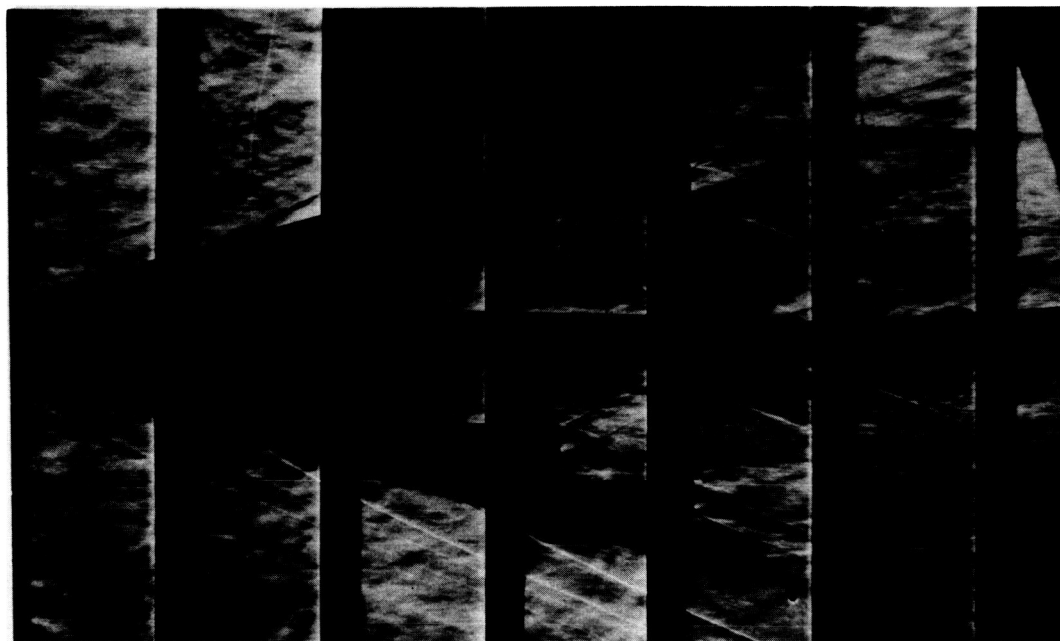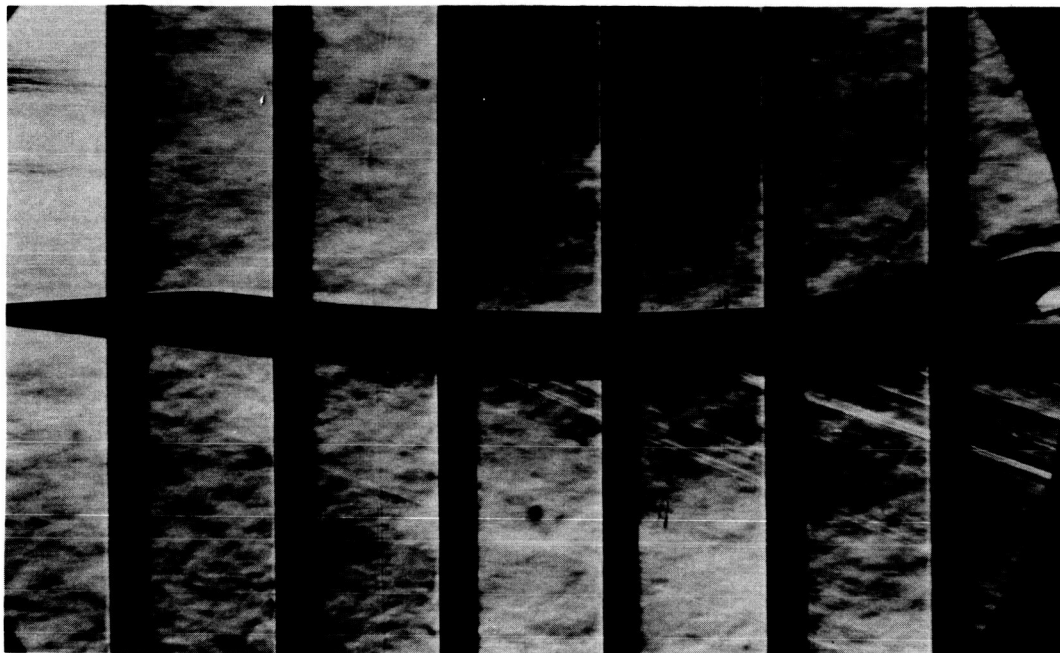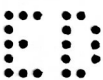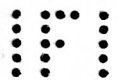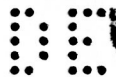
(b) M = 2.96; α = 1.43°.   L-63-8

Figure 27.- Continued.

(c) M = 3.20; α = 1.37°.
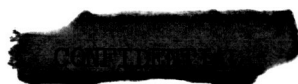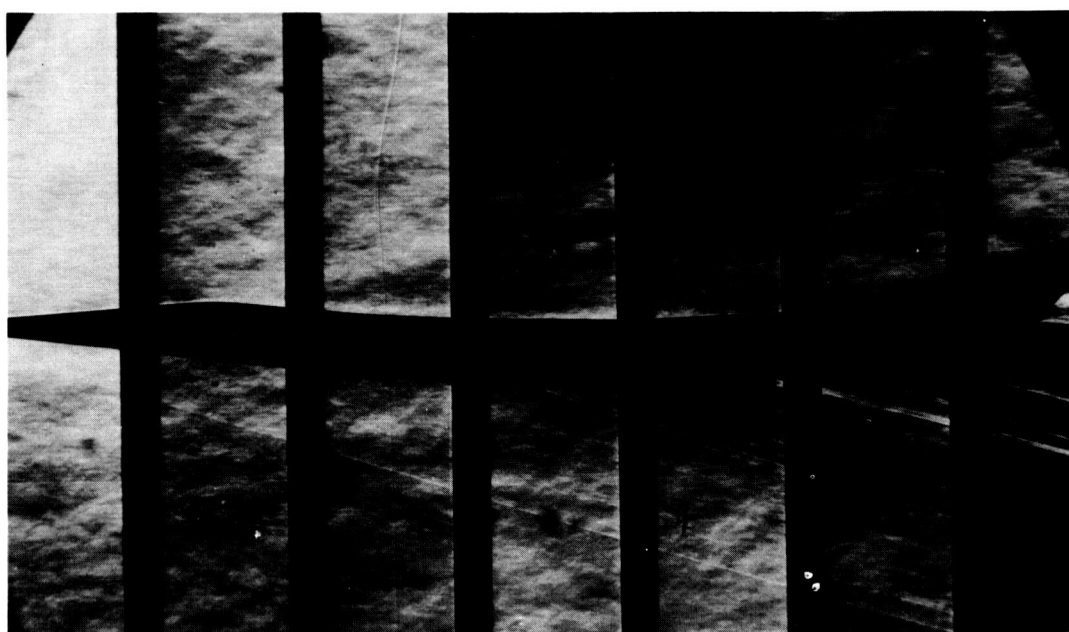
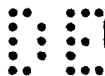(d) M = 3.50; α = 1.17°.   L-63-9

Figure 27.- Concluded.
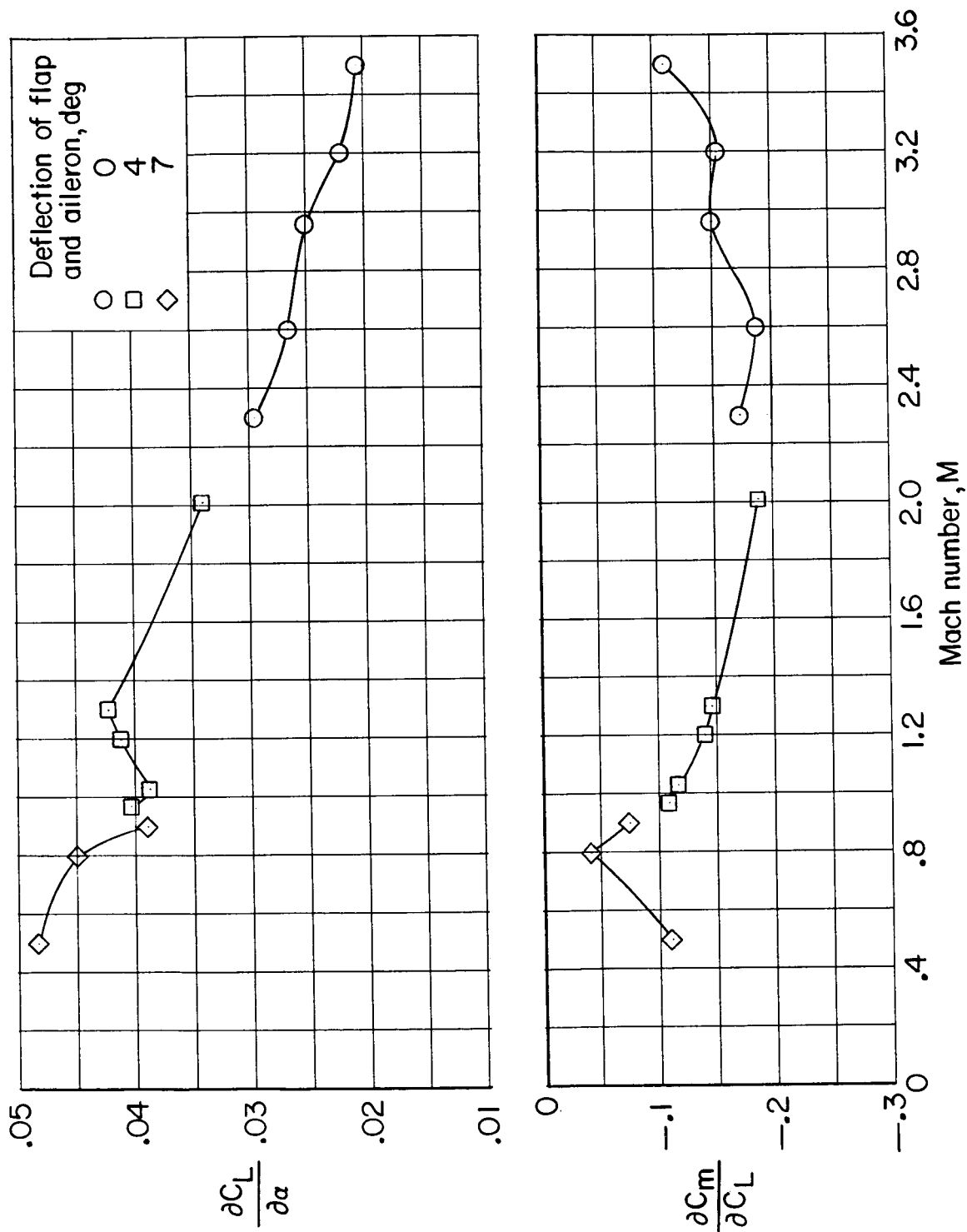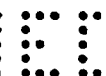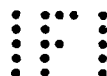
Figure 28.- Variation with Mach number of lift-curve slope and longitudinal stability parameter, measured at C_L for $(L/D)_{max}$ (full scale). Basic configuration; leading edge drooped.
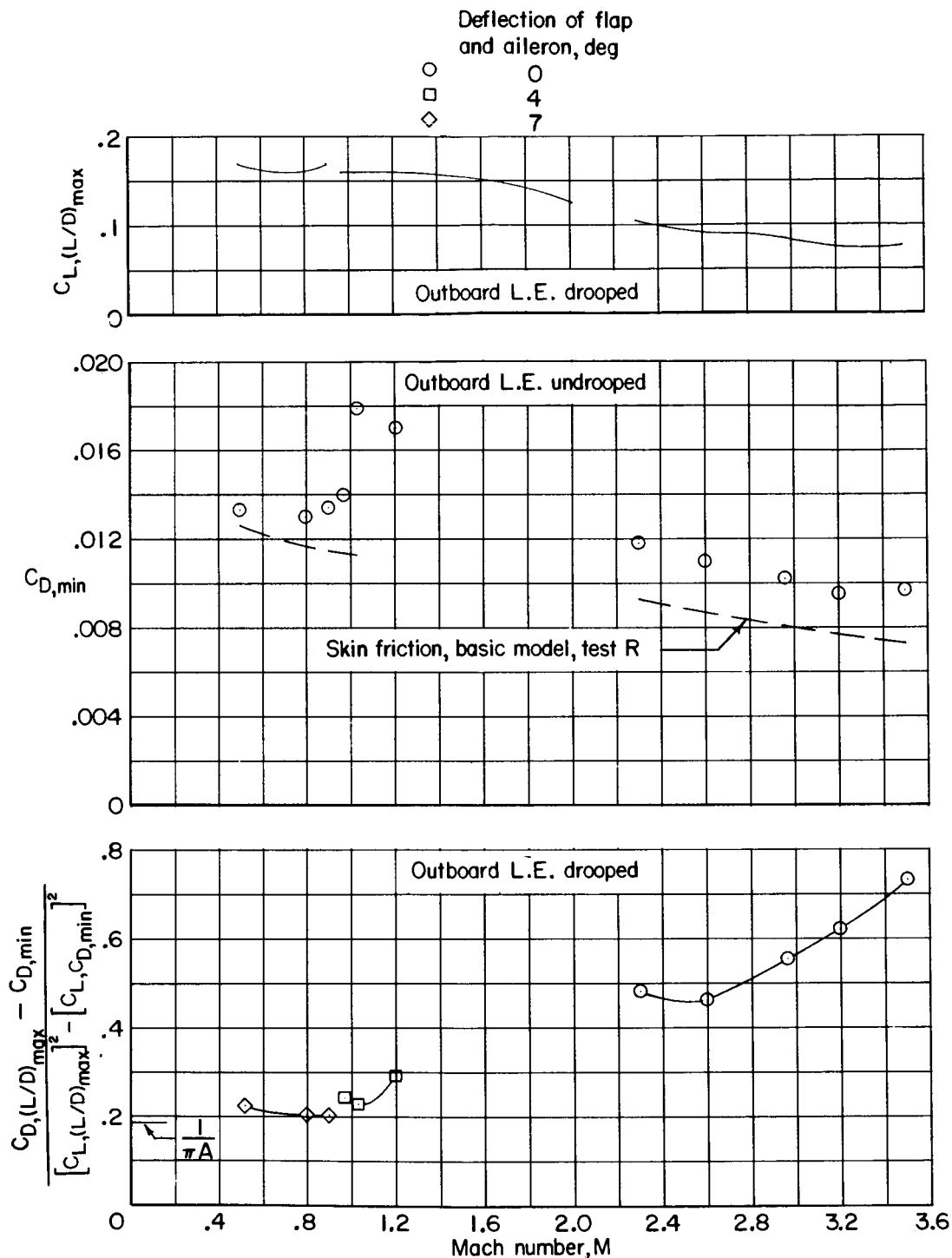
Deflection of flap
and aileron, deg

○　　　　0
□　　　　4
◇　　　　7

Figure 29.- Variation with Mach number of estimated full-scale lift coefficients for $(L/D)_{max}$, model minimum drag coefficients (leading edge undrooped), and drag-due-to-lift factors (leading edge drooped). Basic configuration.
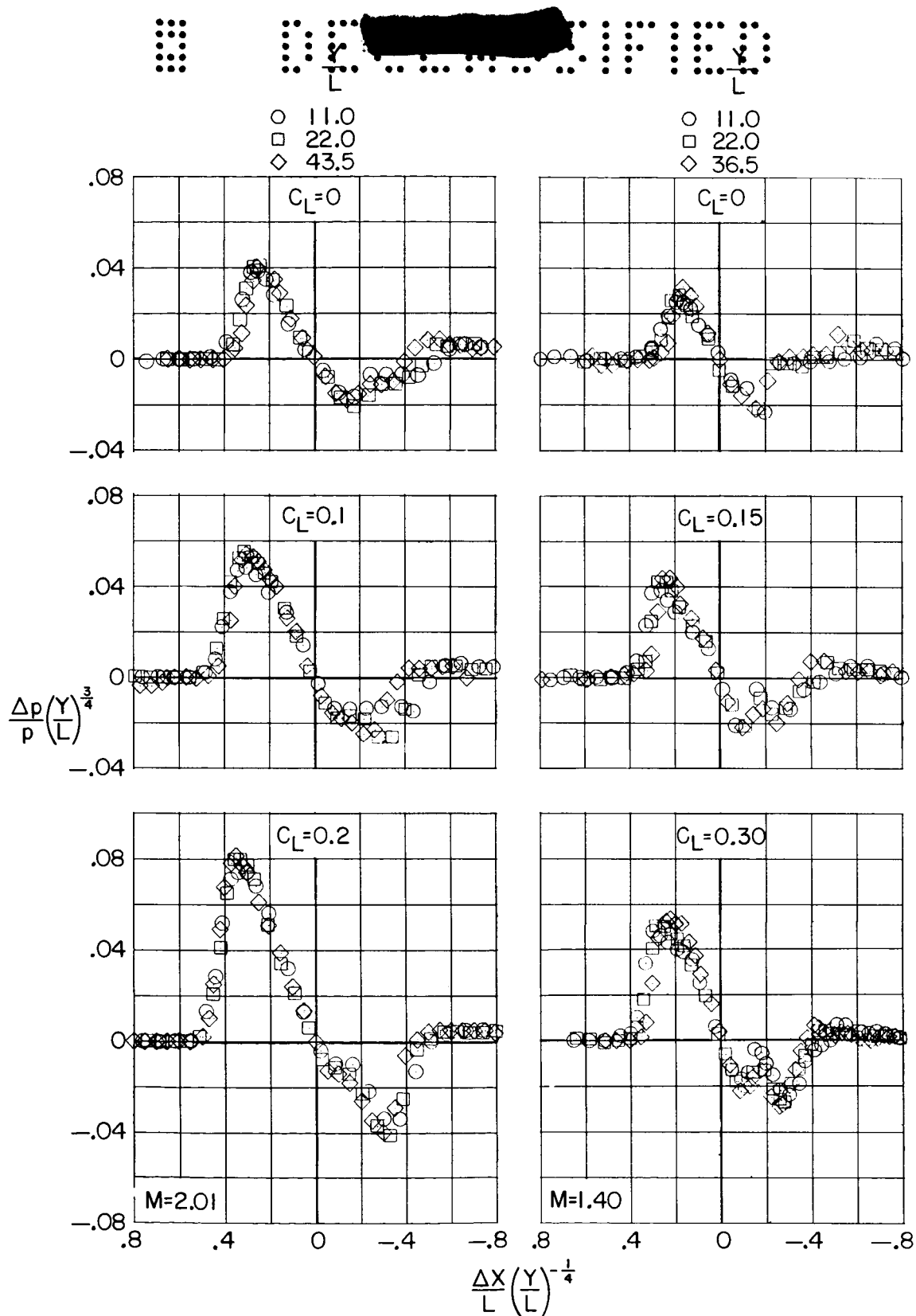
Figure 30.- Pressure signatures of sonic-boom model of basic configuration at Mach numbers of 2.01 and 1.4.

○ Basic configuration
□ Reduced fuselage

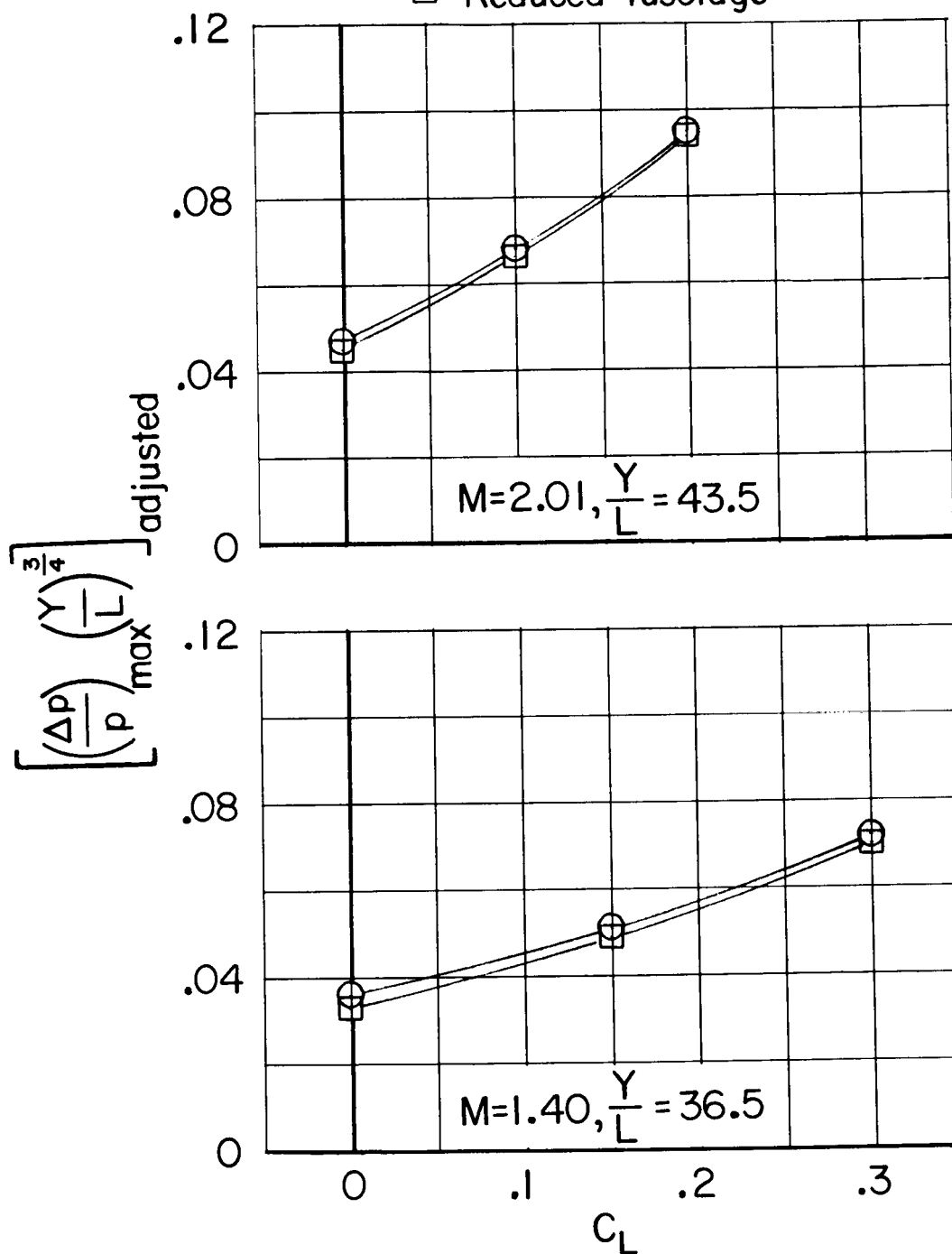$$\left[\left(\frac{\Delta p}{p}\right)_{max} \left(\frac{Y}{L}\right)^{3/4}\right]_{adjusted}$$

$M = 2.01, \frac{Y}{L} = 43.5$

$M = 1.40, \frac{Y}{L} = 36.5$

C_L

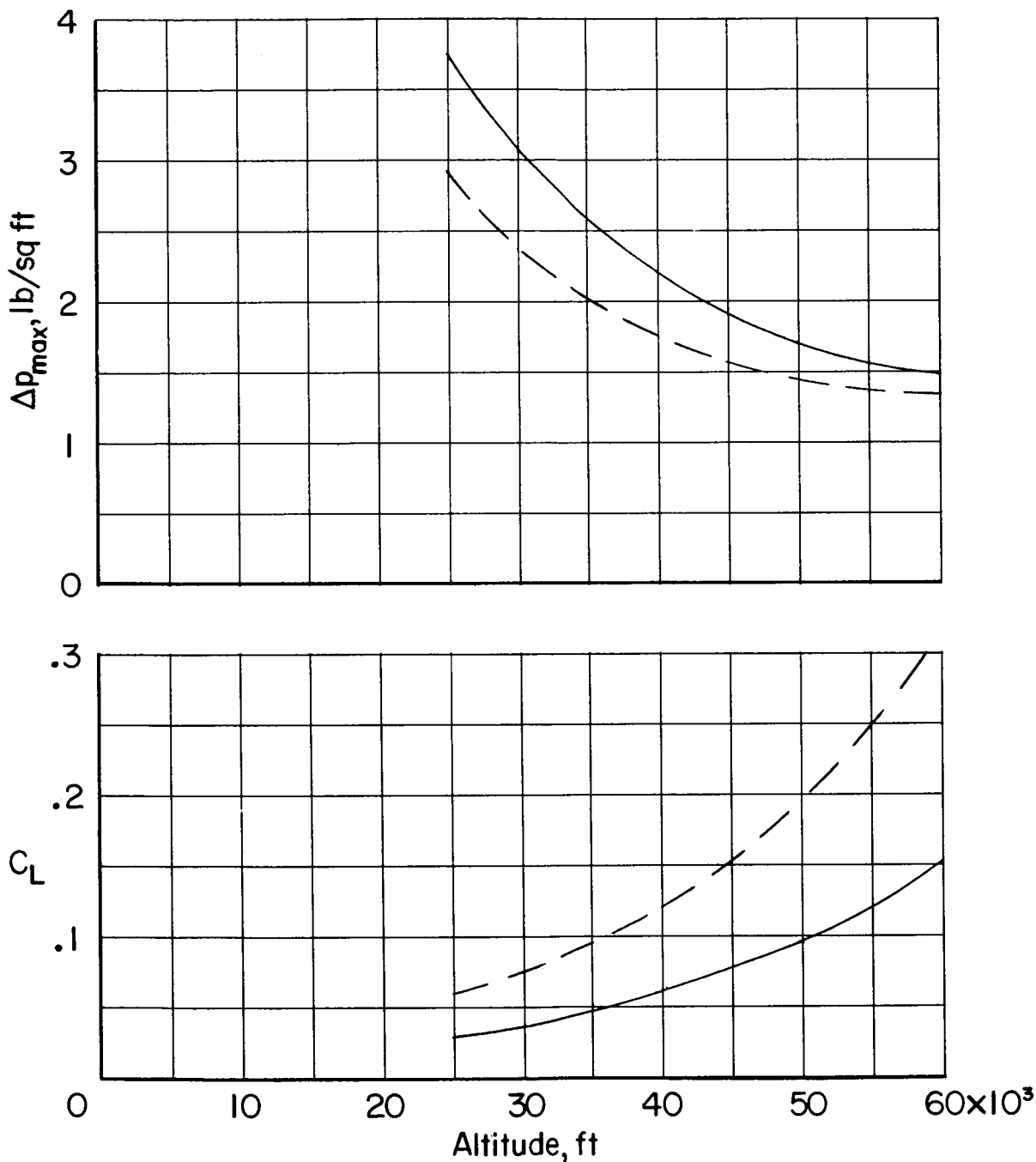Figure 31.- Variation of maximum sonic-boom overpressure with lift coefficient at several Mach numbers.

Figure 32.- Variation with altitude of maximum sonic-boom overpressure at ground and lift coefficient for small fuselage configuration at W/S = 65 lb/sq ft.